UAB

Universitat Autònoma de Barcelona

Tectonics of dyke swarms: Insights from case studies and analogue modelling

Ana Isabel Martínez Poza

UAB
Universitat Autònoma de Barcelona

Tectonics of dyke swarms: Insights from case studies and analogue modelling

Ana Isabel Martínez Poza

A thesis submitted to the
Universitat Autonòma de Barcelona
for the degree of Doctor of Philosophy

Co-Directed by Elena Druguet and Jordi Carreras.

U A B
Universitat Autònoma de B

Departament de Geologia
Universitat Autònoma de Barcelona
Programa de Doctorat en Geologia

MIET
grup de recerca

Agradecimientos

Acknowledgements

En primer lugar, me gustaría agradecer al MINECO y al MEC por las becas que he obtenido a lo largo de mi vida académica y que han sido las responsables de que llegue hasta este nivel de formación y conocimientos.

Por supuesto a mis padres, que sin su esfuerzo, en todos los sentidos de la palabra, nunca habría podido llegar hasta aquí. Ellos me han enseñado que con trabajo se puede llegar hasta donde se quiera y me han dado los valores necesarios para conseguirlo.

A mis jefes, Elena y Jordi, porque me han dado siempre libertad de opinión y decisión, me han sabido guiar y me han ayudado cuando he estado perdida. Sin ellos esta tesis no hubiera sido posible. Y a Lina Marcela, por acompañarme al empezar esta tesis y enseñarme tanto en tan poco tiempo.

A mis compañeros de doctorado, todos juntos hemos sufrido estos cuatro años nuestras penas y frustraciones. Ojalá que todos consigan lo que desean en este mundo académico y profesional, porque se lo han ganado.

Al resto de profesores y secretarias del Departamento de Geología de la UAB, siempre ayudando en todo lo posible y sacando una sonrisa por los pasillos.

Al profesor Allen Glazner y el Departamento de Geología de la UNC, porque esas dos estancias en EEUU han sido muy provechosas académica y profesionalmente. Y a Carolina Muñoz, Roger Putnam y John Bartley, todos ellos me ayudaron en la campaña de campo del IDS en California y sufrieron conmigo cruzar cada día el arroyo Big Pine y cargar con piedras desde 3000 m de altitud. Carolina, gracias por sufrir la altura conmigo esos 10 días, no hubiera podido tener mejor compañera de campo.

Al resto de profesores y compañeros de otras universidades que he conocido durante cursos y congresos, siempre enriqueciendo de nuevos conocimientos e ideas.

Gracias a todos mis amigos y familiares que siempre me han preguntado cómo iba y me han dado ánimos.

Y por último a Miguel A., que siempre me ha apoyado y animado haya estado en otro continente o en la misma ciudad. Y nunca ha dejado que la tesis haya podido conmigo. Muchas muchas gracias.

GRACIAS

Resumen

Los patrones de enjambres de diques aportan evidencias sobre las condiciones de paleoesfuerzos, cinemática cortical y regímenes tectónicos. El objetivo principal de esta Tesis es discernir y caracterizar en tres dimensiones los patrones estructurales de enjambres de diques magmáticos. Para ese propósito, se ha llevado a cabo el estudio de casos de cuatro diferentes escenarios geológicos y dos series de experimentos de modelización analógica. La comparación entre los resultados obtenidos a partir de los diferentes estudios de campo y de modelización ha permitido avanzar en el conocimiento de los factores mecánicos y tectónicos asociados al emplazamiento y deformación de diques.

Se puede realizar una distinción entre patrones simples y más complejos mediante la comparación entre contextos geológicos y tectónicos distintos y mediante la ayuda de la modelización analógica. Los casos más simples se han observado en contextos extensionales en la corteza media-superior. Los enjambres se caracterizan por intrusiones paralelas que se propagan a lo largo de fracturas perpendiculares a σ_3. Sin embargo, las heterogeneidades presentes en las rocas encajantes, tales como diaclasas, producen modificaciones en los patrones de intrusión, puesto que el magma utiliza ciertas fracturas pre-existentes para la intrusión. Esta situación caracteriza en diferente grado los enjambres de Aiguablava (Cordillera Costera Catalana) y del SE de Cerdeña. Como consecuencia, en cada situación se da un patrón de segmentación de diques distinto. Los modelos analógicos recrean este tipo de relaciones y permiten comprobar dichas diferencias.

Los otros dos contextos regionales estudiados (*Independence Dyke Swarm* en Sierra Nevada, California, y varios enjambres de diques máficos del Anti-Atlas de Marruecos) revelan patrones estructurales más complejos. Su intrusión en la corteza media y, sobretodo, subsiguiente deformación, tuvieron lugar durante eventos orogénicos bajo condiciones de mayor presión litostática y esfuerzos diferenciales menores. Aunque del mismo modo que en los casos precedentes el mecanismo de intrusión fundamental fue la hidrofractura, las condiciones tectónicas orogénicas y las propiedades mecánicas del sistema dique-roca encajante (comportamiento frágil-dúctil) muestran una influencia importante en el desarrollo de estructuras. Es relativamente común en estas situaciones la aparición de sistemas conjugados de diques híbridos, así como de patrones *en echelon*. Además, debido a contrastes de competencia entre diques y rocas encajantes, la deformación tiende a localizarse durante y después del emplazamiento, generando foliaciones y zonas de cizalla. Dicho fenómeno ha sido reproducido en una serie de experimentos analógicos de deformación frágil-dúctil alrededor de diques parcialmente fundidos.

Resum

Els patrons d'eixams de dics aporten evidències sobre les condicions de paleoesforços, cinemàtica cortical i règims tectònics. L'objectiu principal d'aquesta Tesi és discernir i caracteritzar en tres dimensions els patrons estructurals d'eixams de dics magmàtics. Amb aquest objectiu s'ha dut a terme l'estudi de casos de quatre diferents escenaris geològics i dues sèries d'experiments de modelització analògica. La comparació entre els resultats obtinguts a partir dels diferents estudis de camp i de modelització ha permès avançar en el coneixement dels factors mecànics i tectònics associats a l'emplaçament i deformació de dics.

Es pot fer una distinció entre patrons simples i més complexos mitjançant la comparació entre contextos geològics i tectònics diferents i mitjançant l'ajut de la modelització analògica. Els casos més simples s'han observat en contextos extensionals en l'escorça mitja-superior. Els eixams es caracteritzen per intrusions paral·leles que es propaguen al llarg de fractures perpendiculars a σ_3. No obstant això, les heterogeneïtats presents en les roques encaixants, com ara diàclasis, produeixen modificacions en els patrons d'intrusió, ja que el magma utilitza determinades fractures preexistents per a la intrusió. Aquesta situació caracteritza en diferent grau els eixams d'Aiguablava (Serralada Costanera Catalana) i del SE de Sardenya. Com a conseqüència, en cada situació es dóna un patró de segmentació de dics diferent. Els models analògics reprodueixen aquest tipus de relacions i permeten comprovar aquestes diferències.

Els altres dos contextos regionals estudiats (Independence Dyke Swarm a Sierra Nevada, Califòrnia, i diversos eixams de dics màfics de l'Anti-Atlas del Marroc) revelen patrons estructurals més complexos. La seva intrusió en l'escorça mitjana i, sobretot, subseqüent deformació, van tenir lloc durant esdeveniments orogènics sota condicions de major pressió litostàtica i esforços diferencials menors. Tot i que de la mateixa manera que en els casos precedents el mecanisme d'intrusió fonamental va ser la hidrofractura, les condicions tectòniques orogèniques i les propietats mecàniques del sistema dic-roca encaixant (comportament fràgil-dúctil) mostren una influència important en el desenvolupament d'estructures. És relativament comú en aquestes situacions l'aparició de sistemes conjugats de dics híbrids, així com de patrons *en echelon*. A més, a causa dels contrastos de competència entre dics i roques encaixants, la deformació tendeix a localitzar-se durant i després de l'emplaçament, generant foliacions i zones de cisalla. Aquest fenomen ha estat reproduït en una sèrie d'experiments analògics de deformació fràgil-dúctil al voltant de dics parcialment fosos.

Abstract

Patterns of dyke swarms provide evidences about paleostress, crustal kinematics and geotectonic regimes. The main aim of this Thesis is to discern and characterize the three-dimensional structural patterns of magmatic dyke swarms. For this purpose, case studies on four different field reference areas and two series of analogue modelling experiments have been carried out. Comparison of the results obtained from different field-based and modelling studies has allowed gaining insight into the mechanical and tectonic factors associated with the emplacement and deformation of dykes.

A distinction from simple to more complex patterns could be made by comparing different tectonic cases and also with the help of analogue modelling. The simplest cases have been observed in mid- to upper-crustal extensional settings. Swarms are characterized by sub-parallel intrusions which propagate along fractures normal to σ_3. However, heterogeneities in the granitoid host rocks, as joints, produce modifications in the intrusion patterns, since magma may use these pre-existing anisotropies to intrude. To different extents, this situation characterizes the Aiguablava (Catalan Coastal Ranges) and SE Sardinia cases. In consequence, particular dyke segmentation patterns are characteristic of each region. Analogue models recreate this type of relations and test the differences in segmentation associated with diverse previously fractured basements.

More complex structural patterns have been recognized in the other studied dyke swarms (Independence Dyke Swarm in Sierra Nevada, California and various swarms of mafic dykes in the Anti-Atlas of Morocco). Their intrusion into the mid-crust and subsequent deformation took place under higher confining pressures and lower differential stresses during orogenic events. Although the main intrusion mechanism was also hydrofracturing as in the other study cases, the particular orogenic tectonic conditions and mechanical properties of the dyke-host rock system (brittle-ductile behavior) had a large influence on the developed structures. Arrays of conjugate sets of hybrid dykes and *en echelon* dykes are more common in these cases. Moreover, as an effect of competence contrasts between dykes and host rocks, deformation localization structures (foliations, shear zones) developed during or after the emplacement. This situation has been reproduced in series of analogue experiments of ductile deformation around partially molten dykes in isotropic rocks.

INDEX

Table 2 XRF data
Table 3 U-Pb data

CHAPTER 1

INTRODUCTION

1.1. SETTING OF THE STUDY

Dykes have been a major indicator of the tectonic regime ongoing during the magmatic intrusion. Because of that, abundant literature has been written about this distinctive feature of the nature.

Usually, large mafic dyke swarms are associated to rifting environments. Frequently characterized by subparallel intrusion of very long dyke segments with large extension. However, after many research, this environment has not been the only proposed setting for the occurrence of large mafic dyke swarms.

Magmatic dykes constitute a key tool for the structural geology and geotectonic interpretation in a region. These structural elements are present in every crustal levels and diverse tectonic setting. The fast emplacement, orientation, morphology, composition and age make dykes important information sources to understand the relationships between magmatic and tectonic processes. They can be relevant indicators of magmatic reservoirs and orogenic processes (Ingram and Hutton, 1994), as well as continental reconstructions (Halls, 1982; Ernst *et al*., 1995). Dykes are important also to recreate paleostress regimes (Anderson, 1951; Pollard, 1973, 1987; Delaney *et al*., 1986; Hoek, 1991; Platten, 2000 and many others), propagation paths (Vanderhaeghe, 2001; Bons et al. 2001, 2009; Brown 2004, 2008, 2010) and emplacement mechanisms (Cadman *et al*. 1990). They are also used as deformation and kinematic markers in middle to lower crust domains (Hanmer and Passchier 1991; Carreras and Druguet 1994; Druguet *et al*. 2008; Druguet and Castaño 2010).

The majority of the studies relate magmatic bodies and deformation processes (Hutton, 1988; Petford *et al*. 2000). Deformation usually increases the mobility of magmatic bodies and creates space for accumulation, transport and injection (Hutton, 1988; D'Lemos *et al*. 1992; Bouchez *et al*. 1997). It is also a controlling factor for volcanic centers, plutonic bodies and dyke swarms (Nakamura, 1977; Delaney *et al*., 1986; Hutton, 1988; Takada, 1994; Glazner *et al*., 1999)

Therefore, the location, time distribution, intrusion time, dimension, orientation, morphology, chemical composition and rheology of large dyke swarms point out the different mechanisms related to dyke generation and deformation.

The aim of this project is to understand the intrusion mechanisms of (mafic) dyke swarms and understand the deformation processes that take place during the injection of the mafic material. The interaction process between dykes and host rock depend on several factors as: rheology, temperature, mechanics and kinematics that will be explained later in this chapter (and also in the discussion chapter).

This work will try to investigate the proposed cases from a structural point of view with the help of other geological tools as petrology, geochemistry, analogue modelling and geochronology.

The main objectives of the project are:

a) Characterized dyke features related to the intrusion mechanisms in deformed and non-deformed dykes.

b) Consequences of the host rock properties in the magmatic intrusion. Heterogeneities in the host rock can suppose a change in the injection path.

c) Effects of the regional stress field during the dyke emplacement and its relation with dyke swarm patterns.

d) Correlation between dyke pattern and the tectonic evolution of each case study.

1.2. CHARACTERISTICS AND FACTORS CONTROLLING DYKE INTRUSION.

1.2.1. Magmatic intrusive bodies.

The intrusive bodies of our interest are dykes (or veins). Depending on the magma composition and tectonic location, dykes may have different features. In a general model, the dyke propagates throughout a non-fractured rock (Rivalta *et al.*, 2014). The thickness is lower than the breadth (third dimension of the dyke, height of the dyke in the vertical plane) and length (dimension along the dyke propagation path). Typical dyke thickness range from 10s cms to 10s meters; length is around 100s meters to 1s kilometers, in the horizontal plane (sills) dyke lengths can reach 10s of kilometers (Toda and Stein, 2002; Tryggvason, 1984, 1986; Wright *et al.*, 2006). Usually, breadth of dykes has the same order of magnitude (or slightly smaller) than the length. When there are dykes of 10s of meters thick and 100,000s of kilometers long they tend to configurate large swarms (Ernst *et al.*, 1995; Fialko and Rubin, 1999; Jolly and Sanderson, 1995; Pollard, 1987). The opening of the dykes is supposed to be along to the minimum compressive stress axis, σ_3, and they propagate perpendicularly to σ_3 (Anderson, 1951). In 2-D models, the propagation of the magma is along the direction of σ_1. In the case of a similar value of σ_{hmin} to σ_{Hmax}, dykes have a low aspect ratio (thin intrusions) and they will intrude in random orientations, e.g. close to free surfaces as volcanoes.

A basic explanation for dyke propagation can be explained as a hot and compressible fluid passing throughout elastic walls, but this non-linear characteristic is only applicable for the model of propagation in fracture tips (Rivalta *et al.*, 2014). Factors as rheology and buoyancy values of the magma vary during the propagation because other process are happening, mainly gas exsolution and crystallization of the magma. Dykes suppose a difficult problem for the mathematical physics; the majority of the questions are simplified to 2-D

models. This imply the linearization of the rock behavior, without taking into account thermal mechanisms, magma changes in rheology and reducing the geometry of the fractures to linear surfaces without heterogeneities and no pre-existing fractures (Rivalta *et al.*, 2014).

Lately, the knowledge of the dyke dynamic has increased due to the advance in geophysical and modelling fields. The most interesting questions for the latest research in the dyke area are: 3-D shape of dykes during propagation; Dynamic controls and geometry of dykes; Effect of the regional stress field and boundary conditions with the host rock.

Usually, they present a tabular morphologies and subvertical disposition. The tabular/laminar morphology can corresponds to the intrusion through fractures produced by the fluid pressure (hydrofracture) (Lister and Kerr, 1991; Rubin, 1995) or the magma can propagate through pre-existing discontinuities and fractures in the host rock (Delaney *et al.*, 1986).

The compositional range for the magmatic material that compose dyke is very broad. And the intrusion range include from lower to upper crust. Mafic dykes tend to be larger than leucogranitic ones, also they are related to extensive settings (rift). This could be caused by the physical propierties like more fluidity, thinned crust and the favourable stress field (σ_1 vertical and σ_3 horizontal). Intermediate dykes tend to be smaller and intrude short distances in deeper crustal levels of orogenic regimes (σ_1 horizontal and σ_3 vertical).

1.2.2. Magmatic dykes: geodynamic regimes.

The occurrence of dykes is related to the regional context, normally linked with divergent and convergent margins. We can find dykes in continental volcanic arcs, subduction orogens, extensional settings like volcanic arcs and back-arcs from an intraoceanic subduction, also mid-oceanic ridges (Petford et al. 2000).

In continental arcs the magmatic bodies have a calc-alkaline composition. Large volumes of granitoides are produced due to continental crust anatexis or differentiation, contamination and fractional crystallization processes. Several types of magmas can be described: metaluminous to slightly peraluminous melts obtained from mantlelic mafic rocks and peraluminous melts produced by anatexis of sedimentary (pelitic) rocks. The typical calc-alkaline suite is developed when differentiation processes occur (Frost *et al.*, 2001; Best, 2003). Dykes from this setting represent the differentiate material from granitoides or partial melting products from gneisses and schists (Pearce, 1996; Petford et al. 2000; Frost et al. 2001; Best 2003; Blatt et al. 2006) and occasionally they are the result of melting the upper mantle.

In convergent settings, dykes can be produced during or post the collisional stage (Harris *et al.*, 1986). The dykes intruded during the collision are caused by the melting of the engrossed lithosphere (middle crust), migmatites and leucogranites are also generated (Hall, 1996). The post-collisional dykes are also anatexis products, but in this case, anatexis is due to a process of the

adiabatic decompression (Petford et al. 2000; Frost et al. 2001; Best 2003; Blatt et al. 2006).

In anorogenic settings, like continental rifts, oceanic ridges and mantelic plumes, there is a large magma production. However, in island arcs and passive ridges the magmatic bodies are mainly mafic dykes. The particular compositional type is caused by partial melting in the mantle or anatexis of crustal basic rocks.

Numerous investigations support the production, magma transport and final intrusion, and consequent deformation, in every geological possible context. Partitioning of the deformation generates shear zones with compressional and extensional areas which benefit the magmatic intrusion (Vigneresse and Clemens 2000). Many examples of strike-slip, transtensive/transpressive settings, are described in the literature (Hutton 1982; Castro 1985; Guineberteau et al. 1987; D'Lemos et al. 1992; Hutton and Reavy 1992; Tikoff and Teyssier 1992; Román-Berdiel et al. 1997; Druguet and Hutton, 1998; De Saint Blanquat et al. 1998; Benn et al. 1998; Brown and Solar 1999; Glazner et al. 1999; Román-Berdiel et al. 2000; Corti et al. 2005). Dykes from compressive/transpressive contexts come from more differentiated magmas than dykes intruded in an extensional/transtensive settings (Cembrano and Lara, 2009).

1.2.3. Spatial distribution of magmatic dykes.

Usually, dykes tend to be organized in systems or swarms. Dyke swarms are constituted by several to hundreds of individual bodies emplaced contemporaneously during an intrusive pulse (Best, 2003). They can be arranged linearly, radially or curvy (Halls 1982; Fahrig 1987; Ernst et al. 1995, 2001) or forming irregular networks as seen in granitic dykes. The dyke orientation of the injected through the crust is dominated by the stress regime, usually it forms tension cracks normal to the minimum stress direction (σ_3). Therefore, the distribution pattern follows the regional or local stress regime during the emplacement (Vanderhaeghe, 2001). The anisotropies in the host rock together with changes in differential stresses in depth affect the orientation and distribution of dykes (Brisbin, 1986).

In the upper crust, the differential stresses are high, then dykes tend to orientate perpendicularly to σ_3 with subvertical dipping (Halls, 1982 and Pollard, 1987). They form regular networks in distensive tectonic settings. In domains of the medium to lower crust, these stresses values are lower and dykes present a weak preferential direction, so intrusions form irregular systems.

1.2.3.1. Dyke networks with preferential orientations

These types of intrusions are typical of basic rocks. Characteristics examples are the Giant mafic swarms (Mackenzie swarm, Canada) with thousands of kms of extension and dyke width between 10 to 50 m and 1000 kms long (Ernst and Baragar, 1992; Ernst et al., 1995). Also

intermediate and felsic dykes can be arranged in this way (e.g. Spanish Peaks, USA).

a) *Lineal swarms*

They have a parallel intrusion pattern. This type of alignments indicates a constant state of stresses (Cadman *et al.*, 1990). However dykes are concentrated in narrow bands and they have a subvertical disposition normal to minimum stress axis. This type is typical from rift contexts (Ernst *et al.*, 1995) and back-arcs (Rivers and Corrigan 2000).

b) *Intersection swarms*

They present a more complex arrangement. Two or more sets are intruded with a preferential orientation that is crosscut between them. They are produced by a change in the regional stresses during the emplacement (Schlische, 2003) or maybe two different sets intruded in a conjugate fracture system (shear/extension pattern) (Escher *et al.*, 1976 and Hanmer *et al.*, 1997)

c) *Other preferential orientation swarms*

Other swarms can present a preferential orientation as a result of intermediate cases between two pattern situations. It could occur an overlapping of regional and local forces (e.g. Spanish Peaks, USA) (Odé, 1957). Another cause can be the magma injection into pre-existing fractures in the host rock (Gudmundsson *et al.*, 2002) (e.g. our study cases in Aiguablava, Sardinia and IDS). The last cause can be a deformation phase after the emplacement, then, the original pattern is modified (Matachewan dyke swarm in Canada and Kangamiut in Greenland).

1.2.3.2. Dyke swarms without preferential orientations

Networks are caotic and they are characteristics of granitoids intruded in medium to lower levels of the crust. They usually have less extension than the mafic swarms. Ductile deformation also affects the disposition of the intrusions (Mehnert, 1968). Usually these complex networks are common in orogenic contexts (transpressive or compressive) and represent different pulses of intrusion (e.g. migmatitic complexes as Cap de Creus) (Carreras *et al.*, 1975; Druguet, 1992; Carreras and Druguet, 1994; Alfonso, 1995; Druguet *et al.*, 1995; Druguet, 1997; Druguet and Hutton, 1998)

1.2.4. Formation and deformation of magmatic dykes.

Another interesting characteristic of dykes is their significance as transporter of mass and heat from the magma source to the upper/medium crust. These circumstances together with the regional deformation control the final shape of the intrusion bodies. Then, shape, size and spatial distribution of dykes reflect the key aspects of crustal melting (Brown, 2008). Dykes register the rheological and mechanical changes linked with transport, injection and deformation processes (Druguet and Castaño, 2008). Magmatic bodies are build up in four stages: melting formation, segregation processes, migration and emplacement (Brown 1994; Bouchez *et al.* 1997; Petford *et al.* 2000; Vigneresse 2004; Bons *et al.* 2009).

i) Magma generation

The main origin of magma melt is anatexia (Sedeholm, 1907). Rocks in lower levels of the crust or upper mantle have the influence of water plus volatiles, if there is an increase in temperature or an adiabatic decompression the melt is produced.

ii) Magmatic segregation and migration/ascension processes

This process describes the movement of the melt through the intergranular space until it accumulates in the reservoir. This mechanism implies a chemical and thermal exchange between rock and melt. The process is dependent on the viscosity and density of the melt, the pressure gradient and the flow rate. This factor depends on the porosity of the rock (Brown 1994; Bouchez *et al.* 1997; Petford *et al.* 2000; Vigneresse 2004; Bons *et al.* 2009).

This process occurs along large distances, from meters to kilometers. The main driven forces of the melt are: 1) Buoyancy of the fluid 2) pressure gradient, responsible of the heterogeneous deformation in the host rock 3) deformation partitioning due to the rheological contrast between magma and host rock (Vigneresse and Tikoff, 1999; Vanderhaeghe, 1999, Weinberg and Mark, 2008).

The interesting migration process for our research is the hydrofracture or dyking (Lister and Kerr, 1991). This is considered as the main magma raisin mechanism in the crust (Spence *et al.* 1987; Sleep, 1988; Emerman and Marrett, 1990; Clemens and Mawer, 1992; Hutton, 1992; Petford *et al.* 1993, 1994, 2000; Rubin, 1993; Brown, 1994; Brown *et al.* 1995; Mériaux and Jaupart, 1998).

This process occurs when the magma rising occurs through fractures generated by the fluid overpressure. This mechanism makes the dykes and magmatic veins propagate to crustal levels. The flow rate is high in comparison to diapirism and it is controlled by the viscous drag of the magma in the conduit (Spence and Turcotte, 1985, 1990; Maaloe, 1987; Spence *et al.* 1987; Turcotte, 1987; Sleep, 1988; Lister and Kerr, 1991; Rubin 1993, 1995, 1998; Mériaux and Jaupart, 1998).

iii)   Emplacement, cooling and deformation of dykes.

The emplacement process supposes the last step in the formation of magmatic intrusions in the crust. Any particular change in the propagation path constitutes the beginning of the emplacement process. Then, this stage starts when the fractures loss the propagation capacity, it can be produced due to a decrease in the fluid pressure caused by a cooling process (Watanabe *et al.*, 2002). The emplacement can be also caused by the presence of heterogeneities or discontinuities in the rock which act as magma stoppers (Clemens and Mawer, 1992 and Hogan *et al.*, 1998).

The intrusion/emplacement process is complex; it is characterized by the mechanical contrast in the magma and also between the host rock and the magma. Moreover, magma suffers very strong rheological changes during the intrusion. Then, mechanical contrasts in the magma and host rock take place under the influence of temperature changes, viscosity, magma pressure, heat flow, stress regime, deformation processes, etc.; this factors rules the intrusion process (Vigneresse and Clemens, 2000) and controls the final configuration of the swarms.   The majority of the ductile to brittle-ductile structures of the dykes reflect only the last stages of emplacement (crystallization) (Pertford, 2003). Therefore, the emplacement study has been divided in specific areas: studying only the mechanisms of emplacement (Paterson and Fowler, 1993), describing the rheology of the magma (Vigneresse *et al.*, 1996 and Petford, 2003) or characterizing the deformation phases implied in the intrusion and its possible tectonic controls (Anderson, 1951 and Ernst *et al.*, 1995).

a) *Emplacement mechanisms*

The magmatic emplacement mechanism is related to the interaction between magma and host rock (Cloos, 1923). Usually, is denominated *dyking* which can be composed of two opposed mechanisms (Pitcher, 1979; Lister and Kerr, 1991; Hutton, 1992; Rubin, 1993): one is forceful emplacement or hydrofracturing if the dyke dilation front (tip) cause tension in the host rock up to the initiation of new fractures where the magma material can migrate (Anderson, 1938; Pollard *et al.*, 1984). Other emplacement mechanism is passive emplacement, magma intrude along pre-existant fractures or free surfaces in the host rock (Castro, 1987; Hutton, 1998 and Paterson and Fowler, 1993). Nowadays, both mechanisms are considered to be combined during the process. Each mechanism will take more importance depending on the depth, dimensions and buoyancy mechanism (Paterson and Fowler, 1993).

b) *Rheological behavior of the magmas*

The intrinsic properties of magmas, mainly viscosity, rule the ascension of the melt through the hydrofracture and it is a key factor for the emplacement (Lister and Kerr, 1991; Hutton, 1992; Rubin,

1993). The mechanical behavior of magmas is constituted by the progressive increase in viscosity at the end of the magma cooling. It factor controls the velocity and mobility of the magma and affect the nature of the injections and the subsequent structures. The magma viscosity values ranges between $10^2 > 10^{15}$ Pa·s and it strongly depends in the temperature and compositional changes (Hallot *et al* 1996; Vigneresse *et al* 1996 and Petford, 2003). Mafic magmas have low viscosity ~100 P·s (at temperatures of 1100 to 1200ºC and <30% crystals) (Vigneresse *et al*., 1996), thus, the fluid flow rapidly and easily through the crust and it can reach long distances. However, granitic magma is more viscous (10^4 to 10^6 Pa·s) (McBirney and Murase, 1984; Ryan and Blevins, 1987; Scaillet *et al*., 1998; Clemens and Petford, 1999), so they flow more slowly.

In early phases of crystallization, magma behaves as a newtonian fluid (Douglas, 1963; Murase and McBirney, 1973; Kushiro, 1980; Spera *et al*. 1988; Dingwell, 1995), but when the fluid is segregated from the magma source, two or more phases are present, fluid plus crystals, with changing proportions. Later on, the rheology of the magma changes to no-newtonian, it can behave as a pseudoplastic to plastic flux (Wickham, 1987; Fernandez and Castro, 1999). There are two critical points in the magma crystallization, one is the rigid percolation threshold (~55% solid), when the crystalline matrix is formed; the second is the particle locking threshold (~75% solid) in which the mobility of the system is completely blocked (Vigneresse *et al.,* 1996 and Vigneresse and Tikoff, 1999).

c) *Dyke/host rock rheological contrast*

This is an important parameter in the formation of dykes since it is related to the mechanical answer of the crustal materials. The rock strength changes with depth so it does its rheology. In continental crust, rocks are cool and have brittle behavior. They respond elastically and they fracture under high differential stresses. On the contrary, in middle to low crustal levels, the rocks deform ductilely. The differential stresses cannot be kept for long time and deformation is characterized by flow mechanisms. Then, magmatic intrusion tends to continue with brittle or brittle/ductile behavior, depending on the depth of the system. In middle and deep levels, the rock proceeding depends on the deformation rates and the intrusion dynamic (Brisbin, 1996 and Best, 2003). This can cause very complex situations, like the change in the host rock from ductile to brittle during the injection moment (Davidson *et al*., 1994). It will change again to ductile temporally affected by the depth and the heterogeneities in the system, competence contrast and type of host rock (Druguet *et al*., 2008; Druguet and Castaño, 2010).

There is an important question proposed by Rubin (1993) about the minimum host rock/magma viscosity contrast necessary to induce a

brittle rather than a ductile behavior. The proposed answer was calculated for rheological conditions where the magma propagation was by fracture vs. viscous deformation of the host rock. The remarks of this study were that if the host rock/magma viscosity ratio ($\eta r/\eta m$) is larger than 10^{11} to 10^{14}, then the host rock behaves elastically during the intrusion. E.g., basaltic and low-viscosity rhyolitic magmas ($\eta m \leq 10^4$-10^6 Pa·s) will intrude in crustal levels. However, with lower viscosity contrast, (10^6-10^8), magma will form diapirs that produce ductile flow in the host rock. Intermediate cases (10^6–$10^8 \leq \eta r/\eta m \leq 10^{11}$–$10^{14}$) show a mixed behavior with a developing tabular shape. More fractures are produced over ductile deformation when the viscosity increases. Experimental studies in this area (Sumita and Ota, 2011) describe how the fluid propagates as a hybrid diapir in the head and a dyke in the tail. The diapir head fills the fracture and the tip propagates and forms a tail shape at the beginning and end of the diapir to form the dyke.

d) Cooling rate in dykes vs. deformation rates

The intrusion/emplacement process is characterized by the thermal disequilibrium from the magma generation to the crystallization phase. There are two conditions needed to be considered: crystallization time and cooling time (from emplacement until the magmatic body reaches the temperature of the host rock) (Paterson and Tobish, 1992). Another point of view contemplates the initial temperature of the magma, the host rock temperature, the thermal conductivity and the shape and dimensions of the body (Jaeger, 1968). Tabular intrusions can be easily modeled by mathematical analysis based on thermal conductivity (Jaeger 1957, 1968; Turcotte and Schubert, 1982; Furlong *et al.* 1991; Hanson and Glazner, 1995; Yoshinobu *et al.* 1998). Cooling times is determined by the dyke thickness and the thermal contrast (ΔT) is set between the solidus temperature of the magma and the host rock temperature. Thus, the cooling time for a dyke of 1m thick will be less than a year, if the ΔT is not close to 0, and the cooling time will be around 1 Ma (Handy and Streit, 1999; Albertz *et al.* 2005). When these models are applied to middle to lower crust, the cooling can be considered like a fast event in comparison to the usual strain rates (~10-14 s^{-1}) (Pfiffner and Ramsay, 1982)

e) Tectonic controls of the intrusion

The stress state is a key aspect in the intrusion/emplacement process. First intrusion models set a wedge pattern for the injection of the fluid in which the overpressure generates tension forces in the tip of the wedge and then, propagation is possible (Anderson, 1951). This model is the base for paleostress analysis with dykes and it is also used in paleogeographic reconstructions (Ernst *et al.*, 1995).

However, this simplistic view is not suitable for other complex situations in lower crustal levels. Then other proposal considered that the shape and orientation of the structures not always corresponds to the regional stress regime, but they are related with active shear zones during the intrusion (Hutton, 1992). The normal disposition to σ_3 of the dykes does not happen in deformed areas, even if they are active or pre-existent (Delaney *et al*. 1986; Tokarski, 1990). In these cases, the opening directions are oblique to the dyke walls.

f) Role of pre-existing fractures in the host rock

Generally, in the crust dykes can go upward through rocks without pre-existing fractures because they have sufficient energy to produce hydrofractures (Rivalta *et al*., 2014). Pre-existing fractures are not needed to mobilise magma through the crust, but in areas with fracture networks, magma may exploit the preferential paths as areas of weakness. In this setting, dykes always intrude in orientations defined by the regional stress field (Delaney *et al*., 1986; Ziv *et al*., 2000). This situation is observed very frequently (as in the study cases present in this work), but it also depends on the orientation of the pre-existing fractures. Fractures with orientations different to the stress field will not be refilled with magma. However, fractures with preferential orientations will become magma paths (Hooper *et al*., 2011; Valentine and Krogh, 2006).

g) Morphology of the intrusion

The final morphologies of the intrusions and the features presents in the dykes and host rock illustrate the particularities of the emplacement and deformation processes. Thus, we can define dykes as key tools to decipher the development of geological domains. An important marker is the longitude/thickness rate, normally lower than 200. The *en echelon* arrays (overlapping or no overlapping segments) are a very common arrangement (Delaney and Pollards, 1981; Du and Aydin, 1991). The interaction between dyke segments produces a change in the stress field of the tips (Hoek, 1991; Ramsay and Lisle, 2000) and it is the responsible of the formation of horns and branching structures.

Discontinuous segments can be formed in dilatation fractures, between riedel-shears (Peacock and Sanderson, 1992) or P-shears (Tikoff and Teyssier, 1992). These types of dykes use to have high aspect ratio and they have a high angle with respect σ_1, then during progressive deformation the structures tend to extends as boudins (Bons and Druguet, 2007). Another frequent feature is its continuous but not tabular geometry. In fact, it has been described subtabular shapes and zigzagged and stepped configurations (Beach, 1980; Hoek, 1991; Druguet *et al*., 2008; Castaño and Druguet, 2008; Martinez-Poza *et al*., 2014). In syn-tectonic dykes usually there is an

anisotropic fabric with a preferential orientation of the minerals originated in the progressive magma crystallization during the emplacement. This fabric is called magmatic fabric; it reflects the changes in viscosity during the syn-tectonic crystallization (Hutton, 1988; Paterson *et al*., 1989).

Primary structures originated in dykes during the intrusion can be modified afterwards due to post-emplacement deformation, with resultant structures as folds, boudins, internal foliation and refractions. In more complex cases as internal foliations, shear zones and mullions, the situation is more complicated. In these cases, dykes have less competence maybe because they are still molten during deformation, thus dykes localize deformation. This situation can occur during and after the emplacement and in both cases, the dyke acts as an incompetent body.

CHAPTER 2

METHODOLOGY

2.1. FIELD STUDIES

2.1.1. Selection of reference areas for the field case studies (dos frágil…)

The aim of this project from the beginning has been the study of mafic dyke intrusions in different crustal depths. For this reason, the following dyke swarms were selected, since they display very distinct range of crustal injection, from the upper to middle crust and also exhibit particular deformation processes.

The case study is a good scientific tool for qualitative studies. Later, all the data acquired in the field works will be analysed in detail, so a quantitative approach can be made. Linking all the data, we can present an interpretation of the geological history of the area.

We selected two areas were we could find a dyke intrusion into a brittle host rock; this is the Aiguablava dyke swarm (Catalan coastal range) and the SE of Sardinia dyke swarm (Sardinia, Italy). Both swarms have very similar characteristics: brittle host rock, granite, granodiorite or leucogranite; mafic injections disposed in sub-vertical dyke-like structures; age range of emplacement; age of host rock; geological setting; injection depth; +

In the other hand, we selected other two field areas with a deeper intrusion range. One is the Independence dyke swarm (California, USA) and the other area is a group of dyke intrusions in several inliers of the Anti-Atlas (Morocco). They display localization of shear zones in the dykes margins, although this is more outstanding in the IDS area.

Each of the four localities will be described in detail in the next chapter dedicated exclusively to the case studies. In every part, the dyke swarms will be fully characterized. Its geological setting, external description, petrology, structural analysis, stress analysis and in some cases also geochronology will be explained. All the areas were selected due to its good outcrop conditions. The majority of the areas expose 3-D sections of the dykes so a full analysis can be achieved.

Dykes provide a good indicator of the tectonic setting and different deformation processes that an area could have suffered. This is why we have chosen areas that may not seem similar in the first look, but later after an in detail study, they could exhibit general trends applicable to other cases in future research. The study cases can help us to construct a catalogue of dyke features related with its own geological context. This data will be very useful to enlarge the existing work in large dyke swarms.

2.1.2. Field data methodology and analysis

During the field works in the four study areas, an in detail acquisition of structural parameters was carried out. We tried to obtain the maximum number of structural data thus a good later analysis could be carried out.

We divided the work in two parts; the first one was mainly data acquisition task in the field. This amount of data implies a later analysis in the office to interpret the measurements. The second part implied laboratory work. It was composed of analytical techniques that help us to characterize rock composition and age.

2.1.2.1. Field and office analysis

Here I present the techniques used before, during and after the field work is completed. Several office analyses can be made after the data is obtained in the field:

A) Bibliography

Previously to the field work, some preparation should be done in order to obtain the bigger and better quantity of data in the field. For this purpose, the first task should be read all the known bibliography about the study area. This will help us to situate the geological setting of the area and find the areas that need more in detail research in order to be understood. We can focus in certain areas and save more time for the following steps.

B) In detail cartography

After the bibliographical work is done, there is big probability that a published geological map of the study area is available. Using this information together with aerial images, field data (foliations, dyke and host rock measurements), field sketches, a good cartography can be elaborated. These maps are built using Canvas X GIS software.
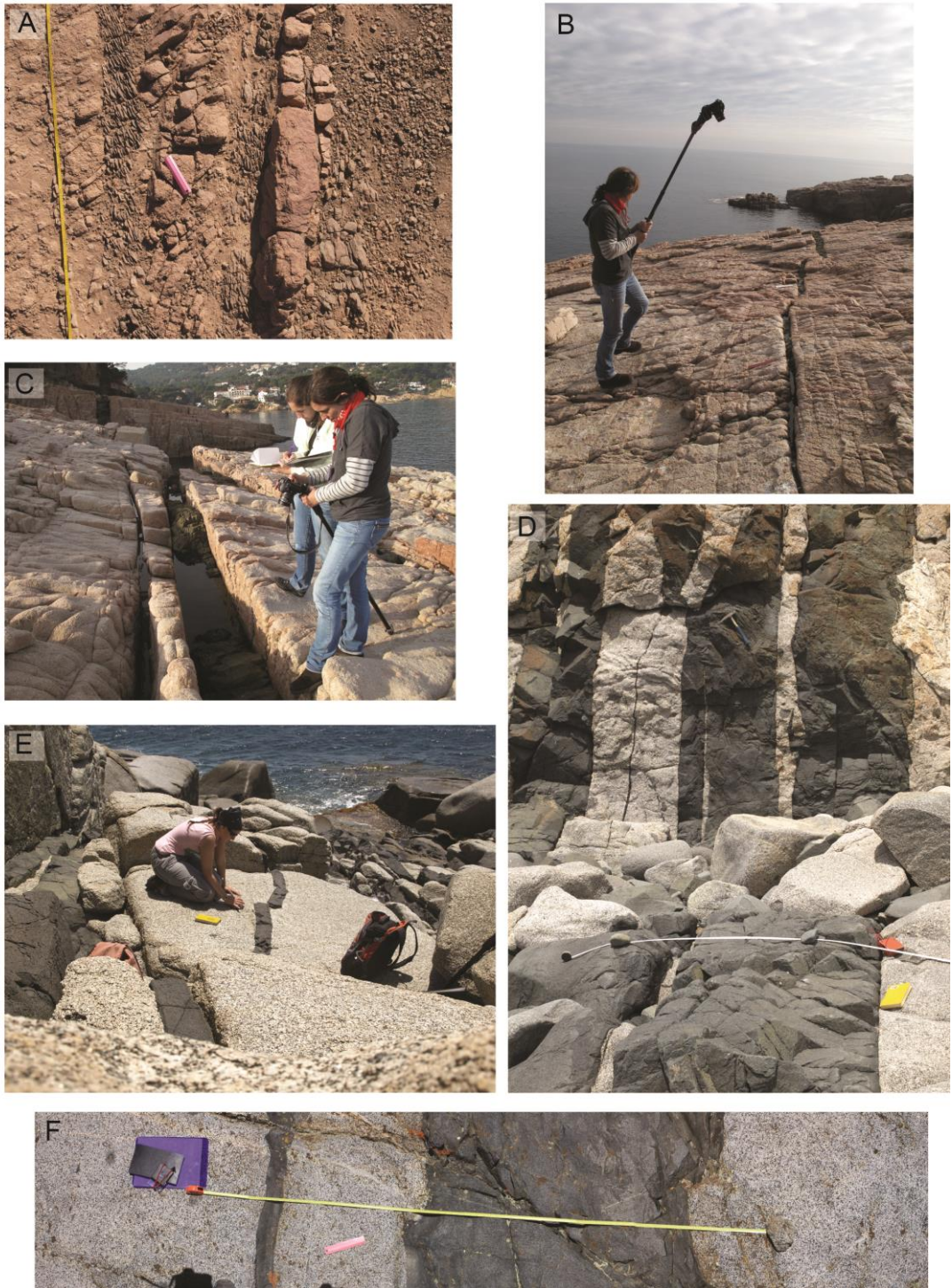
Fig. 2. 1. A) Example of setting to do stitched photograps, B) and C) Photo acquisition with the monopod, E) Structural measurements acquisition, D) and F) Vertical and horizontal stitch setting.

C) Photo acquisition and analysis

During the field work, one of the most important labours is photography. Not only to situate the field stations and record the local geology, but also because it is very important for the later study in the office. There should be taken photographs of every remarkable feature found in the field, in our case, in the dykes. The most important pictures should be from the dyke-host rock margin and dyke structures. Together with series of stitched photographs taken with a monopod (situated normal to the surface of the outcrop and at ~1-2 m high), which would help us to record the extension of the dyke we want to study in detail.

In the field we used reflex digital cameras (Canon 500D) to get the better quality possible. Before we take a photograph, we orientate the framework with a ruler that marks the North, so we can orientate the photograph when we analyse it. For the stitched photographs we usually clean the horizontal surface first (with scrub brushes), and later we mark the North with a ruler. Another important step, since usually there are taken several photographs, is to put a measuring tape in the extension of the dyke, so later it is easy to reconstruct.

Later, using processing software like Canon PhotoStitch 3.1, Adobe Photoshop and Adobe Illustrator, the images can be stitched and interpreted.

D) Structural measurements

Other essential duty is the systematic taking of structural data. In our case, we measure: dyke orientation (dip and trend), joint orientation (dip and trend) in the host rock and inside the dyke mass. Moreover, we measure apparent dilation directions when possible in vertical and in horizontal sections. Also we measure stepped structures so later we can applied Bussell's method (1989). In some areas we measured as well foliations, aplite veins, mylonite zones and we took dyke widths in several points to have some control in the subsequent analysis.

Later on, the structural measurements are plotted using stereographical projection softwares like Stereonet (Allmendinguer, 2002).

E) Rock sampling

Every case area was sampled so a good petrological and microstructural characterization could be made. In the IDS zone we took more quantity of rock so later geochemical and geochronological analysis could be carried out.

Few samples were taken oriented, then when the thin sections were studied, the microstructures could be located precisely.

2.1.2.2. Laboratory analysis

After the sampling of rocks in the field, different laboratory analyses were carried out:

A) Optical microscope analysis

   Thin sections were obtained from the rock samples. Later, the samples from Aiguablava, Anti-Atlas and Sardinia were analyzed under an optical microscope at the UAB MIET lab. While the samples from the IDS case were studied at UNC (University of North Carolina at Chapel Hill) during my research stay, also using an optical microscope.

   Microstructures, textures and mineral assemblage were obtained from the thin section examination.

B) SEM analysis

   The SEM analysis was carried out only in some of the more characteristic IDS samples. For this procedure was used the scanning-electron microscope (SEM backscattered images) Tescan SEM with semi-quantitative EDS capabilities, in the UNC laboratory. I used the instrument to look in detail into some outstanding microstructures and also to look for zircons in the sample, so it confirms a geochronological analysis could be performed.

C) Major elements analysis

   The major elements analysis was carried out in the different facilities that have the UNC Geology Department. This analysis required different steps. It started with the sample preparation and rock-crushing until they had a grain size of 1/16mm.

   The following step was the evaluation of the LOI, for this, the resultant powder was weighted (as well as the crucible), then dried in an oven at ~120º C for ~1h, so the humidity was extracted and measured. The final step was a second oven, in this case in a fumace at ~1000ºC (~1h). Here we oxidized the F^{+2} to F^{+3} and eliminated the structural H_2O.

   Afterwards, the dried powder was treated in the Katanax K1 automatic fluxer to create the disks that the X-Ray Fluorescence spectrometer (Rigaku Supermini wavelength-dispersive XRF spectrometer) would need to measure the major elements.

D) Geochronology

   LA-ICP-MS implies a lasing through the surface of the mineral (zircon in our case) and the resultant aerosols are measured in a mass

spectometer. This technique was first intruduced in the U-Pb geochronology in the 90s (Feng *et al*., 1993; Fryer *et al*., 1993; Hirata and Nesbitt, 1995). Later it has been the most used method for U-Pb systems due to its good results and high resolution. The LA-ICP-MS technique includes two steps, firstly the laser ablation procedure and secondly, the ICP-MS. The first system is composed by a short wavelength laser (<266 nm). This wavelength is more efficient for the
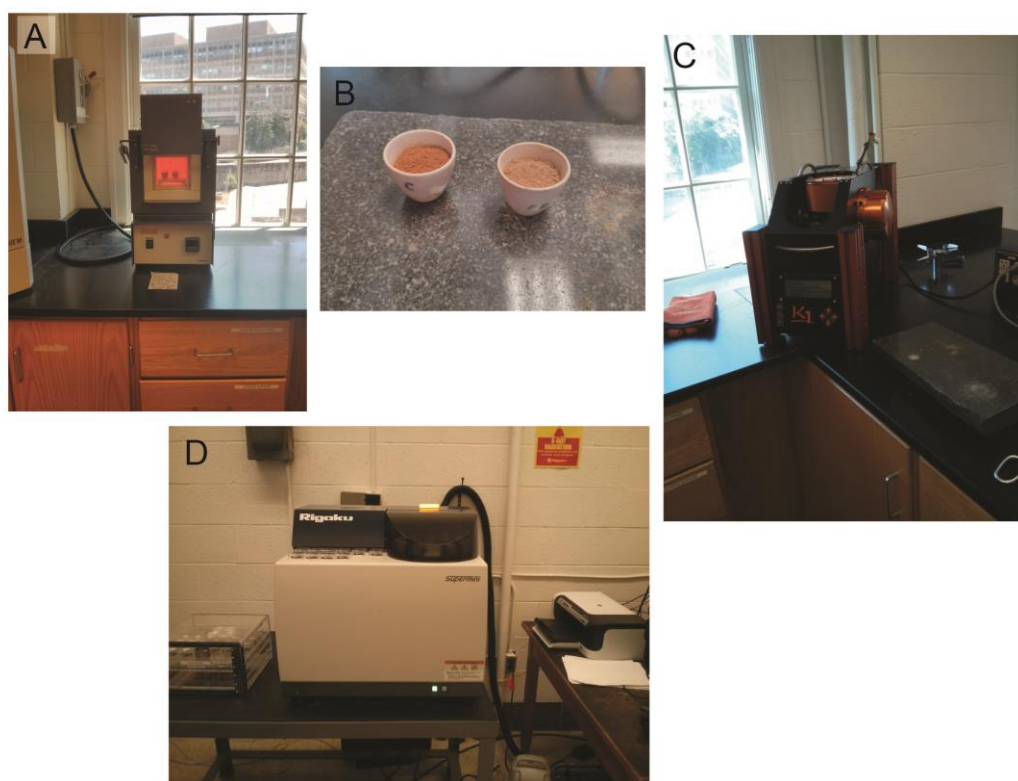
Fig. 2. 2. A) Fumace oven, B) Two samples in cruciable after the fumace at ~1000ºC, notice the red colours of oxidation, C) Katanax K1 automatic fluxer and D) Rigaku Supermini wavelength-dispersive XRF spectrometer.

procedure and imply less heating of the sample and isotopic fractionation (Guillong *et al*., 2003; Günter and Heinrich, 1999; Günter *et al*., 1997). The sample is processed in the cell with the laser and the resultant particles are vacuum to the plasma torch. The gases can be studied depending on the instrument sensitivity (Guillong and Heinrich, 2007; Günter and Heinrich, 1999; Horn and Günter, 2003). The measurements and shape of the sample cell can influence the interaction of the plasma and the movilized particles (Cottle *et al*., 2009; Kosler and Sylvester, 2003; Muller *et al*., 2009; Pisonero *et al*., 2006). The type of collector and magnetic sensors imply the uncertainty vaules in the measurement, mainly produced during the ablation or in the transport and ionization stage. The U and Pb fractionation depend on the depth of the spot (Hergenroder, 2006; Horn *et al*., 2000; Kosler *et al*., 2005; Paton *et al*., 2010), the aerosol production and the particle size distribution (Guillong *et al*., 2003; Günter and Heinrich, 1999; Günter *et al*., 1997). Moreover, the differences in the matrix material can biases the U/Pb fractionation

(Black *et al.*, 2004; Kosler *et al.*, 2005). The precision of single measurements with this type of technique is delimited by a standard
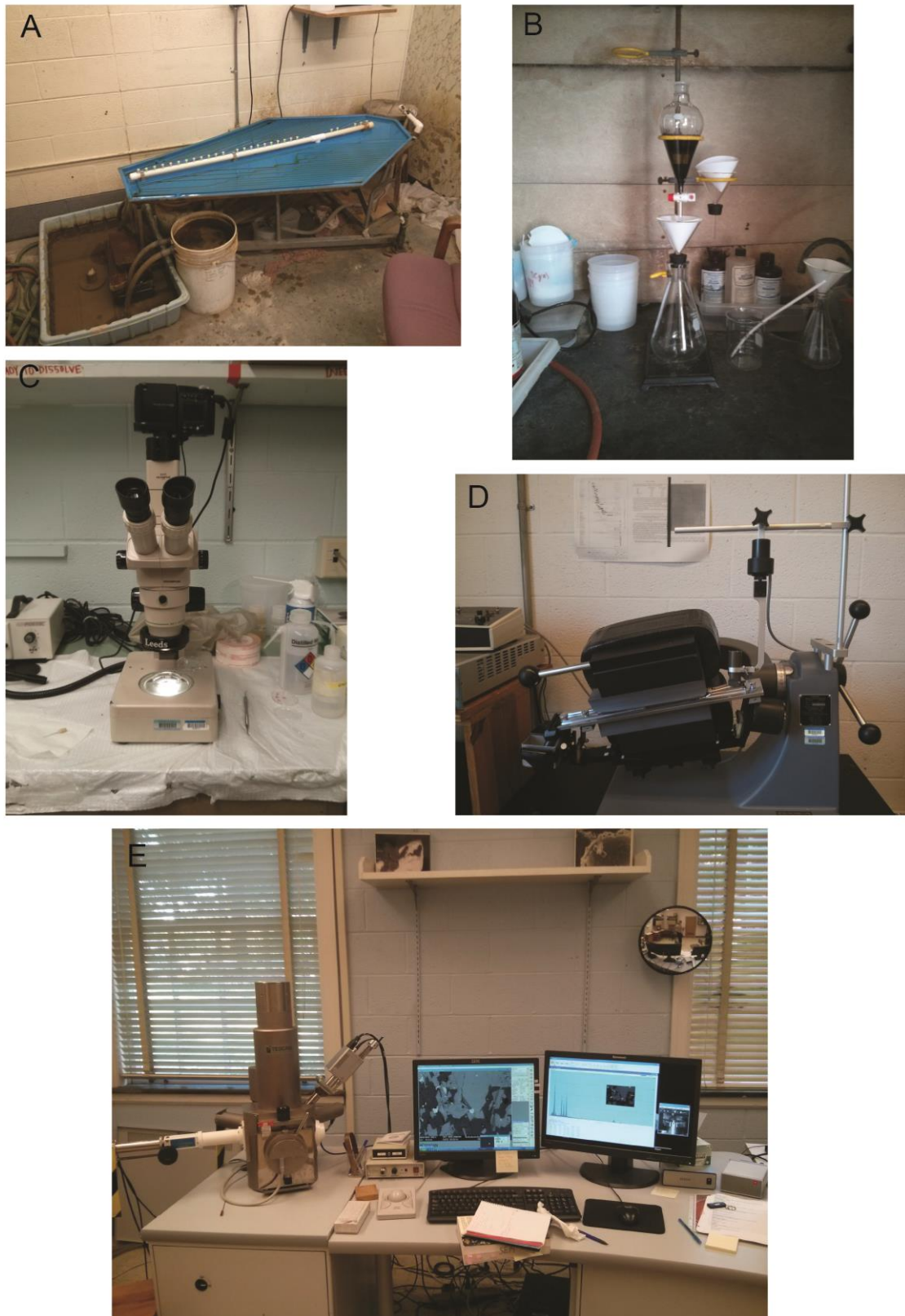
Fig. 2. 3. A) Water separation shaking table table, B) Heavy liquids separation setting in a security fume hood, C) Magnifying glass in the picking laboratory, D) Frantz magnetic separator and E) Tescan SEM.

variability of 2% (Horstwood, 2008; Sylvester, 2008). Latelly, this geochronological procedure has been widely used in many laboratories. Then, many new software has the data interpretation and uncertainty detection as their main focus (Chang *et al*., 2006; Gehrels *et al*., 2008; Horstwood, 2008; Paton *et al*., 2011; Petrus and Kamber, 2012; Sylvester, 2008; van Achterbergh *et al*., 2001). The analysis and data interpretation has been tried to be standarized as a new path in this geochronological method, so a higher precission could be achieved with the LA-ICP-MS procedure (Schoene, 2013).

The selected samples selected for the geochronological study were processes in the separation, picking and heavy liquids laboratories of the UNC. The final objective was to separate zircons and titanites from the sampled rock. In order to get them, we applied several separation steps.

First, in the crushing lab, we reached a size of 200-300 μm. Later we proceeded with the water separation shaking table and collected the heavy and medium fraction of the samples. Afterwards, we continued with the heavy liquids procedure. We used methylene iodine (ρ = 3.32 g/cm^3) as heavy liquid. Then, we mounted the system needed to separate the heavy minerals from the lighter ones and follow the waiting times. The separated part was dried out and passed through a Frantz magnetic separator, so only the non-magnetic minerals would remain. The final separation steps was handpicking of the zircons and titanites using a magnifying glass. Later the minerals were mounted in epoxy and the sections were polished and mapped to have a good guide for the later analysis. Finally, the samples were sent to UC Santa Barbara geochronology laboratory to be analysed with the LA-ICP-MS technique (LASS, laser-ablation split-stream inductively coupled 6 plasma mass spectrometer). The final results were treated with the Iolite and Isoplot software (Paton *et al*., 2011 and Ludwing, 2008, respectivelly).

2.2. ANALOGUE MODELLING

The second methodology applied to this project has been the performance of analogue modelling in order to reproduce the situations found in the nature.

It supposes an experimental approach that contributes to the study of dyke injection processes and later effects of deformation phases. This technique pretends to do a semi-quantitative analysis of the structures produced by the experimental models. The analogue models are not systematized in our case, only the deformation rate is constant in all the experiments. However, this is not a limitation for the contribution that this experimental works can do for the research.

All the experiments were performed in the Analogue Modelling laboratory of the MIET Research Group, at the Autonomous University of Barcelona.

2.2.1. Deformation machine

The tests were conducted in the MIET lab with the collaboration of Lina M. Castaño. The Machine used for the deformation corresponds to a type of kinematic press machine for experimental deformation ―BCN-Stage" build in the 90s (Carreras and Ortuño, 1990). The apparatus is composed by a deformation cell, arranged in a parallelogram shape, with the borders sets parallel to the X and Y axis. Every pair of walls moves along an axis connected with an electric engine (both X and Y respectively). The machine is controlled by the LabView 3.1 software. It lets set the deformation velocity and the non coaxiality (Means *et al*., 1989), from pure shear to simple shear. The setting also has a hot air fan and temperature probes to control the temperature in the room. In the upper part, the deformation cell has a crystal top, to protect the experiment and set semi confined conditions. It is also useful to take photographs of the experiment during its duration. The photographic system is located vertically at ~1.5m of the top of the apparatus and it has a systematic photo capture system every 10 minutes.

2.2.2. Analogue materials

The materials used for the experiments are basically plasticine and couverture chocolate. The material properties are already studied in detail as analogue materials. In addition, they are cheap and easy use for constructing the models.

The plasticine is usually used as analogue material for middle to lower crust (McClay, 1976; Zulauf and Zulauf, 2004; Druguet and Carreras, 2006; Druguet and Castaño, 2010). It behaves as a viscoelastic non-Newtonian fluid (Turcotte and Schubert, 1982; Ranalli, 1995). We used it as the host rock of our intrusive bodies, simulating the conditions of a portion of middle-upper crust. The brand of this plasticine is Oclu-plast S.L. and it behaves as an elastoviscous non-lineal material (Gómez-Rivas, 2008) with an effective viscosity ~10^7 Pa·s.

The coverture chocolate simulates cooling magma (Druguet and Carreras, 2006), depending the temperature we reach in the experiment, since viscosity is temperature dependent (as in the magmatic processes). Molten chocolate (36-40ºC) behaves as Bingham fluid. When the chocolate crystallise, it constitute a crystalline solid with greater stiffness than the plasticine, so the rheological contrast is coherent with the observed in the nature between mafic magma and host rock. Therefore, the incompetent mode of the couverture opposite to the plasticine let develop very similar structures as found in the field. We used coverture chocolate from Nestlé S.A. with a viscosity ranging from <100 Pa·s and <107 Pa·s at the experimental temperatures of 30-26 ºC.
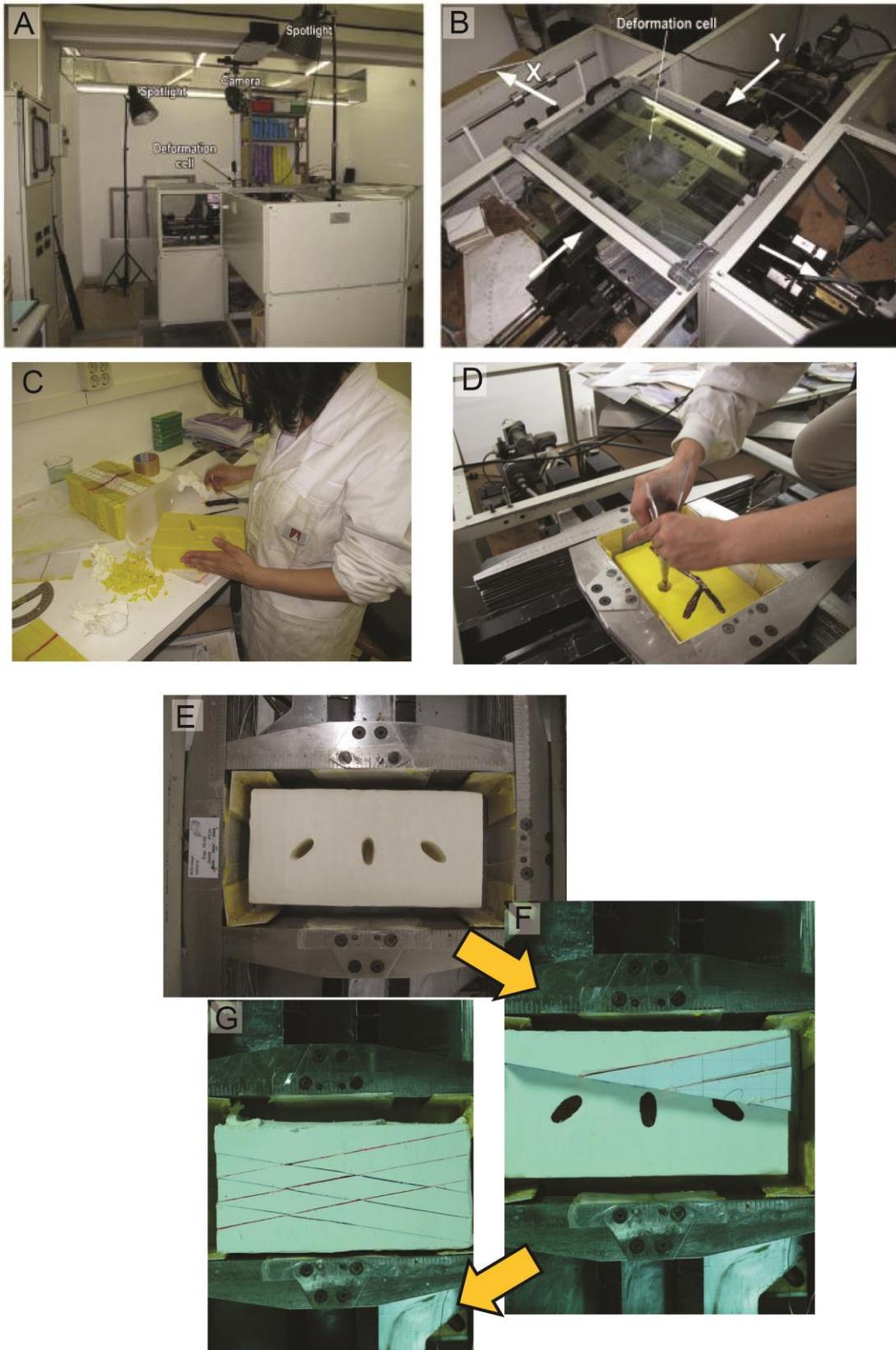
Fig. 2. 4. A) BCN-Stage apparatus, B) BCN-Stage deformation cell disposition, C) and D) Model preparation, E), F) and G) Model setup (Exp. 16.02) in the deformation cell.

2.2.3. Experimental setting

The deformation conditions for all the experiments were pure shear with a constant strain rate of 2.5×10^{-5} s^{-1}. The compression occurs along the Z axis of the apparatus and the extension occurs along the Z axis. The bulk shortening is not constant for each model and it depends on the duration of the tests, but it ranges between 3 to 7.5 hours. Therefore, taken into account the measurements of the model blocks (30x15x10 cm), which we can consider rather constant, the shortening along the Z axis supposes around 30-50%.

All the extension of the analogue modelling test was recorded every 10 minutes by the photo acquisition system. Consequently, a film with the evolution of the model can be made afterwards, and also every step of the process can be analysed in detail.

The models try to be an approximation to the nature, mainly in the rheological and kinematical approach. However, it is not possible to reproduce the geometrical and dimensional characteristics in the laboratory. We build a homogeneous block of plasticine, where later we will drill holes with different shapes (depending on the model) that will be filled with chocolate. Likewise, we will create fractures recreating joints in the host rock.
The analogue simulation supposes a simplification of the real world that tries to help us to understand the processes implied.

CHAPTER 3

CASE STUDIES

3.1. AIGUABLAVA: PASSIVE DYKE EMPLACEMENT INTO PREVIOUSLY FRACTURED BASEMENT DURING POST-OROGENIC REGIONAL EXTENSION OF THE MID-UPPER CRUST.

3.1.1. Introduction

Magmatic dykes provide data about sources and location of magma reservoirs, magma transport (e.g. Bons *et al*., 2001; Brown, 2010; Clemens and Mawer, 1992; Vanderhaeghe, 1999), intrusion and emplacement mechanisms (e.g. Brown and Solar, 1999; Cadman *et al*., 1990; Hutton, 1988) and are important kinematic markers in both, deformed mid- and lower crustal domains (e.g. Druguet *et al*., 2008; Hanmer and Passchier, 1991) and in the upper crust (e.g. Airoldi *et al*., 2011; Babiker and Gudmundsson, 2004; Cadman *et al*., 1990; Glazner *et al*., 1999; Paquet *et al*., 2007). Furthermore, dyke swarms, particularly mafic ones, are essential for the interpretation of geodynamic processes and paleogeographic reconstruction of continents (e.g., using palaeomagnetic and geochronological studies; Ernst *et al*., 1995; Halls, 1982; Hanski *et al*., 2006; Srivastava, 2011), and in determining magmatic flow and regional paleostress conditions (Anderson, 1951; Delaney *et al*., 1986; Hoek, 1991; Hou, 2012; Neff, 1973; Ode, 1957; Platten, 2000; Pollard, 1973; Rubin, 1995).

Lamprophyres are among this kind of intrusive rocks which typically form dyke swarms. They are generally grouped as porphyritic rocks with ferromagnesian phenocrysts (biotite, amphibole or pyroxene) and usually contain feldspar, which is confined to the groundmass (Le Bas and Streckeisen, 1991). Although lamprophyre and lamprophyric rocks have no petrogenetic significance (Mitchell, 1994), their singular nature has generated wide interest in geological research during the last three decades. This is especially because of their importance in deep-mantle studies and their supposed association with kimberlites and lamproites (Woolley *et al*., 1996).

This paper examines the Aiguablava lamprophyric dyke swarm in the Catalan Coastal batholith of NE Iberia from a structural point of view. The high quality exposures and the variety and clarity of structures bring evidence for intrusion of the dyke swarm into a pervasive fracture network in the host rocks, and this stands out as the main emplacement model recognized since the last decade (Carreras and Gimeno, 2000; Enrique, 2009; Gimeno, 2002; Passchier, 2007). Indeed, the area has become a classic locality to observe the cross-cutting relationships between different generations of dykes and joint sets (Druguet et al., 2013). However, except for preliminary work by Martínez-Poza *et al*. (2012), no systematic and exhaustive structural analysis of the dykes has been performed. In contrast, several petrological and geochronological studies have been carried out (Enrique, 2009; Enrique *et al*., 2012; Esteve *et al*., 2014; San Miguel Arribas, 1952; San Miguel de la Cámara, 1936; Solé *et al*., 2003; Ubide, 2013; Ubide *et al*., 2008, 2010).

Self-propagating dyke-fractures (Lister and Kerr, 1991; Spence and Turcotte, 1985) and dyke intrusion into previously fractured rocks became established in the 1980's as two end-member mechanisms for dyke transport and emplacement. The fundamentals of the second of these mechanisms were established by Delaney *et al.* (1986) and Pollard (1987). They gave some criteria for the identification of dykes intruded along pre-existing fractures and formulated the condition for fracture re-opening. Accordingly, for dyke emplacement, magmatic pressure (P_m) must equal or exceed the tectonic normal stress (σ_n) acting on the fracture surface.

$$P_m \geq \sigma_n \quad (1)$$

Later works by Baer *et al.* (1994) and Jolly and Sanderson (1995) provided feasible methods to measure the relative magmatic pressure and state of stress during dyke emplacement, using dyke orientation data. The relationship between dyke and vein emplacement and fracture networks has been broadly investigated in subsequent studies (André *et al.*, 2001; Gudmundsson *et al.*, 2002; Hoek, 1991; Le Gall *et al.*, 2005; Mazzarini and Isola, 2007; Tokarski, 1990; Ziv *et al.*, 2000).

The objectives of this research are to characterize the three dimensional relationships between the pre-existing jointing and the lamprophyric dykes and to determine the geo-mechanical conditions associated with the intrusion of the dyke swarm. The following methodologies have been applied to achieve the above objectives: (i) statistical measurement of fracture networks using a circular scanline method on aerial orthophotographs, (ii) characterization of dyke intrusion patterns at different scales and differently oriented exposure surfaces, (iii) estimation of the net dilation direction for the dyke swarm applying a stereographic analytical technique, (iv) 3-D analysis of the stress state during dyke emplacement by the combined use of stereographic projections and Mohr circles, and (v) estimation of the amount of regional extension from scanlines on photographs.

3.1.2. Geological and petrological settings

The studied lamprophyre dyke swarm in the Aiguablava pluton (Costa Brava) is part of the Catalan Coastal Ranges batholith in NE Spain (Fig. 3.1). The Catalan Coastal Ranges batholith, emplaced into late Neoproterozoic and Paleozoic rocks at intermediate and shallow crustal levels, is composed of several magmatic intrusions, with compositions varying from granodiorite to monzogranite to leucogranite. The estimated age of the batholith is Lower Permian (Enrique, 1990), corresponding to the late- to post-Variscan magmatism that is also represented by other granitoid plutons in the basement of the Pyrenees.

The Aiguablava pluton was dated as ≈288 Ma (Ferrés, 1998; Losantos *et al.*, 2000). The Aiguablava pluton is made of a pinkish medium to fine-grained biotite-leucogranite, mainly composed of quartz, K-feldspar and sodic plagioclase, with minor biotite and garnet as accessory minerals (Enrique, 1990; Gimeno, 2002). A widespread network of aplite–pegmatite veins is associated
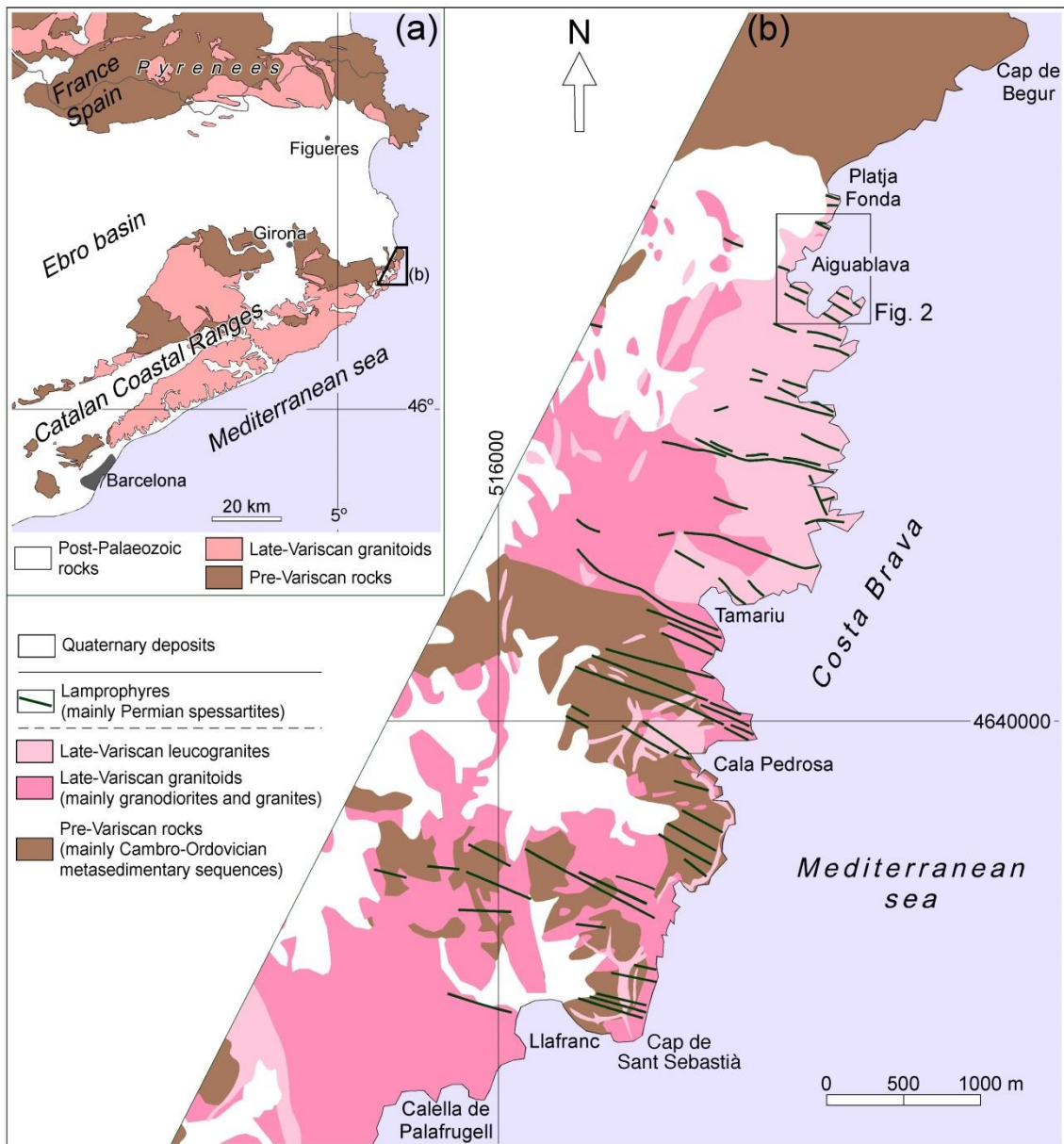
Fig. 3. 1. Geological setting of the study area. (a) Map of the Variscan of the Eastern Pyrenes and northern Catalan Coastal Ranges where the Costa Brava batholith is located. (b) Geological map of NE Costa Brava batholith where the main lamprophyric dykes are sketched. The mean trend of the dyke swarm in the whole area is N113°. The square indicates the study area in Aiguablava.

with this intrusive body. The presence of miarolitic cavities suggests that magma crystallization occurred in the shallowest parts of the magmatic system. Towards the north, this leucogranite intrudes into K-feldspar megacryst-bearing granodiorite and into phyllites of the Begur massif, where these rocks are also crosscut by the lamprophyric dykes (Enrique, 2009).

The Aiguablava lamprophyric dykes can be grouped in at least three distinct petrographical types (Enrique, 2009):

(1) An extensive system of ≈N110°–N115° trending sub-vertical dykes (Figs. 3.1 and 3.2) of dark greenish-gray color and thickness varying between a few centimeters and a few meters (Figs. 3.3 and 3.4). They have been classically

considered as having a predominant calc-alkaline spessartitic composition (Enrique, 2009; San Miguel Arribas, 1952; San Miguel de la Cámara, 1936), although a more recent study by Ubide *et al.* (2010) places these rocks between the sub-alkaline and alkaline fields. Whole-rock K–Ar dating indicates a 253 ± 5 Ma, Upper Permian age (Losantos *et al.*, 2000). They are aphanitic to fine-grained, containing partly altered clinopyroxene, olivine and biotite phenocrysts. Calcite and chlorite are common in the groundmass together with plagioclase and amphibole. Chilled margins of aphanitic texture devoid of phenocrysts and angular xenoliths of the leucogranitic host rock are common in dm- to m-thick dykes. The local presence of vesicular texture at the dyke margins suggests dyke emplacement at a shallow crustal level (Gimeno, 2002). In some cases the thickest dykes display a rather complex internal structure consisting of either a wall-parallel textural banding or low-angle mutual cross-cuts. These features could be related to a late multi-stage dyke assembly in the evolution from the volumetrically most abundant spessartitic dykes to the less abundant bostonitic ones which are described here below.

(2) A less voluminous group of sub-vertical dykes of alkaline affinity is also recognized in the study area (bostonites; see Enrique, 2009). These are easily distinguishable from the spessartite dykes by their characteristic chocolate-brown color. Although bostonite dykes have not been dated yet, field cross-cutting relationships indicate that they postdate the spessartitic dykes (Fig.3. 4a). Locally, they form *composite dykes* combined with the spessartite ones, as observed in the Punta des Mut area (Enrique *et al.*, 2012).

(3) Apart fromthe above two dyke types (spessartite and bostonite), a few sub-horizontal ultrabasic camptonite dykes of alkaline affinity are also recorded (Esteve *et al.*, 2014; San Miguel Arribas, 1952; San Miguel de la Cámara, 1936). These were dated at ≈76 Ma (Upper Cretaceous age) by the amphibole 40Ar/39Ar method (Solé *et al.*, 2003), and are thus unrelated in time and geodynamic context to the earlier Permian lamprophyres. In the study area they are represented in Sa Planassa zone by a single ca. 2.5mthick sub-horizontal sheeted intrusion (Fig. 3.2). They have an across dyke zoned porphyritic texture characterized by the accumulation of phenocrysts (clinopyroxene and amphibole) at the base of the dykes, which is inferred to be on account of gravitational fractionation (Gimeno, 2002; Ubide *et al.*, 2008).

On a wider regional context, mid- to late-Permian mafic calcalkaline to alkaline magmatism is present elsewhere in the Pyrenees, the Iberian Range, the Spanish Central System, the Cantabrian Chain, the French Massif Central (Perini *et al.*, 2004) and in the Corso-Sardo block (Ronca *et al.*, 1999). However, there is a lack of general agreement on the geodynamic framework of these intrusions, which have mostly been interpreted from petrogenetic and geochemical approaches. The intrusion of the latest camptonitic dykes has been interpreted in the context of the alkaline magmatism associated to the Mesozoic regional extensional event which marked the evolution on the margins between the Iberian and European plates. This process was the result of the Pangea breakup and the subsequent opening of the North Atlantic ocean. Other examples of this alkaline magmatic activity are found in other localities of the

Catalan Coastal Ranges, in the Corbières massif (NE of the Pyrenees) and in the Western Pyrenees (Solé *et al*., 2003; Ubide, 2013).

As stated in Section 1, there is a widespread network of joints that was presumably developed during decompression and cooling of the plutonic host rocks during the Lower Permian (Enrique, 2009), and the emplacement of all three described lamprophyre groups is apparently controlled by some of these joints (Gimeno, 2002; Martínez-Poza *et al*., 2012; Passchier, 2007). Furthermore, dykes are much more abundant in the leucogranite host rocks, where the fracture network is also more intensely developed. The lamprophyre dyke swarm also extends along a larger area towards the south (Fig. 3.1). Our work is mainly focussed on the more widespread first (spessartite) and second (bostonite) generations of sub-vertical lamprophyre dykes.

3.1.3. General pattern of subvertical joints and dykes

We performed a structural analysis on six selected areas around the Aiguablava bay where the lamprophyre dykes are well exposed (Fig. 3.2a). From NW to SE, these areas are Platja de N'Astàsia, Punta des Pi, W Aiguablava, E Aiguablava, Sa Planassa and Punta des Mut. In order to obtain a first characterization of the patterns of both the joint systems and the dyke swarms at the map scale, a trend frequency analysis has been performed on the four areas conformed by sub-horizontal outcrops (Platja de N'Astàsia, Punta des Pi, Sa Planassa and Punta des Mut; Figs. 3.2 and 3.3). These zones range in dimension from 7000 to 10,000 m2. We used the circular scanline method of Mauldon *et al*. (2001), a widely used approach in statistical measurement of fracture networks. The circular scanline method is independent of trace orientation and thus it is not subject to directional biases as in the straight scanline method. The cartographic base used for this analysis consists of aerial orthophotographs at scale 1:5000 from ICC (http://www.icc.cat/vissir3) that have been digitally enlarged to optimize visualization of the dyke and join systems (Fig. 3.2b). On each of the four areas shown in Figs. 3.2 and 3.3, we measured the orientation of joint and dyke traces intersected by overlapping triplets of concentric circles of radii 1, 2 and 5 m, in a similar manner as suggested and performed by Umili *et al*. (2013). The public domain software ImageJ (Abràmoff *et al*., 2004) was used to measure fracture trace orientations, and the results from the four areas were integrated and evaluated in conjunction.

The sub-vertical fracture network consists of multiple joint sets and a main trend for dyke arrangement (Figs. 3.2c, and d and 3.3). The subvertical joint pattern consists on two systematic major orthogonal sets at N23°, N113° and secondary sets at ≈N0° and ≈N90°, among others (Fig. 3.2c). Joints of these principal sets have straight traces with lengths varying from a few meters to a few hundreds of meters and spacing below 2m for most arrays (Fig. 3.3). Intersections between joints of different sets are commonly of the X- and T-types (Pollard and Aydin, 1988). The sub-vertical dykes have a mean N113° trend, thus corresponding to the trend of one of the principal fracture sets. Since the technique implies repeated measurement on individual joint or dyke traces, the results represent a statistical estimation of frequency of fracture trends per
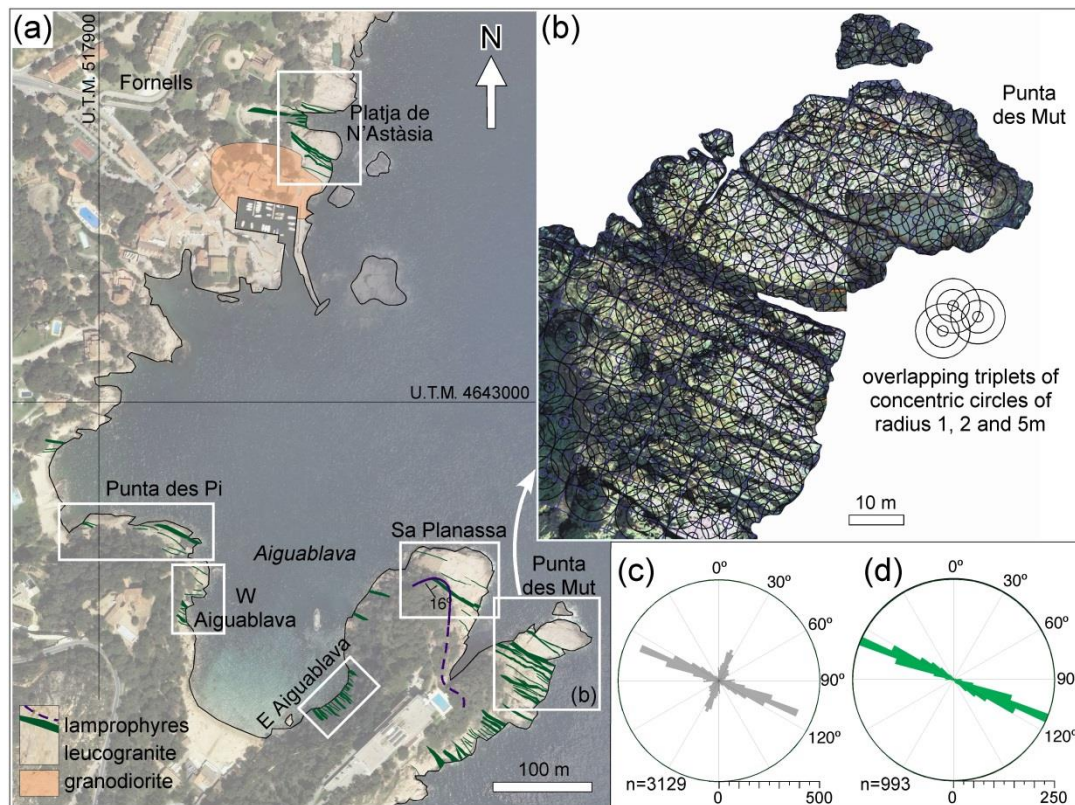
Fig. 3. 2. (a) Aerial orthophotograph of the study area in the surroundings of Aiguablava (digital orthophotograph fromhttp://www.icc.cat/vissir3/; ©Institut Cartogràfic de Catalunya). The white boxes represent the areaswhere structural analyses have been performed. **(b)** Aerial orthophotograph of the Punta desMut area (digital orthophotograph is ©Institut Cartogràfic de Catalunya) showing the grid of overlapping circles used to statisticallymeasure the strikes of joints and dykes, applying the circular scanlinemethod of Mauldon *et al.* (2001). The same grid and techniquewere also performed on Platja de N'Astàsia, Punta des Pi and Sa Planassa areas. **(c)** and **(d)** Rose diagrams of fracture trends measured from the aerial orthophotograph (c: dyke walls and joints; d: dyke walls only).
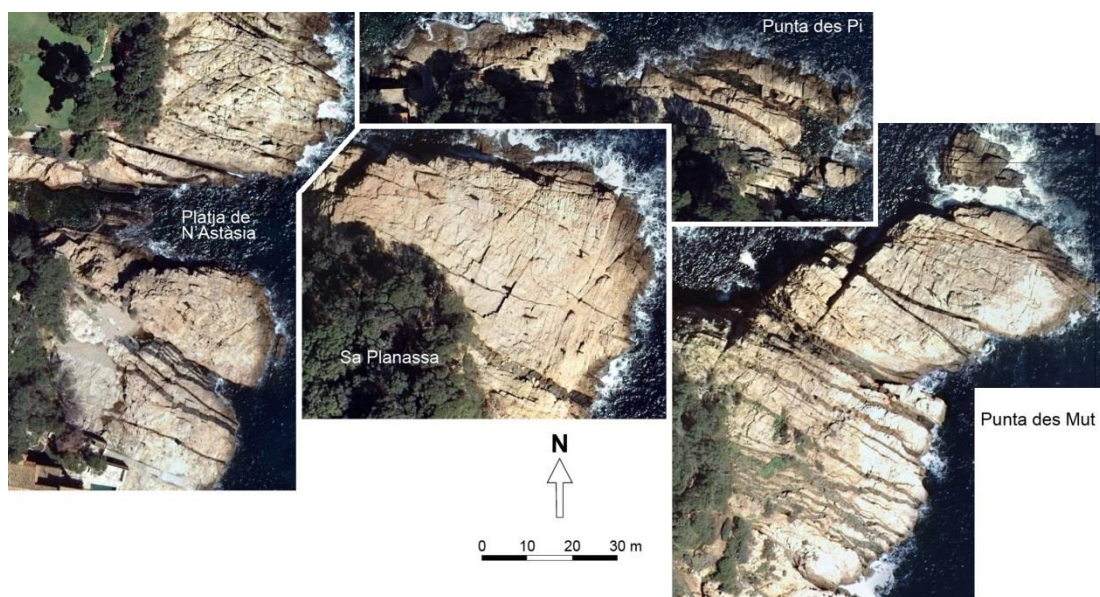
Fig. 3. 3. Aerial orthophotographs of the four sub-horizontal areas covered for the trend frequency analysis of joint and dyke systems at the map scale. Digital orthophotograph is ©Institut Cartogràfic de Catalunya, http://www.icc.cat/vissir3/.

45

surface. In the case of the dykes, the relative deviation in orientation from the mean N113° trend is consistent with the slight zigzagging of single dykes displayed on the aerial photographs (Fig. 3.3). The dyke frequency analysis shows that a 67% of the measured dyke segments have a N113°±10° trend, whereas only about 2% of the dyke segments are at a high angle to this main trend, coincident with a joint set in the same direction. Many of the remaining 31% of the measured dykes have orientations related to other secondary joint sets present in the host rock. Thus, the overall macroscopic dyke swarm consists of regularly aligned dykes that follow an average N100°–N125° trend, and minor segments of variable orientations.

This first 2D appraisal from sub-horizontal sections of sub-vertical fracture and dyke arrangement is complemented and corroborated by the pattern observed on steep outcrops at the cliff areas of Aiguablava (Fig. 3.4). A slightly irregular zigzagging on dipping dykes and the presence of a gently N-dipping systematic joint set (generally devoid of dyke) are other particular features observed on the escarpments.
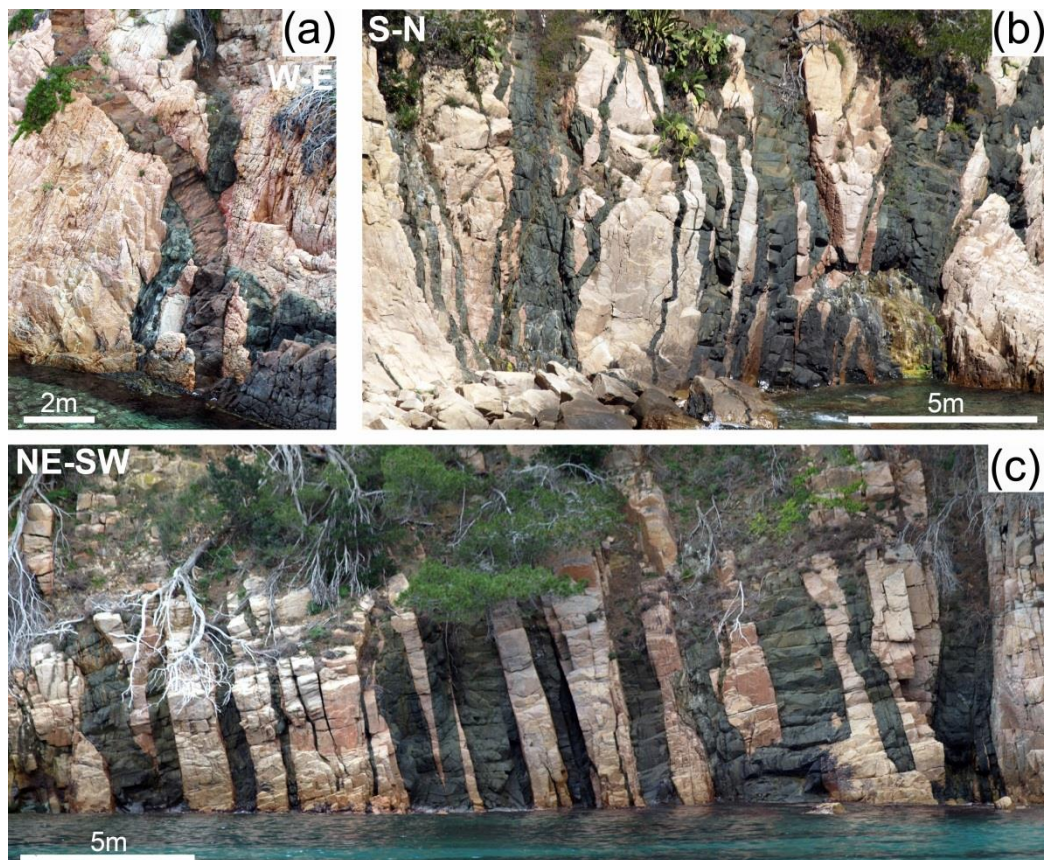
Fig. 3. 4. Photographs of the dyke swarm at the coastal cliffs. (a) A bostonite dyke (brownish) cross-cutting a spessartitic one (dark green) on the northern cliff of Platja de N'Astàsia. The lamprophyre dyke swarm on the western (b) and eastern (c) sub-vertical cliffs at Aiguablava. Notice the pervasive set of gently N-dipping fractures.

3.1.4. Outcrop-scale structural patterns

A 3-D detailed structural analysis has been performed at the mesoscopic, outcrop scale. This involves qualitative geometrical characterization and orientation analysis (described in this section) and several quantitative methods to estimate the conditions of dyke emplacement (developed in following sections).

3.1.4.1. Joint pattern

As documented in the previous section, both the leucogranitic host rocks and the lamprophyre dykes are affected by a dense network of multiply oriented, mutually crosscutting fractures that give the rock masses a blocky appearance. The majority of these fractures correspond to joints that do not show any apparent aperture or offset, although they are occasionally filled with thin quartz or calcite veins or veneers. Although joints have linear traces at the map scale (Fig. 3.3), they display more irregular geometries at the outcrop scale. This particularly applies to the shorter fractures and may consist of curved traces, en echelon arrays and/or branching terminations.

The stereoplot in Fig. 3.5a shows multiple sets of steeply dipping joints which contrast with the clustered dyke orientations around a N100°–N125° trend, confirming the trends observed from the 2D analysis (Fig. 3.2). Furthermore, a set of gently N-dipping joints is well differentiated, which corresponds to the orientation of the Upper Cretaceous camptonite dykes mentioned in Section 2.

Since this work is based upon the assumption that dykes emplaced into previous joints, it seems pertinent to ascertain which set or sets of joints predate the sub-vertical lamprophyre dykes. However, such discrimination has become difficult because field observations point towards a complex fracture pattern that resulted from development of early fracture sets related to cooling and decompression of the granite batholith, followed by further fracturing associated to the emplacement of the sub-vertical dyke swarm itself, and subsequent tectonic and uplift events and the intrusion of the Upper Cretaceous camptonite dykes that caused new fractures postdating the vertical dykes.
Multiple field observations (see e.g. Figs. 3.6–9) allowed us to gain insight into the timing of different join sets relative to the lamprophyre sub-vertical dykes, which are summarized here below.

(1) A swarm of aplite–pegmatite and quartz veins is widespread in the leucogranite host. They clearly predate the lamprophyre dykes (Figs. 3.7a and b and 3.9), probably representing the last differentiates of the Aiguablava pluton. They show a rather constant orientation which is sub-parallel to a ≈N20° trending joint set (Fig. 3.5c) and at a high angle to the mean trend of the mafic dykes. This may indicate that the felsic veins would have intruded into a≈N20° trending joint set which was already developed prior to lamprophyres or was probably formed at the latest pluton cooling stages.
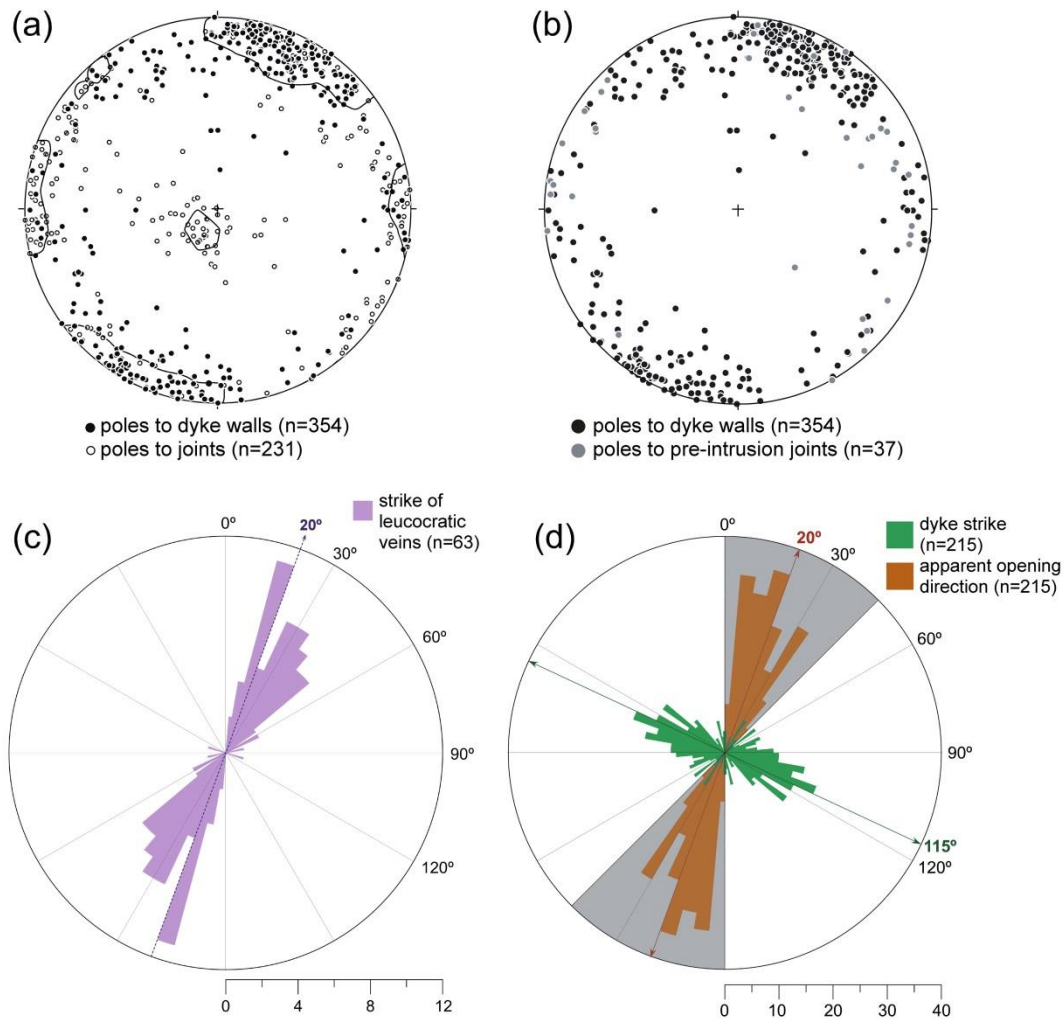
Fig. 3. 5. (a) and (b) Lower hemisphere, equal area stereoplots of poles to dyke segments and joints. Contours at 2% per 1% area are depicted in (a). In (b), only poles to joints that surely predate dyke intrusion are plotted. (c) Rose diagram of strikes of sub-vertical leucocratic veins (aplite, pegmatite and quartz) revealing a NNE–SSWdominant trend, parallel to one of the dominant joint sets (see Fig. 2c) and normal to the main trend of the dyke swarm as seen in (d) or in Fig. 7a. (d) Rose diagram depicting frequency of pairs of strikes of dyke segments and their corresponding apparent opening directions. The gray area corresponds to a 45° range in opening directions, which represents a small angle comparedwith the larger dispersion in strike of dyke segments. All data in (a) and (b) taken from the six selected areas except for E Aiguablava cliffs (unaccessed), and data plotted in (c) and (d) from the sub-horizontal outcropping zones.

(2) There are also many joints from the ≈N20° trending set and from other dyke-oblique joint sets that are cut and offset by the lamprophyre dykes (Fig. 3.7a and c).

(3) There is clear field evidence for dykes exploiting pre-existing fractures, most dykes representing opened previous joints of the dominant N110° trending set.

(4) In many cases where the join network is well developed, dykes display a segmented, zigzag geometry, evidencing changes in dyke propagation direction through differently oriented joints (Figs. 3.7a, c, d, and e and 3.9). These features will be described in detail in the next sub-section.
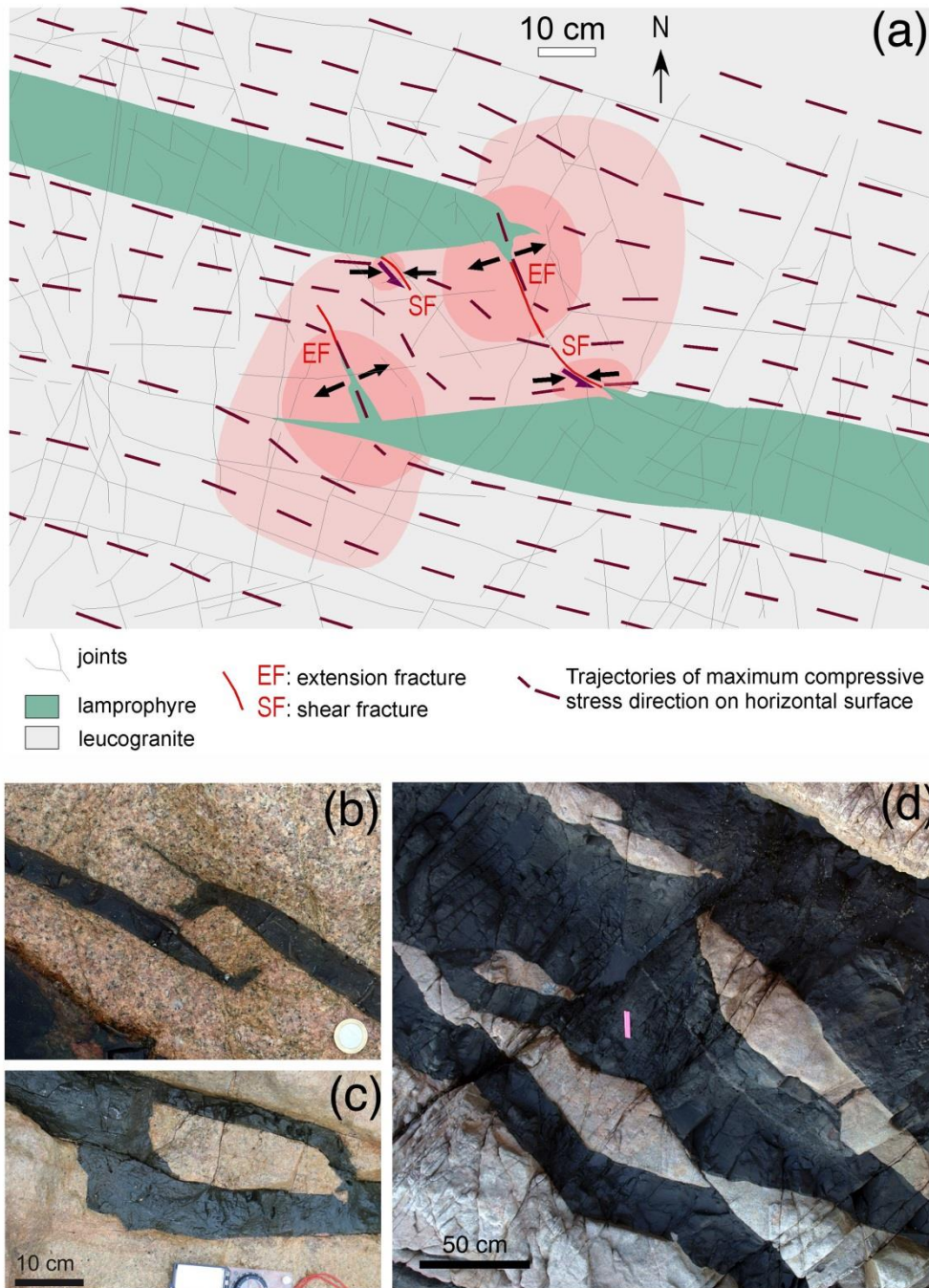
Fig. 3. 6. Examples of geometries resulting from dyke interaction. They all correspond to sub-horizontal exposure surfaces. (a) Interpretative sketch of the stress field generated between the tips of two parallel overlapping dyke segments fromSa Planassa area (based on Pollard and Aydin (1984) approach using an analogy between oceanic ridge segments and an opening crack in an elastic solid). A zone of local stress concentration is outlined by two contours ofmean normal stress. The dashed lines represent the trajectories of the maximum compressive principal stress following the dyke paths. Converging trajectories induce shear fracturing (SF) and diverging trajectories induce crack opening by extension fracturing (EF). (b) Host rockbridge and sudden curvature of dyke segments between two overlapping dykes at Platja de N'Astàsia. (c) and (d) Rafts of host rocks due to dyke coalescences at Platja de N'Astàsia and W Aiguablava outcrops respectively. North is upwards in all photographs.

(5) For certain joint sets, there are contradictory joint-dyke crosscutting relations, such as joints of identical orientation that arbitrarily appear to cut or to

be cut by the lamprophyre dykes (Fig. 3.9). This suggests episodes of fracture reactivation during and after emplacement of the mafic dyke swarm.

(6) Geometrically contrasting joint patterns are frequently observed inside and outside the lamprophyres which may hinder their interpretation. That is, joint patterns in the leucogranitic host and inside the dykes show marked differences with regard to spacing and orientation (Fig. 3.7f and g). A possible interpretation is that differing joint arrays reflect different cooling patterns as they represent separate magmatic events. Another explanation for the different joint orientations is that they result from the process of fracture refraction across rocks of contrasting mechanical properties (such as the finer grained character of lamprophyre compared to leucogranite) during a single post-dyke fracturing event. Most likely, both effects may locally overlap in space to contribute to many of the observed complex arrangements.

As a result of this analysis, about 20% of the measured joints that were not exploited by the dykes are cut by the dykes and, thus, they surely predate the dykes. They show variable orientations, forming several sets (Fig. 3.5b). The rest of the fractures fall into the uncertainty of being either early joints that are reactivated or purely syn- to post dyke joints.

3.1.4.2. Dyke intrusion patterns

The most common feature of the Aiguablava dykes at the m- to cm-scale is their deviation from planarity, showing segmented, usually offset geometries which contrast with the quite regular arrangement observed at the map scale. Although segmentation is a 3-D feature, it is more noticeable on sub-horizontal than on sub-vertical outcrops.

The stereographic projections and rose diagram in Fig. 3.5a, b and d allow visualizing that several of the pre-existing joint sets were exploited by magmatic dykes. The most favorable joints for dyke emplacement are those of the ≈N100°–N125° set, along which a majority of dyke segments were intruded (Fig. 3.5a, b and d). Additionally, other joint sets were exploited, and this fact contributed to the segmented geometry of many individual dykes.

The process of segmentation in magmatic dykes has been widely described in the literature. Segmentation structures, including en echelon segmentation (Delaney and Pollard, 1981), offsetting, stepping and curved geometries, can be sometimes used to infer dyke propagation direction, magma flow and the stress state (Rubin, 1995). Several mechanisms can be responsible for dyke segmentation (Weinberger *et al.*, 2000). These are mainly grouped into host rock mechanical controls, either structural (intrusion into fractured or foliated host rocks, e.g. Hoek, 1991) or lithological (intrusion across layered rocks, e.g. Baer, 1991; Druguet *et al.*, 2012; Gudmundsson, 2002) and the interaction of regional and local magma pressure-related stresses (e.g. Olson and Pollard, 1989; Pollard and Aydin, 1984).
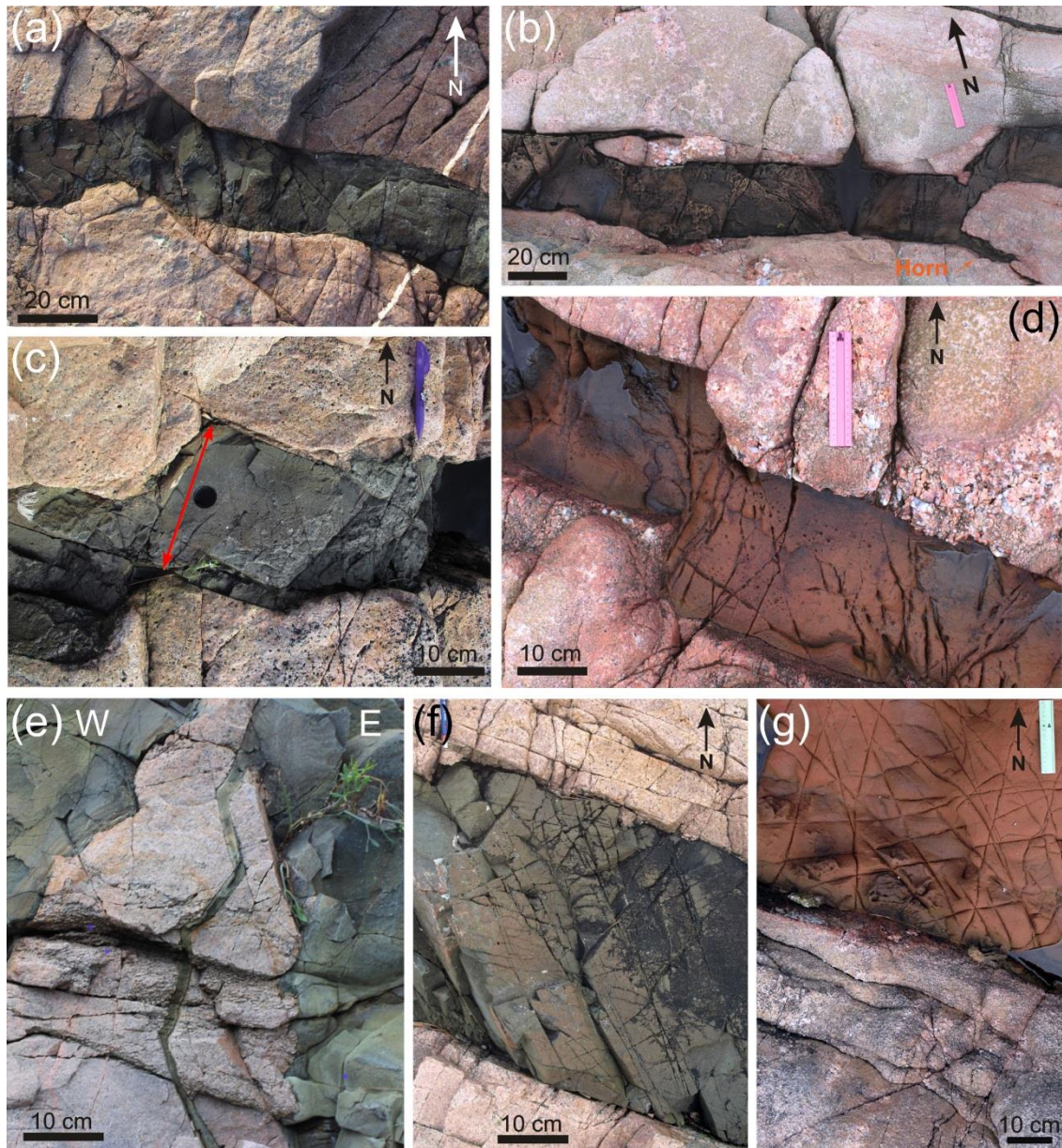
Fig. 3. 7. Examples of continuous segmentation structures in dykes. Photographs taken on sub-horizontal outcrops except for (e). (a) Segmented dyke fromSa Planassawith stepping along a secondary joint which is partly intruded and offset. The dyke also cuts, and is cut by, other joints, and cross-cuts a leucocratic vein at a high angle (right side of photograph). (b) Bostonite dykewith a stepped geometry that likely resulted fromjoining through secondary joints, leaving horns or thin projections of the main dyke. Locality: Punta des Pi. (c) Left stepped dyke at Sa Planassa.Notice the offset, unexploitedN–S joints. The defacing core hole is not our authorship. (d) Right stepped dyke fromPunta des Pi. (e) Sub-vertical viewof a zigzagging apophysis between twomajor lamprophyre dykes fromPlatja de N'Astàsia. (f) Joint patterns in the leucogranitic host and inside the dyke showing a marked dissimilarity in terms of fracture spacing and orientation. Locality: Platja de N'Astàsia. (g) Another example of contrasting jointing patterns in host-rock and dyke from Punta des Pi.

3.1.4.2.1. Discontinuous offset dyke segments

Discontinuous dykes show straight long segments parallel to the N100°–N125° joint set (Figs. 3.5d and 3.6a, b). They are arranged non systematically as variably right or left stepping offsets with non overlapping or overlapping morphologies (Fig. 3.6). Such offsetting leaves a bridge of host rock between dyke tips. The interaction between the two close-spaced dyke segments produces a perturbation of the remote stress field, as described and modeled by Pollard and Aydin (1984), Rogers and Bird (1987), Hoek (1991), Ramsay and Lisle (2000) and Tentler and Amcoff (2010). Horn structures can develop either by bending of the dyke tips area (Fig. 6a) and/or switching dyke propagation direction along new or reworked secondary fractures (Fig. 3.6a and b). An illustrative example of perturbation of the stress field around the overlapping dyke segments is shown in Fig. 3.6a. Pairs of extension and shear fractures are developed at opposite sides of the interaction zone. This structural pattern allows drawing stress paths and contours, showing the rotation of the direction of maximum compressive stress on the sub-horizontal outcrop surface around the rock-bridge zone. According to models by Olson and Pollard (1989) and Weinberger *et al.* (2000), the prevalence of small curvature around dyke tips would indicate a low to moderate crack interaction and a larger control of the remote differential stresses for the Aiguablava case.

3.1.4.2.2. Continuous offset dyke segments

Continuous dyke segmentation is more conspicuous and has several likely forming mechanisms. One is by the merging of two propagating dyke tips, either throughout pre-existing secondary or newly developed dilatant joints (Nicholson and Pollard, 1985). In the case of overlapping dyke segments, the host rock bridges broke, developing into raft structures (Fig. 3.6c). In the non-overlapping case, the segments join through a connecting segment (connector), but horns or thin projections of the main dyke may continue beyond the offset for a short distance (such as observed in Fig. 3.7b). The resulting geometry in this last case may be not exclusive of linkage of two non-overlapping dykes of opposite propagation senses, but could also be the effect of one single dyke that undergoes a local offset during its propagation, as interpreted by Currie and Ferguson (1970) for lamprophyres from Ontario. Closely adjacent sub-parallel dykes may also become connected by apophyses at a high angle, giving rise to angular, rhomb-shaped rafts of the leucogranitic host (Fig. 3.6d).

Another mechanism for continuous dyke segmentation is inferred from the commonly observed stepped and zigzag patterns (Figs. 3.7a, c, d, and e and 3.9). In this case, the stepping segments are caused by the propagation of the magma through the local joint network, alternately along the main ≈N110°–N115° and the secondary ≈N30°, ≈ N95° and ≈N170° trending joint sets preferentially. Steps and zigzags are also present on sub-vertical sections due to deflection in dip of the exploited joints (Figs. 3.4 and 3.7e), although the effect is less marked than in flat exposures, consistent with the smaller variation in dip of the different join sets. Step and zigzag patterns can be recognized because of matching of offsets on opposite dyke walls (Figs. 3.7a, c, d, and e

and 3.9c). Analogous to dykes from Antarctica (Hoek, 1991), the apparent dyke opening direction remains approximately normal to the whole dyke envelope. Following the studies of previous workers in other parts of the world (Airoldi *et al*., 2011; Basson and Viola, 2003; Gil-Imaz *et al*., 2012; Hoek, 1991; Le Gall *et al*., 2005; Riley *et al*., 2005) the zigzag patterns are indicators of propagation of a single dyke controlled by the variably oriented pre-existing joints; these are useful to estimate dyke dilation direction (Bussell, 1989; Baer and Beyth, 1990; see next section).

Apart from the above structures, branching (bifurcations and apophyses) and localized damage zones at dyke terminations are also rarely observed.
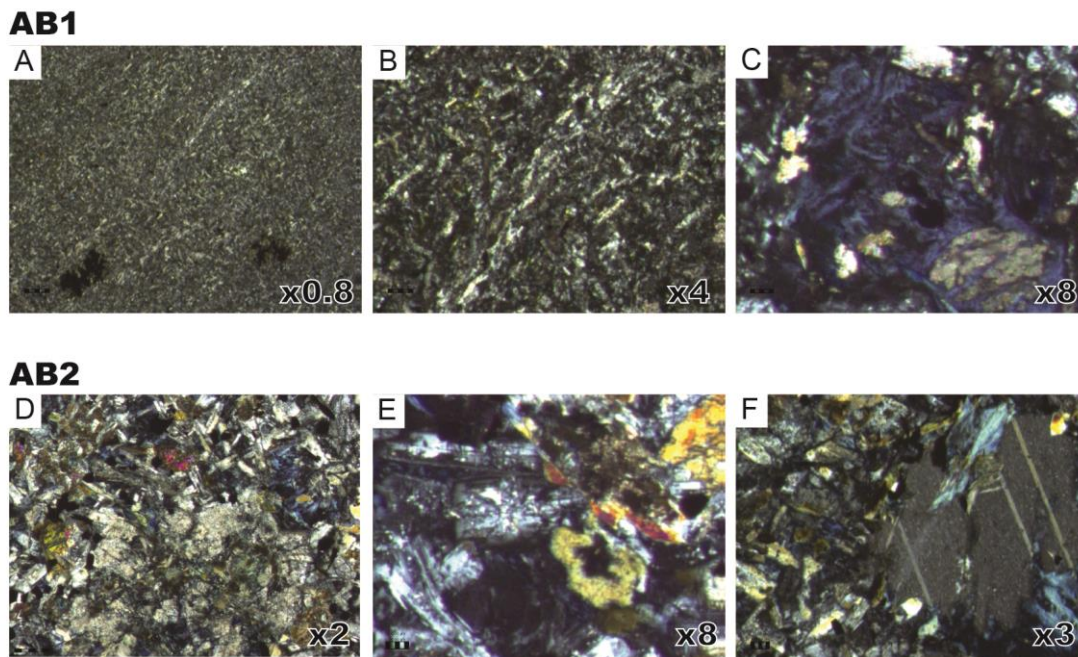
Fig. 3. 8.

3.1.5. Petrographic description

Only two samples were collected from the field, since we wanted to preserve as much as possible the outcrop. The area where we can observe the dyke intrusions is protected because of it geological interest.

AB-1

This sample correspond to a bostonite dyke. It has a clear color and fine grain size with some oxide minerals standing out (Fig. 3. 8. A). When observed with cross-polarized light, an emerging foliation is detected in some elongated plagioclases. It present an intersectal texture, with some plagioclases oriented aleatory (Fig. 3. 8. B). The mineral assemblage is: plagioclase, opaque minerals like Fe. Oxides, magnetite and cromite, Kfds and chlorite (alteration product) (Fig. 3. 8. C).

AB-2

This sample is from a dyke in the N'Astàsia area. It has a very fine grain as well, with plane polarised light we can observe large plagioclases. No internal fabric is detected, it presents a microcrystaline intersticial texture (Fig. 3. 8. D). The mineral assemblage is: plagioclase (albite), chlorite, clinopiroxene, opaque minerals and calcite (alteration product together with the chlorite) (Fig 3. 8. E and F).

3.1.6. Analysis of dyke dilation direction

The structural analysis performed on the six selected areas give clear evidence that most dykes opened in a sub-horizontal NNE–SSW direction close to normal to the main trend of the dyke swarm (≈N110°– N115°) and to the trend of 67% of the measured dyke segments (Figs. 3.2d and 3.5d). Evidences for that include offset of markers in the host rock that are present in all outcrops (sub-vertical and subhorizontal), such as aplite–pegmatite veins (Figs. 3.7a and b and 3.9) and pre-existing joints (Figs. 3.7a and c and 3.9), and matching pairs of offset edges in continuous stepped or zigzag dykes (Figs. 3.7a, c, d, and e and 3.9). 215 dyke segment strikes and their corresponding apparent opening directions were measured on sub-horizontal outcrops. The results (rose diagram in Fig. 3.5d), indicate a total variation of dyke opening directions between N000° and N045°which is a small span compared to the much larger variation of dyke wall orientation (total 180° azimuth span). This rather constant trend of apparent opening directions allow us to infer that the lamprophyre dyke swarm mainly consists of sub-vertical open-mode fractures consistent with a regional minimum principal stress axis (σ3) oriented NNE–SSW. This also determines that the only hybrid extension-shear fractures correspond to dyke segments with orientations deviating from the main ≈N110°–N115° trend, such as the short segments of stepped dykes (Fig. 3.7a, c, and d).

3.1.6.1. Net dilation direction inferred from the Bussell's method

A more precise 3-D analysis has been carried out to estimate the strike and dip of the net dilation direction for the dyke swarm, applying the stereographic analytical technique of Bussell (1989). The approach has been applied in several studies of dyke emplacement (e.g. Baer and Beyth, 1990; Riley *et al*., 2005; Taylor and Randall, 2000; Vétel and Cartwright, 2010) and is based on the concept that a dilation plane, defined by the offset edge and the apparent dilation direction, contains the average dilation direction. Dilation planes were obtained from the whole Aiguablava area by measuring (i) the apparent dilation directions measured on stepped and zigzag dykes and (ii) strikes and dips of pairs of adjacent non-parallel plane segments (dyke wall surfaces) or their intersection lines (offset edges) (Fig. 3.10a). By this method, the mean dilation direction can be determined from the best-fit intersection of multiple dilation planes. The obtained mean dilation direction for the whole sub-vertical dyke

swarm is 019/02, that is NNE–SSW and sub-horizontal (Fig. 3.10b), which fits satisfactorily with our previous analysis and is inferred to correlate with the orientation of the regional least compressive stress axis σ3.
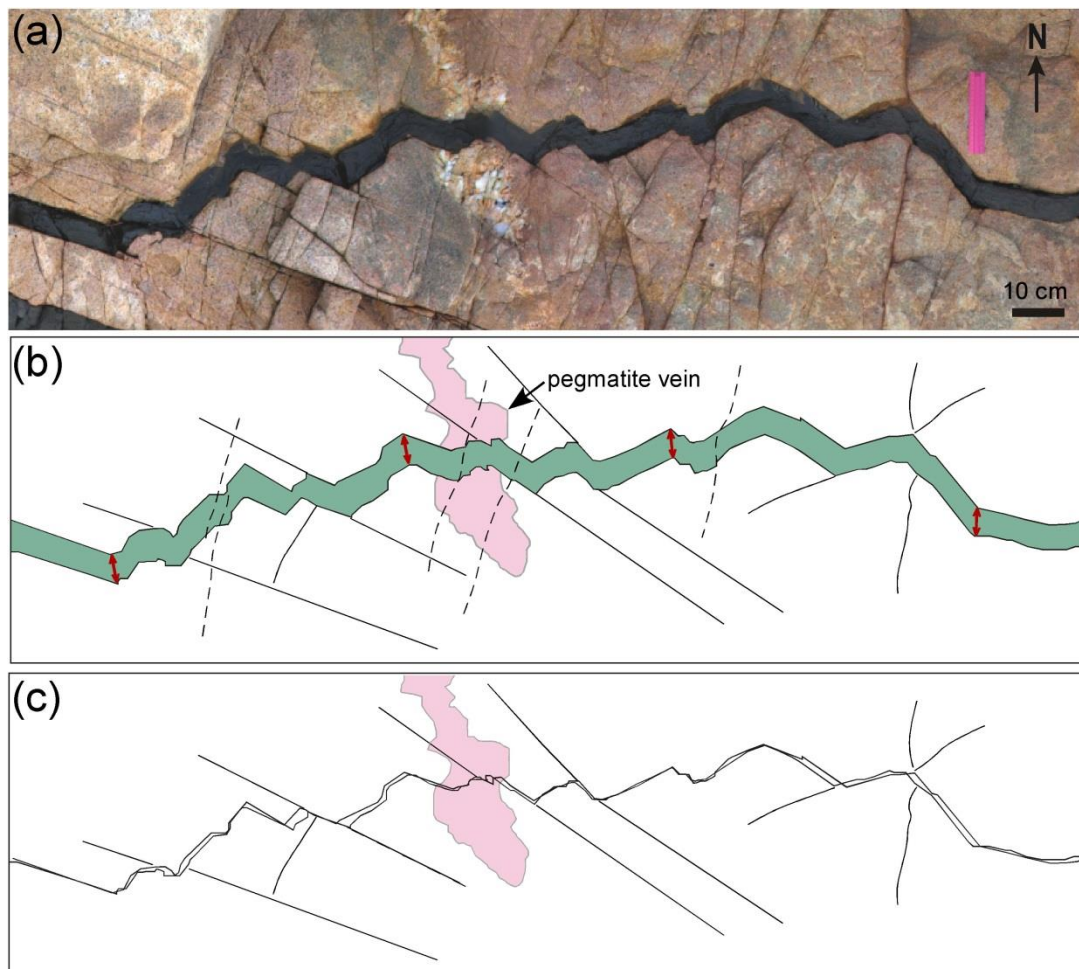
Fig. 3. 9. Small zigzag dyke from Platja de N'Astàsia (sub-horizontal outcrop). (a) Photograph. (b) Sketch with indication of the main pre-dyke (solid lines) and post-dyke (dashed lines) joints and the apparent dilation direction (arrows). (c) Reconstruction of initial fracture shows the likely propagation path along pre-existing joints.

3.1.6.2. Fit with direction of maximum dyke thickness

For any stepped or zigzag vein (or dyke) with constant dilation D (in orientation and magnitude), the thickness of any segment is $W = D\cos\alpha$ (Baer *et al*., 1994), being α the angle between the dilation direction and the normal to the segment azimuth along which the magnitude of W is measured. Thus, segments with α=0 correspond to pure extension fractures (i.e. segments perpendicular to the dilation direction and to σ3) and they will have the maximum thickness $W_{max}= D$ (Fig. 3.11a).

On the basis of this geometric assumption we can relate strikes and thicknesses of dyke segments to estimate the regional dilation or extension
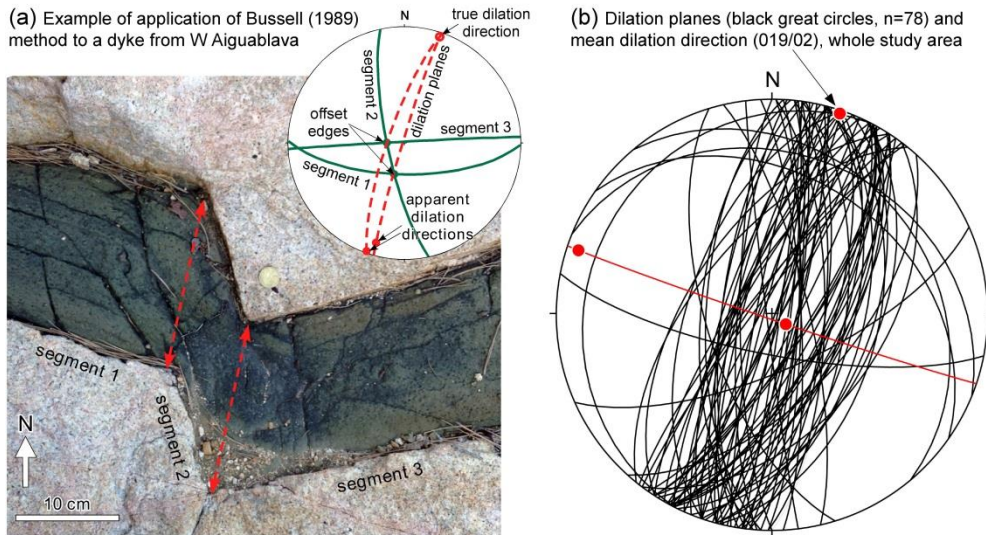
Fig. 3. 10. **Results on dilation direction analysis performed on segmented dykes from the six selected areas around Aiguablava by applying the Bussell (1989)method. (a) Example of how a true dilation direction is obtained frompairs of dyke offset edges and apparent dilation directions. Horizontal treat at W Aiguablava area. (b) Stereoplot of the whole set of dilation planes and the mean true dilation direction determined by the Bussell's method.**
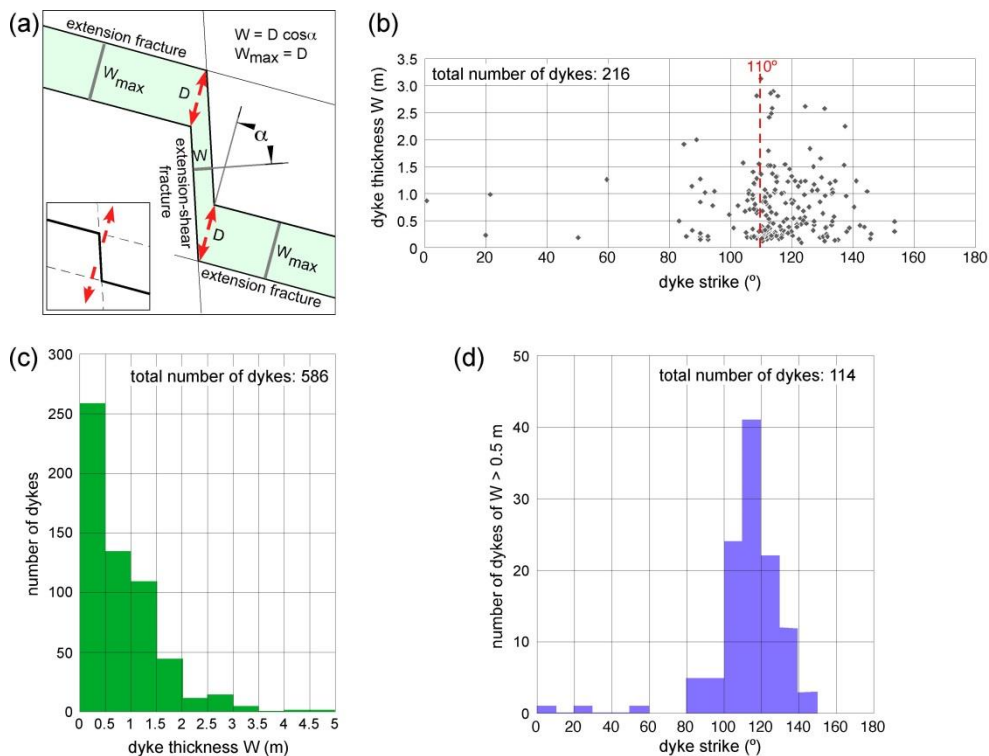
Fig. 3. 11. **Fig. 10. (a) Idealized sketch showing the variation of dyke segment thickness (W) with dyke azimuth for a constant direction and amount of dilation (D).Maximumthickness(Wmax)will be attained by dykes oriented normal to dilation direction. α is the angle between the dilation direction and the normal to the dyke segment (Baer *et al.*, 1994). (b) Plot of dyke segment strike vs. dyke thickness recorded from aerial photographs of the four sub-horizontal outcrops investigated in this study (see Section 5.2). Only dykes striking between ≈N100° and ≈N140° reach thicknesses in excess of 2m. (c) Frequency histogramof dyke thickness distribution. Measures are fromaerial and vertical cliff photographs of the six study areas. (d) Frequency diagram of dyke segments exceeding 0.5 m in thickness. More than 50% of these dyke segments have strikes between N100° and N120°.**

direction (Baer *et al.*, 1994; Le Gall *et al.*, 2005) and compare the results with the net dilation direction obtained by the Bussell's method. For this purpose we measured dyke thicknesses on the aerial photographs (Fig. 3.3) and on photographs of the vertical cliffs (Fig. 3.4b and c).

The results shown in Fig. 3.11b, c, and d indicate that dyke thicknesses rarely exceed 2 m and that the scarce segments exceeding this dimension are oriented within the mean N100°–N140° trend, with maximum thicknesses at ≈N110°, which fits orthogonally with the N019° strike of the net dilation direction.

3.1.7. Regional paleostress field and magmatic pressure

We have performed a 3-D analysis of the state of stress during dyke emplacement using the method proposed by Jolly and Sanderson (1997). Accordingly, Mohr circle is constructed for the opening of preexisting fractures, and the relative state of stress and magma pressure is estimated from patterns of poles to dilatant fractures (veins or dykes). Based on a 3-D approach introduced by Baer *et al.* (1994) and the 2D Mohr circle analysis of Delaney *et al.* (1986), this method involves the use of stereographic projections and 3-D Mohr circles.

The relative state of stress and magma pressure is expressed with the parameters driving pressure ratio (R′), which describes the difference between the principal stress axes and the magmatic pressure (Baer *et al.*, 1994), and the stress ratio (φ), which describes the relative magnitude of the principal stress axes, defining the shape of the stress ellipsoid (Angelier, 1984; Baer *et al.*, 1994).

$$R' = \frac{P_m - \sigma_3}{\sigma_1 - \sigma_3} \qquad (2)$$

$$\Phi = \frac{\sigma_2 - \sigma_3}{\sigma_1 - \sigma_3} \qquad (3)$$

The stress ellipsoid is prolate for φ=0, oblate if φ=1 and intermediate φ values indicate triaxial stresses with σ1 N σ2 N σ3. When R′ b 0 there is no possible fracture opening; when R′ N 0, fractures can open depending on the stress ratio (Baer *et al.*, 1994). If the poles to dyke walls form a cluster distribution around the minimum principal stress axis (σ3), magma pressure will be lower than the intermediate stress (σ2). On the contrary, if dyke poles are more scattered defining a girdle and leaving a gap zone devoid of poles around the maximum principal stress axis (σ1), magma pressure will be higher than the intermediate stress axis (Fig. 3.12a and c).

The symmetry in distribution of dyke poles gives the location of the principal stress axes (Jolly and Sanderson, 1997). The mode of calculating the symmetry axes is using Bingham statistics (Mardia, 1972), included in the Stereonet

software, from which the orientations of the principal stress axes are obtained. When the fluid pressure is less than the intermediate stress σ2, the angles σ1 and σ2 (σ1 is measured in the σ2–σ3 plane and σ2 is measured in the σ1–σ3 plane) define the cluster of poles (Fig. 3.12a). When the magma pressure is higher than the intermediate stress σ2, the angles σ2 and σ3 (σ3 is measured in the σ1–σ2 plane) define the girdle of poles (Fig. 3.13c). The values for the stress ratio and the driving pressure are calculated with the following equations (Jolly and Sanderson, 1997):

$$\Phi = \frac{\sigma_2 - \sigma_3}{\sigma_1 - \sigma_3} = \frac{\tau_{max\,1}}{\tau_{max\,2}} = \frac{1+\cos 2\theta_2}{1+cos2\theta_1} \qquad (4)$$

$$\Phi = \frac{\sigma_2 - \sigma_3}{\sigma_1 - \sigma_3} = \frac{\tau_{max\,1}}{\tau_{max\,2}} = 1 - \frac{1-\cos 2\theta_2}{1-cos2\theta_3} \qquad (5)$$

$$R' = \frac{P_f - \sigma_3}{\sigma_1 - \sigma_3} = \frac{a}{2\tau_{max2}} = \frac{(1+cos2\theta_2)}{2} \qquad (6)$$

Eq. (4) applies to the situation where Pm b σ2 and Eq. (5) to that of Pm N σ2. This technique has been previously applied to hydrothermal vein systems by André *et al*. (2001), McKeagney *et al*. (2004), Mazzarini and Isola (2007), Mazzarini *et al*. (2011) and Mondal and Mamtani (2013), and recently extended to stochastic models by Yamaji *et al*. (2010), Yamaji and Sato (2011) and Sato *et al*. (2013).

For the Aiguablava case, the poles to dyke segment walls forma subhorizontal elongate cluster (Fig. 3.12d), indicating the prevalence of steeply dipping WNW–ESE trending dykes, as previously shown in Fig. 3.5a and b. The elongate clustered distribution of dyke poles would actually reflect a pattern in between that of a clustered (where Pm b σ2, Fig. 3.12a) and that of a girdle distribution (where Pm N σ2, Fig. 3.12a), and similar to the pattern where Pm=σ2 (Fig. 3.12b), suggesting that the magmatic pressure (Pm) was close to the intermediate principal stress axis (σ2) at the time of intrusion. The orientations of the principal stress axes estimated from the symmetry of dyke poles (Fig. 3.12d) are: sub-vertical maximum stress (σ1), WNW–ESE intermediate stress (σ2) and NNE−SSWminimum stress (σ3). The orientation of σ3 is consistent with the dyke opening direction value deduced from the field data and estimated through application of Bussell (1989) method. The relative magnitudes of stress and magma pressure, that is, the stress and driving pressure ratios are calculated using σ1 and σ2 angles and the Eqs. (4) and (6).We obtain a stress ratio of φ= 0.29, corresponding to a close to prolate stress ellipsoidwith σ1 N σ2≫σ3, and a driving pressure ratio for the dykes of R′= 0.27, corroborating that the magmatic pressure was lower but almost equal to the intermediate principal stress axis (σ2) and lower than the mean stress. With these values the 3-D Mohr circle in Fig. 3.12e is constructed.
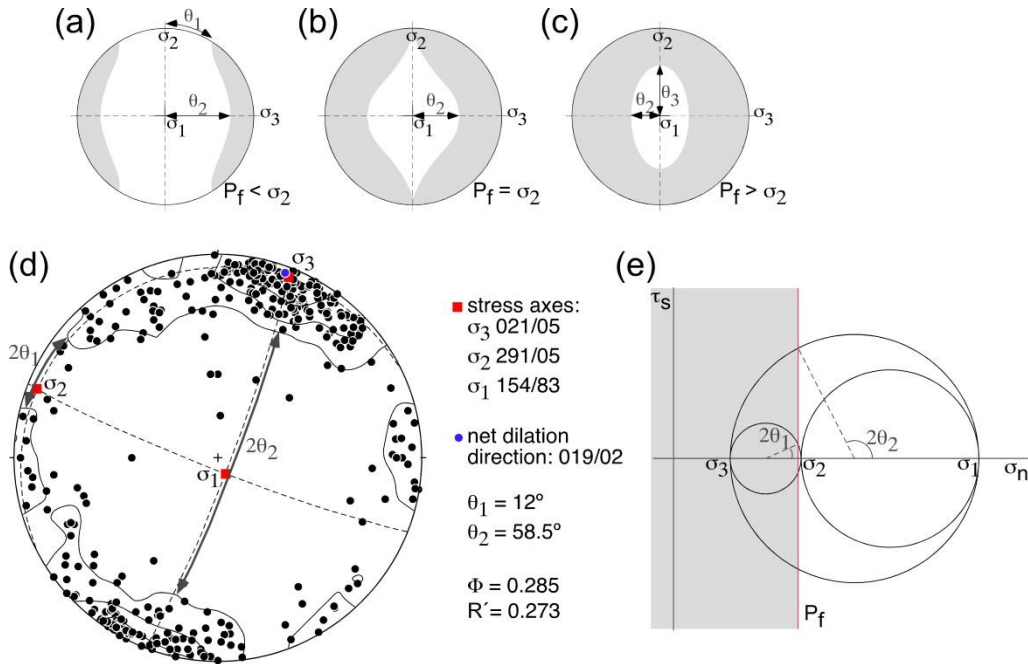
Fig. 3. 12. Panel labels (a), (b) and (c) are equal area, lower hemisphere stereoplots showing the theoretical distribution of poles to dilatant fractures (gray areas) for Pf b σ2, Pf=σ2 and Pf N σ2 respectively, for hypothetical caseswith vertical σ1 (method based on Jolly and Sanderson, 1997). (d) Equal area, lower hemisphere stereoplot of poles to dyke segment walls fromall measured dykes in Aiguablava. The contoured area (contours at 1, 4 and 8% per 1% area) indicates the orientations of fractures thatwere able to dilate duringmagma intrusion. Orientations of the principal stress axis (σ1, σ2, σ3) are derived from the cluster-like distribution of dyke poles and the angles σ1 and σ2. The mean dilation direction obtained from application of the Bussell's method is depicted for comparison. (e) 3-D Mohr circle producing a stress ratio (φ) of 0.29 and a driving pressure ratio (R′) of 0.27.

3.1.8. Estimation of the amount of regional extension

In order to get insight of the magnitude of regional extension associated to the intrusion of the Aiguablava dyke swarm, we applied the method proposed by Jolly and Sanderson (1995). Measurements were based on dyke-transverse scanlines on the same photographs used for the analysis of dyke thickness (Figs. 3 and 4b and c). The percentage of true extension (TE) is determined by the sum of dyke thicknesses measured parallel to the line (t), minus half the thicknesses of the first and last dykes in the traverse, divided by the sum of the space between the dykes (spacing, s), which is expressed with the equation (Jolly and Sanderson, 1995):

$$TE = \frac{\sum_{i=1}^{n} t_i - \frac{1}{2}(t_1 + t_n)}{\sum_{i=1}^{n-1} s_i} \times 100 \qquad (7)$$

Results for the Aiguablava bay area are shown in Fig. 3.13. The area with the highest true extension corresponds to the vicinities of W and E Aiguablava, with a mean value of ≈40%. Although extension roughly decreases from south to north, the dyke swarm is very irregular in distribution, with a sub-swarm of dykes at Platja de N'Astàsia and a large coastal exposure zone almost devoid of dykes between Platja de N'Astàsia and Punta des Pi. Taking into account the

absence of dykes in this last area, an average ≈12% extension associated to dyke intrusion is estimated for the whole Aiguablava bay area.

(a)

Line	Punta des Mut (% TE)	Sa Planassa (% TE)	Punta des Pi (% TE)	Platja de N'Astasia (% TE)	W & E Aiguablava (% TE)
1	54.50	9.57	63.07	21.52	41.71
2	59.32	10.77	0	18.21	41.04
3	48.54	9.85	0	21.63	37.46
4	35.73	8.63	0	31.06	
5	54.96	13.52	0	31.84	
6	53.04	18.89	0	35.91	
7	33.24	23.51	0	34.97	
8	35.03	0	112.07	35.68	
9	37.52	0	42.65	24.02	
10	94.86	0	31.93	0	
11	26.76	0	33.66	0	
12	0	13.39	40.64	0	
13	0	9.24	22.75	0	
14	0	0	0	0	
mean	38.11	8.38	24.77	18.20	40.07
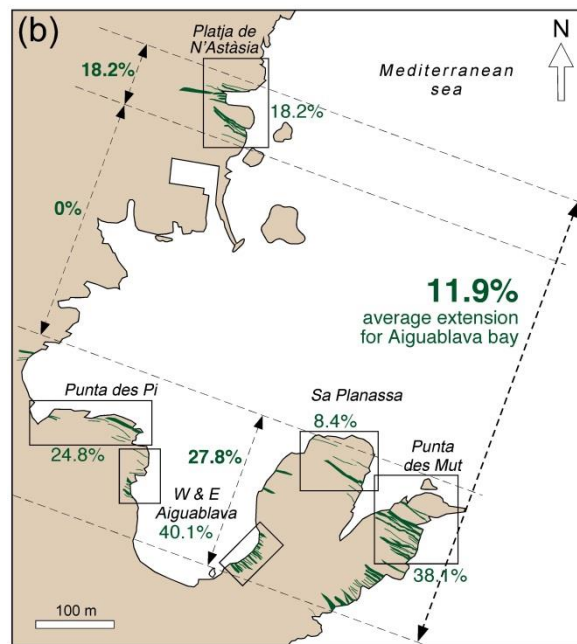
Fig. 3. 13. Estimation of extension associated to dyke intrusion in the Aiguablava bay area. (a) Table of true extension percentages (% TE following Eq. (7)) measured along various transects (up to 14 lines per area), and mean TE values obtained for each area. The spacing between transects was 5 m, except in Aiguablava W, where a single scanline was performed, and Aiguablava E, where two 2.5 m-spaced scanlines were performed. (b) Schematic map depicting main dyke traces and location of the mean extension values per area and the average extension of 11.9% for the whole bay.

3.1.9. Discussion and conclusions

The present detailed 3-D structural analysis confirms the previous qualitative hypothesis of emplacement of the Aiguablava vertical dyke swarm into a network of older joints, and allows us to constrain a 3-D model for the conditions of emplacement of the dyke swarm, which is synthetized and discussed in this section, followed by a discussion on regional correlations and geodynamic implications.

3.1.9.1. Model for the intrusion of the Aiguablava dyke swarm

The fracture pattern affecting the host leucogranites at the onset of dyke intrusion would likely be similar but less intensely developed than the present-day pattern. This consists on a polygonal network of multiple intersecting sub-vertical joint sets and a gently N-dipping joint set, mostly developed during pluton cooling and decompression. The gently N-dipping set, together with the subvertical ≈N20° and ≈N100°–N125° ones conform the three master joint sets in the area (Figs. 3.2c, 3.5a and b and 3.14).

The most suitable joints for dyke intrusion are those of the≈N100°–N125° set, along which a majority of dykes were intruded (Figs. 3.5a, b, and d and 3.14). Additionally, other secondary joint sets were exploited, including the subvertical ≈N60° and ≈N170° sets, a fact that highly contributed to dyke segmentation, in particular to development of the characteristic continuous step and zigzag geometries. Thus, both field observations and analytical procedures indicate that the older joint network largely controlled the orientations for dyke intrusion.
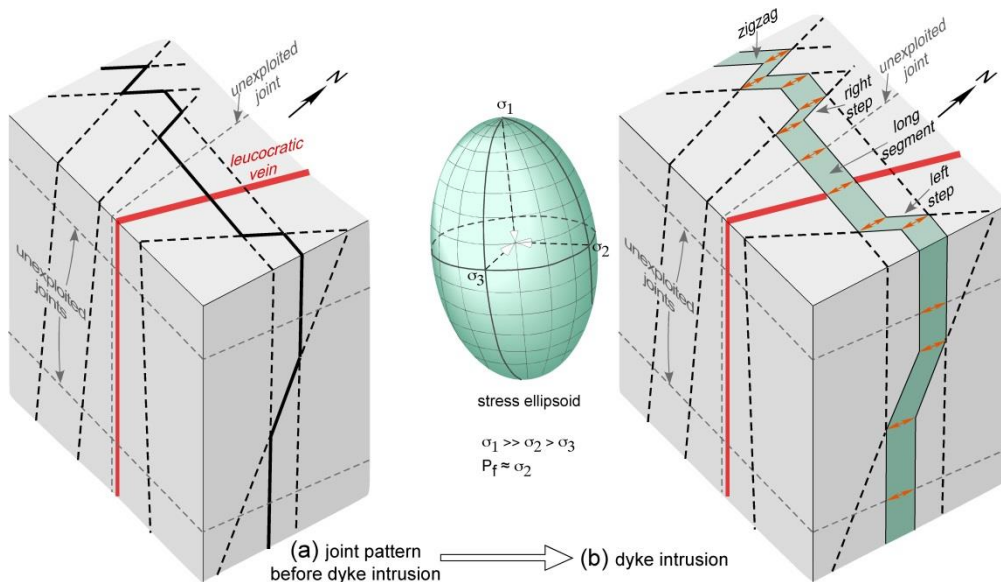
Fig. 3. 14. 3-D interpretative sketches of the pre-intrusion (a) and intrusion (b) stages of the Aiguablava segmented dykes along various joint sets with a rather constant NNE opening direction, parallel to σ3. The stress ellipsoid has been drawn from the Mohr circle construction in Fig. 11.

However, the occurrence of dominant dyke orientation along the ≈N100°–N125° trend and a prevalent sub-horizontal NNE–SSW normal to- wall net dilation direction, indicates that dyke intrusion was controlled by the external regional stress field.

3.1.9.1.1. Regional stress field and tectonic regime

The tectonic stress field estimated from the paleostress analysis can be expressed with orientation of the principal stress axes (sub-vertical σ1, WNW–ESE σ2 and NNE–SSW σ3). The NNE–SSW σ3 is parallel to the mean dilation

direction determined using the method developed by Bussell (1989), and perpendicular to the mean dyke swarm direction.

The relative stress magnitudes or stress ratio (φ= 0.29) is depicted as a sub-vertical close to prolate stress ellipsoid in Fig. 3.14.

These orientations and relative magnitudes of the principal stress axes are consistent with differences observed between dyke patterns in horizontal and vertical sections. That is, the higher degree of segmentation and variability in segment attitudes are observed in subhorizontal outcrops that correspond to the σ2–σ3 plane. On the contrary, dykes are relatively straighter on the steep exposures at W and E Aiguablava, which correspond to the σ1–σ3 plane of relative higher differential stress. Thus, the deduced paleostress values support the segmentation model of the dyke swarm.

The inferred sub-vertical value of σ1 implies that an extensional tectonic regime operated during dyke intrusion. And as calculated in Section 7, despite the rather irregular dyke spacing distribution, an average of 12% crustal extension associated to dyke intrusion is estimated for the study area.

3.1.9.1.2. Magma pressure and its relation with principal stress

The magnitude of magma pressure relative to the maximum and minimum stresses is represented by the driving pressure ratio (R′, Baer *et al.*, 1994). This has also been estimated by means of the paleostress analysis fromwhich a value of R′=0.27 has been obtained.

The closeness of this ratio with the stress ratio implies that magma pressure (Pm) was lower but close to the intermediate principal stress (Fig. 3.12). The relative low magnitude of magma pressure compared to the maximum principal stress is compatible with the scarcity of damage zones and branching structures in and around dyke walls and tips. Instead, we find straight or slightly deformed horn structures which reflect local perturbations of the stress field due to dyke interactions.

Fluctuation of magma pressure in between different magmatic pulses (e.g. Sibson *et al.*, 1988) is inferred to be small, with magma pressure likely falling from maximum values close to σ2 to values just above σ3. An argument for that is the similarity of the recorded intrusive structures from the earliest (spessartitic) to the latest (bostonitic) dykes.

A concluding remark is that the structure of the basement controlled the local, outcrop scale geometry of dykes. Intrusion was highly favored by the presence of pre-existing joints in the host rocks. The stress field at the time of intrusion was characterized by conditions of extensional tectonics and a slightly overpressurized magma. Thus, dykes would have intruded into upper crustal granitic rocks under an intermediate state between passive and forceful emplacement (Fig. 3.11e). The interplay between the influence of inherited joints in the host rocks and the stress field contemporaneous to dyke

emplacement controlled the intrusion mechanisms and the final 3-D arrangement of the dyke swarm.

3.1.9.2. Regional correlations and tectonic implications

This study points towards NNE–SSW-directed crustal extension as a tectonic framework in the Late Permian for the emplacement of the Aiguablava dykes in a fractured granitic basement. This would apply to the whole Aiguablava sub-vertical dyke swarm, including the two main compositional types (spessartite and bostonite), which share the same intrusive patterns and structural trends, despite the fact that bostonite-type dykes are relatively younger than the spessartite-type ones (evidenced by local cross-cutting relationships). Furthermore, the regional trend of the dyke swarm extends towards the south (Fig. 3.1b), to the entire Costa Brava batholith and thus, one can consider extrapolating the inferred regional extensional regime to this broader area of the Catalan Coastal Ranges.

As referred to in the Introduction, mafic dykes of Permian age are present in various Variscan domains of NE Iberia (Catalan Coastal Ranges, western Pyrenees and Iberian Range), in the Spanish Central System, the Cantabrian Chain, the French Massif Central and in the Corso-Sardo block. Different geodynamic models have been suggested for the emplacement of this variety of dykes. Based on geochemical signatures, calc-alkaline and sub-alkaline spessartites from the French Massif Central and the Cantabrian Chain have been associated to the presence of subduction systems during the Variscan orogeny that would have modified the mantle source (Perini *et al*., 2004).

Lamprophyres from the Spanish Central system have been interpreted either in the context of crustal-scale dextral shearing (Doblas and Ubanell, 1991), sinistral transtension (Scarrow *et al*., 2011) or in the context of a widespread rifting event developed from Carboniferous to Permian (Orejana *et al*., 2008).

In NE Iberia, there is evidence of continuous magmatism from Late Carboniferous to Late Permian in a tectonic setting changing from transpression to extension (Debon and Zimmermann, 1993; Lago *et al*., 2004). Perini *et al*. (2004) did not find evidence to apply their subduction system model to all the Iberian domains. However, a Late Carboniferous–Early Permian subduction of the Paleotethys following the main Variscan orogeny has been inferred for the whole Western Mediterranean domain (Ziegler and Stampfli, 2001) and recently in the Pyrenean domain by Pereira *et al*. (2014). According to Debon and Zimmermann (1993), the lamprophyres from the Western Pyrenees (most intruded into the Cauterets–Panticosa pluton), were emplaced during a transtensive episode that would mark the transition from orogenic calc-alkaline to anorogenic alkaline magmatism. Santana *et al*. (2006) proposed that dyke intrusion took place during the same dextral transpressional regime that was involved in the emplacement of the main Variscan plutons. A recent model by Gil-Imaz *et al*. (2012) postulate dyke intrusion under a N–S regional extension, which is roughly consistent with the NNE–SSW extension that we have deduced for the Costa Brava. However, in the interpretation of the Panticosa

dykes by Gil-Imaz *et al.* (2012), the maximum compression axis is horizontal E–W, reflecting a strike-slip regime that differs from our results from Aiguablava. It is interesting to note that the Panticosa dykes also intruded into a pre-existing fracture network (Gil-Imaz *et al.*, 2012; Santana *et al.*, 2006).

Late Permian doleritic and lamprophyric dykes are also widespread in Corsica and Sardinia, and they have been mainly associated to a post-orogenic phase that predated an intracontinental rift-related event (Buraglini and Traversa, 2000; Gaggero *et al.*, 2007; Ronca *et al.*, 1999). The Corso-Sardo swarms display quite regular linear patterns comparable to that of Aiguablava, especially in Sardinia, although they differ in orientation, the Sardinian dykes being oriented close to N–S.

This dissimilarity in dyke orientation is partly due to the Neogene drift event that produced an anticlockwise rotation of the Corso-Sardo block of an amount between 30° and 50° with respect to the stable Western European plate (Cohen, 1980; Speranza *et al.*, 2002). However, additional causes are required to account for trend divergences between the Catalan and the Sardinian dykes. Differences in orientation of the regional stresses and/or the previous fractures at the time of intrusion are among the most probable causes.

The extensional tectonics inferred from the Costa Brava dykes is supported by the presence of Late Permian–Early Triassic sedimentary basins associated with a prevalent extensional regime in Eastern Iberia (López-Gómez *et al.*, 2002). This distensive period could represent the latest stage in the evolution from Variscan compression/transpression to late Variscan (Early Permian) strike-slip tectonics in a Paleotethys subduction environment, and to Late Permian extension associated to Neotethys opening. The general trend from calc-alkaline to alkaline compositions observed in many Permian dykes in the Variscan basement of Iberia could be related to this geodynamic evolution.

3.2. SARDINIA: DYKE EMPLACEMENT INTO LESSER FRACTURED BRITTLE HOST ROCKS IN THE MID-UPPER CRUST.

3.2.1. Introduction

Dykes are among the most interesting structural elements used in paleostress and paleostrain analysis (Anderson, 1951; Delaney *et al.* 1986; Pollard, 1987). This is because in propagating dykes the transport of a viscous fluid or magma is coupled with host rock fracturing and deformation (Rubin, 1995). The external stress field and tectonic regime play an important role in dyking, but other factors like magmatic pressure and the interaction with rock layering or with pre-existing fractures also have to be taken into account (Rivalta *et al.* 2015).

The structural patterns of mafic dyke swarms have been classically used as evidence for deciphering geodynamic conditions and crustal scale tectonic settings, as shown by a large number of papers and special volumes dedicated to this topic (e.g. Halls, 1982; Parker *et al.*, 1990; Ernst *et al.*, 1995; Hanski *et al.*, 2006; Srivastava, 2011). When these dyke swarms are subvertical and are exhibited along large continuous or scattered areas, they are suitable for performing tectonic analyses from aerial or satellite photographs and, thus, inferring geotectonic settings.

This is the case in southeastern Sardinia where a large mafic dyke swarm of Permian age intruded into granitoid rocks of the Sàrrabus massif. Dykes are subvertical and roughly parallel to each other in a NW-SW direction.

The main objectives of this research are to characterize the three-dimensional structural pattern of the SE Sardinia dyke swarm and to determine the mechanical and tectonic conditions associated with the intrusive event. In addition, this paper aims to compare the results from this study with those previously obtained for another approximately coeval lamprophyre dyke swarm in the Catalan Coastal batholith of NE Iberia (Martínez-Poza *et al.*, 2014). Indeed, the methodologies used in the present study are the same as those applied to the Catalan Coastal dyke swarm. This will allow direct, mutual comparison and correlation. Furthermore, some insight is gained at plate-scale into the geodynamic evolution of the western Mediterranean region from Permian to present times.

3.2.2. Geological setting

Dyke swarms stands out in the SE of Sardinia. They are embedded in the Sàrrabus massif, a late Variscan plutonic complex composed by a sequence of different granitoid types (Brotzu and Morbidelli, 1974; Brotzu *et al.*, 1983). This study foccusses on the Permian mafic dyke swarm located in the southern part of the Sàrrabus massif, along the coastal shore in the surroundings of Villasimius (Fig. 3. 15).
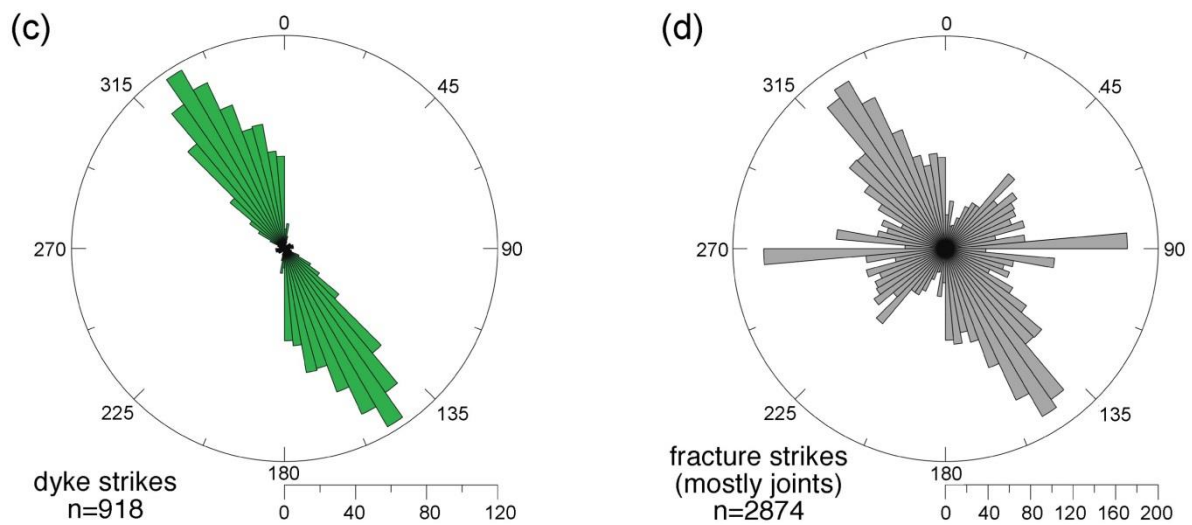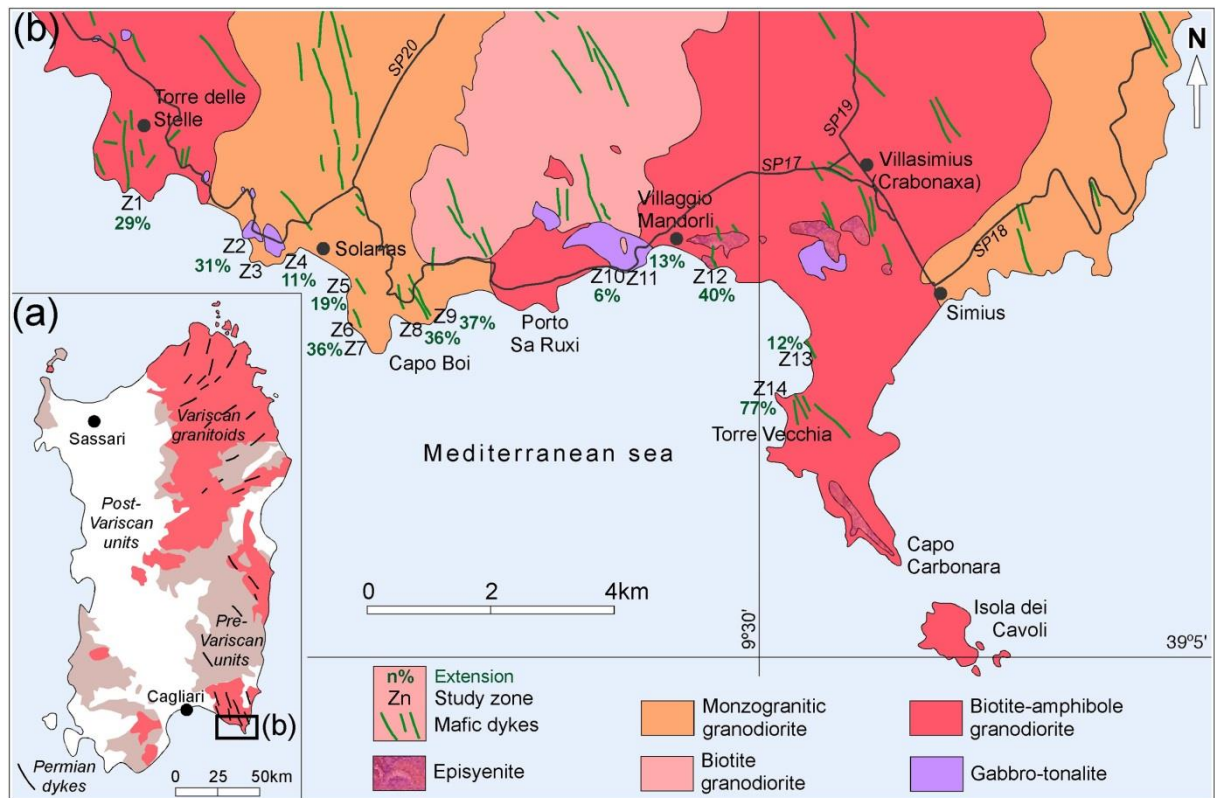
Fig. 3. 15. Geological setting of the study area. (a) Main lithological units of Sardinia. (b) Geological map of the south Sàrrabus pluton. Simplified from Carta Geologica di base della Sardegna in scala 1:25.000. http://www.sardegnageoportale.it   Rose diagrams of dyke wall strikes (c) and fracture strikes (d) measured on the 14 selected study areas from aerial photographs from Google maps. Along the coastal line, the study zones are indicated together with the respective calculated percentages of extension.

The Paleozoic basement of Sardinia (Fig. 3. 15a) is the result of the collision between Gondwana and Armorica plates in the South European Variscan framework. All penetrative deformation structures, metamorphism (which increases from SW to NE Sardinia) and large calc-alkaline magmatic activity belong to the Variscan event (Secchi and Lorrai, 2001), without any substantial effect of the Alpine orogenesis (Vaccaro *et al*., 1991). However, Helbing *et al.*

(2006), based on the different trends of post-Variscan mafic dykes in NE and SE Sardinia, postulate a periclinal structure attributed to the Alpine event.

3.2.2.1. Late Variscan magmatism

Calc-alkaline intrusions are spread pervasively in Sardinia and Corsica, configuring the so-called Sardinia-Corsica batholith (Atzori *et al*., 2000; Gaggero *et al*., 2007).

They consist of medium and high-K calc-alkaline basic and intermediate plutonic rocks associated with metaluminous and peraluminous dykes (Ronca *et al*., 1999).

Several authors have grouped the plutons depending on their emplacement phase, syn- or late-orogenic, starting with gabbrotonalitic to gabbro-monzogranitic and finishing with leucogranites (Bralia *et al*., 1982; Ghezzo and Orsini, 1982). L-type (metaluminous) and s-type (peraluminous) granitoides are found (Bralia *et al*., 1982, Secchi *et al*., 1991) as well. The origin of the granitic and leucogranitic rocks is proposed to be by partial melting of the continental crust (Bralia *et al*., 1982, Guasparri *et al*. 1984, di Pisa *et al*., 1988, Ghezzo and di Vincenzo, 1996).

The southern section of the Sardinia-Corsica batholith was developed between 340-288 Ma (U/Pb on zircon, Cocherie *et al*., 2005). This is associated with the orogenic collapse and tectonic unroofing along a localized transpressive or transtensional setting, active between the Late Carboniferous to Early Permian (Gaggero *et al*., 2007) and the subsequent plate reorganization (Ziegler *et al*., 2001).

The Sàrrabus massif extends over an area of ~400km^2 with shallow intrusion characteristics and a fairly long intrusion time span (290-270 Ma; Atzori *et al*., 2000). It is composed by several intrusive phases that display high-K calc-alkaline affinity. The shallow characteristics are shown in the low-grade regional metamorphism and the small contact metamorphism around plutons (with the presence of andalusite-cordierite hornfelses) (Secchi and Lorrai, 2001). The Sàrrabus units are divided by sharp and discordant contacts, with WNW-ESE and NS trends that are extensional trends in the post-collisional structures of the Variscan orogen (Cortesogno *et al*., 1998).

Looking in detail the geologic map of the research area (Fig. 3.15b), four different petrological types of granitoids can be distinguished in the Sàrrabus massif (Secchi and Lorrai, 2001; Fig. 1b). These are from older to younger: gabbro-tonalites, biotite- amphibole granodiorites, monzogranitic granodiorites, biotite-granodiorite and episienites.

During the Early Permian, a large area of Sardinia was affected by an important episode of explosive acid volcanism, associated with an extensional phase (Cassinis *et al*., 2003). Dated ages from felsic dykes in the earliest phase, using

Rb-Sr and 40Ar-39Ar methods (Vaccaro *et al*., 1991), cluster around 300-290 and 270 Ma.

In addition, basaltic dykes, with transitional composition (olivine basalt to traquibasalt) and aplitic veins and dykes were later intruded (Permian) and are very extended in the study area. Mafic dykes are the object of our study.

3.2.2.2. The Permian mafic dyke swarm

Later in the Permo-Triassic times, the granitoides from the Sàrrabus massif were intruded by a dyke swarm with different compositions (monzosyenites, basalts and rhyolite) (Secchi and Lorrai, 2001). In the southern-east part of the island, the dykes crosscut the Sàrrabus Late Carboniferous granitoides, while to the north they intrude the metamorphic basement (Ronca *et al*., 1999).

The dyke swarms represent around the 25% of the volume of the Sardinia batholith (~6000 km2) (Secchi and Lorrai, 2001; Vaccaro, 1990, 1991). The dykes show an emplacement along preferred directions (Vaccaro, 1990, 1991). The orientation of the dyke swarm is mainly NNW-SSE (N140-160º), with secondary directions at ≈N-S (Ronca *et al*., 1999). Comparing them with the late-Hercynian stress patterns (Arthaud and Matte, 1975, 1977a, 1977b), these trends seem to be parallel to the maximum compressive axis (σ1) and into a left side fault system, respectively (Ronca, 1996; Ronca and Traversa, 1996). Normally, the dip is sub-vertical and the thickness ranges between 1-15 m, (up to 30 m in Cala Pira) (Atzori *et al*., 2000).

These dykes were classified in groups by several authors (Atzori and Traversa, 1986, Atzori et al., 2000; Brotzu and Morbidelli, 1974; Pirinu, 1991; Ronca, 1996; Ronca and Traversa, 1996, Ronca *et al*., 1999). Generally, the dykes have been grouped in four different types, which also represent an intrusion sucession: 1) Fine to medium grained dykes of two-mica leucogranite with calc-alkaline affinity, up to 2m thick dykes of aplitic-micropegmatitic leucogranitic composition with muscovite-pegmatite pockets (Ronca *et al*., 1999). 2) 10-30 m thick dykes of biotite or biotite-muscovite porphyries, microgranites and aplites associated. 3) 0.5-10 m thick, fine grained mafic dykes. They correspond to calc-alkaline basalts, basaltic andesites and andesites (Ronca *et al*., 1999). Locally we can observe *composite dykes*, as a result of autointrusion (Scala Carbonada, Cabu Oi) (Secchi and Lorrai, 2001). Finally, a small group of tholeiitic basalt dykes that were supposed to be related to the late-Permian hypabyssal activity (Traversa and Vaccaro, 1992). All of them show pervasively alteration.

The origin of the mafic dykes is well constrain after the petrographic and geochemical analysis, which give mantle derived signal, although there is a minor volume of less evolved basic rocks which suffered crystal fractionation (Ronca *et al*., 1999). Major elements in the dykes (high K_2O) can be compared with the ones in the Sàrrabus granitoides (Brotzu *et al*., 1993) which are consider to be from a primitive magma source. Atzori *et al*., (2000) attributed the origin of the basic composition dykes to be mantelic because of the high Mg values and Cr and Ni contents, and the enrichement in LILE and LREE (Ronca

et al., 1999). The correlation with HFSE in the basic intrusions indicates a single but heterogeneous magmatic event (Atzori *et al.*, 2000).

The studied dykes do not present any sign of the Hercynian deformation phases. The southern part of the Sàrrabus granitoids seems to have been intruded after the Hercynian orogeny.

The granitoides in the SE of Sardinia (Sàrrabus mainly) were emplaced around 311-295 Ma, the dyke magmatism in the area occurred after that in a post-collisional phase, during a short period of time (290-260 Ma) (Nicoletti *et al.*, 1982; Pirinu, 1991; Brotzu *et al.*, 1993; Ronca *et al.*, 1999). The early intrusions are a few peraluminous muscovite-bearing rhyolitic dykes, dated as 290 Ma. A second phase of thicker rhyolitic dykes was emplaced around ~270 Ma. The later emplacement of basic and intermediate dykes took place after the occurrence of the felsic ones, around 259 Ma. A final phase of basaltic and tholeiitic dykes could represent the final stages of the Late-Permian basaltic activity (Ronca *et al.*, 1999). Because of this, dykes are supposed to be due to a post-tectonic (Late Carboniferous-Upper Permian) magmatism (Ronchi et al., 1998).

For Ronca *et al*. (1999) the age of the last dyke intrusion is not good enough for the time expand of the intrusions in the Sàrrabus area. This age is older age than in the northern dykes. Therefore, the calc-alkaline activity did not possibly occur in the central and southern part of Sardina later than 290 Ma. The calc-alkaline hypabyssal magmatism lasted until the Autunian in the Sàrrabus massif (Ronca *et al.*, 1999). There is more geochronological and geochemical work needed to constrain the time when the basaltic activity occurred during the Permian volcanism (Traversa and Vaccaro; 1992; Ronca and Traversa, 1996).

3.2.3. Methodology

Our analysis is based on structural data obtained from fieldwork along a W-E coastal section between Torre delle Stelle and Torre Vecchia (Fig. 3. 15b), combined with examination of aerial photographs from the same area. The specific methodologies applied to characterize and interpret the SE Sardinia mafic dyke swarm are:

(1) Statistical analyses on aerial photographs (®Google Maps) of dyke and fracture trend frequencies using a circular scanlines method. Also, dyke dimensions and percentages of regional extension are measured from scanlines on the aerial photographs (enlarged for measurements up to a ≈1:200 scale). The outcropping area along the coastal section was divided into 14 study zones (Z1-Z14 in Fig. 3. 15b).

(2) 3-D description of dyke and fracture patterns at the outcrop scale on differently oriented exposure surfaces in 12 of the 14 study zones (zones 6 and 7 were not accessible by foot).

(3) 3-D estimation of the mean net dilation direction for the whole dyke swarm applying a stereographic analysis.

(4) 3-D paleostress analysis of the mafic dyking event by the combined use of stereographic projections and Mohr circles.

This multi-methodological approach was previously used to describe a comparable mafic dyke swarm in NE Iberia (the Aiguablava dyke swarm; Martinez-Poza *et al.,* 2014). In the following sections we will further explain these techniques and give the most relevant results for the SE Sardinia dyke swarm.

3.2.4. General features of dykes and fractures from aerial photographs

3.2.4.1. Strike patterns of dykes and fractures

Dyke and fracture directions were measured by applying the circular scanlines method of Mauldon *et al.* (2001) to aerial photographs of the 14 study zones. Figs. 2a and b show examples of how the measures were taken from a grid of overlapping circles of radius 1, 3 and 5m. We measured strike directions of dyke walls and fractures at all points where these are intersected by the various circles. This statistical method implies measuring a single dyke or fracture several times. Thus, the data shown in Figs. 3. 15c and d actually refers to strikes of fracture and dyke wall segments.

The subvertical dykes have a dominant ~N140-N165º trend, defining a principal dyke set with mean direction at N150º (Fig. 3. 15c). Although representing a minority in terms of frequency, two other secondary sets are distinguishable, one at N10º (~N-S), and the other at ~N77º. Since the orientation pattern is rather homogeneous, many of the secondary directions are interpreted to correspond to short segments of long dykes. Other directions deviate from the main trend, especially those at ~N-S, it seems to correspond to dykes of a second magmatic pulse, based on a few crosscutting relationships observed in the aerial photographs.

Fractures (mostly joints, as they do not show apparent displacement at the aerial photograph-scale) have a much wider range of orientations (among others, N150º, N90º, N100º and N45º by order of frequency, Fig. 3. 15d). This multiple joint network is present both in the host rocks and in the dykes. At the scale of this analysis, a clear distinction cannot be established in terms of orientation between fractures inside dykes and in the granitoid host rocks. From the parallelism of dykes and joints in the N150º direction (Figs. 3. 15c and d), we can preliminary infer some genetic relationship; either dykes at N150º exploited pre-existing joints or both dykes and joints belong to the same tectonic-magmatic event.
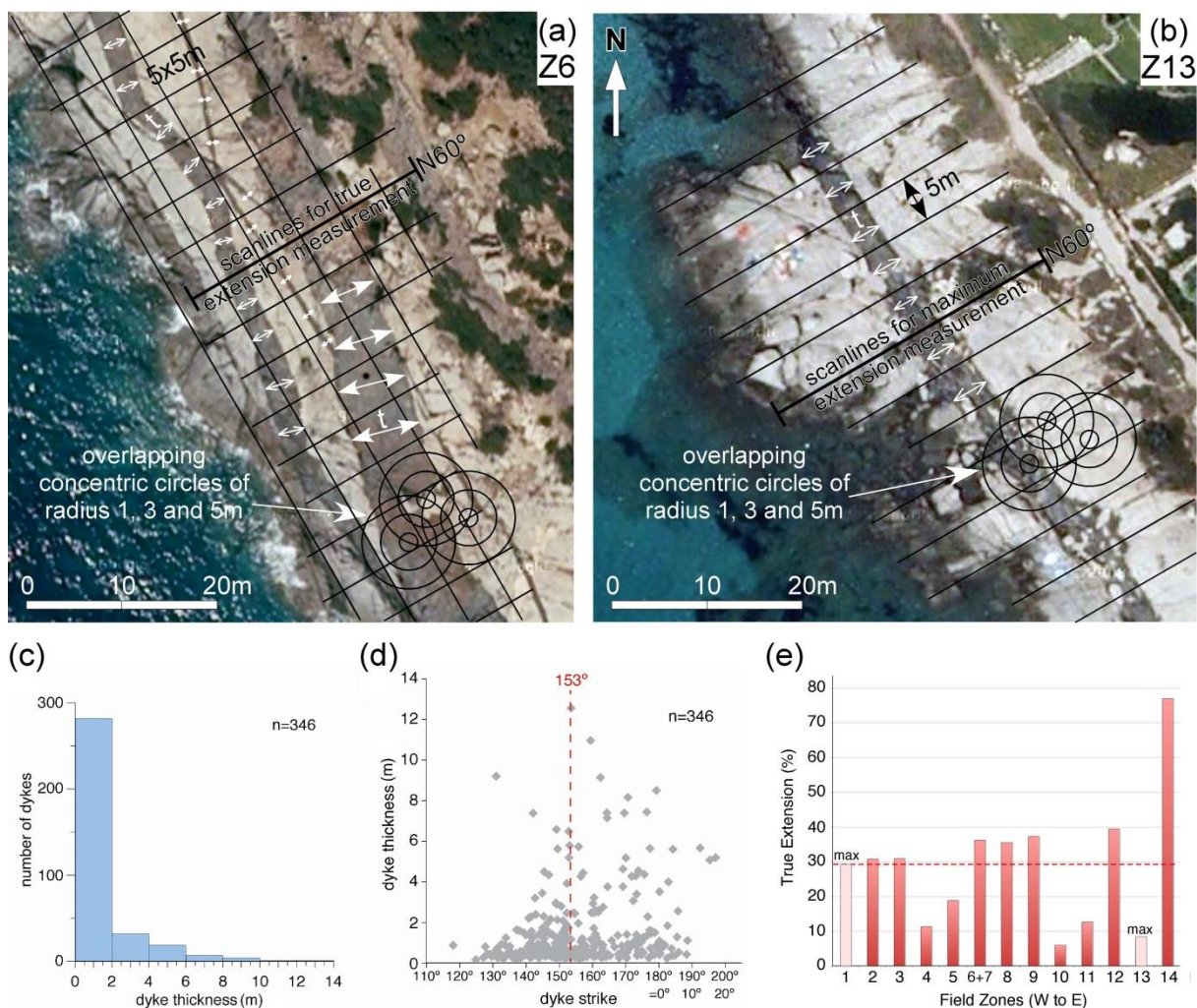
Fig. 3. 16. Illustrations of the methods and results from the regional-scale analysis of the SE Sardinia dyke swarm. (a) and (b) Examples of measures taken on aerial photographs (Google Maps), showing a grid of overlapping circles used to statistically measure the strikes of fractures and dykes (applying the circular scanlines method of Mauldon *et al*. 2001) and the regularly spaced gridded scanlines for dyke thickness (t) and extension appraisals. (c) Frequency histogram of dyke thickness distribution. (d) Plot of dyke strike vs. dyke thickness. (e) Histogram of % extension for each of the 14 analyzed zones.

3.2.4.2. Dyke dimensions (length and thickness)

Lengths of dykes vary from a few centimetres to a few hundred metres. They have not been systematically measured because dykes that are discernible at the aerial photo-scale tend to be longer than the outcrop dimensions (Figs. 3. 16a and b). The longest measured dyke is 280 m long in Z13, followed by a dyke 170 m long from Z6. The longest continuous dykes are all oriented between ≈N140 and ≈N170, coinciding with the trend of the dominant set. Dyke thicknesses were determined using a 5x5m grid, taking one thickness value (t) per square (Figs. 3. 16a and b). They vary from less than a metre to 13 m, with about 80% of the measured dykes not exceeding 2 m thick (Fig. 3. 16c). Dyke thickness shows a positive correlation with dyke length and thus the thickest dykes also match in direction with the trend of the dominant set (Fig.

2d). Aspect (length/thickness) ratios in the order of 50-100 can be roughly estimated.

3.2.4.3. Estimation of regional extension

The estimation of the component of horizontal extension associated with the intrusion of the dyke swarm is important since it provides insight into the magnitude of regional extension related to this magmatic event, assuming that the minimum principal compressive axis (σ_3) is normal to the sub-vertical dyke swarm and thus, sub-horizontal. Measurements were done on the aerial photographs of the 14 zones along scanlines oriented perpendicular to the trend of the swarm in a N60° direction, with a separation between lines of 5 m (Figs. 3. 16a and b). The number of scanlines in each area varies from 10 to 76 lines, depending on the outcrops areas.

We estimated True Extension (TE) based on Jolly and Sanderson (1995) method. This is defined by the sum of dyke thicknesses along one line (t), minus half the thicknesses of the first and last dykes in the traverse, divided by the sum of the space between adjacent dykes (spacing, s), as expressed with the equation (Jolly and Sanderson, 1995):

$$\text{TE} = \frac{\sum_{i=1}^{n} t_1 - \frac{1}{2}(t_1 + t_n)}{\sum_{i=1}^{n-1} s_i} \times 100 \quad (8)$$

This expression cannot be used in zones 1 and 13 where the outcrops consist of a single dyke embedded in granitoid (see Fig. 3. 16b). In these cases, we estimated a maximum extension value (Tmax) defined by the dyke thickness (t) divided by the sum of the outcropping space in the granitoid at each side of the dyke, which is the length of the scanline (L) minus the thickness of the dyke (t):

$$T_{max} = \frac{t}{(L-t)} \times 100 \quad (9)$$

Average true extension values or maximum extension values are obtained for each zone (Figs. 3. 15b and 3. 16e). Distribution of the dyke swarm is heterogeneous and so it is regional extension. The highest extension percentage corresponds to the easternmost zone 14 (~77%, Figs. 3. 15b and 3. 17a) and the lowest to zone 10 (~6%). An average ~29% extension associated to dyke intrusion is estimated for the whole study area.

3.2.5. Dyke and fracture patterns at the outcrop scale

Besides the presence of a general straight parallel NNW-SSE trending pattern of the dyke swarm, a more detailed 3D structural analyses performed through outcrop-scale fieldwork reveals the existence of a more complex structural pattern involving cross-cutting relationships between joints and dykes, intrusion modes, dyke segmentation types and interactions between dykes and fractures (Figs. 3. 17 to 3.21).
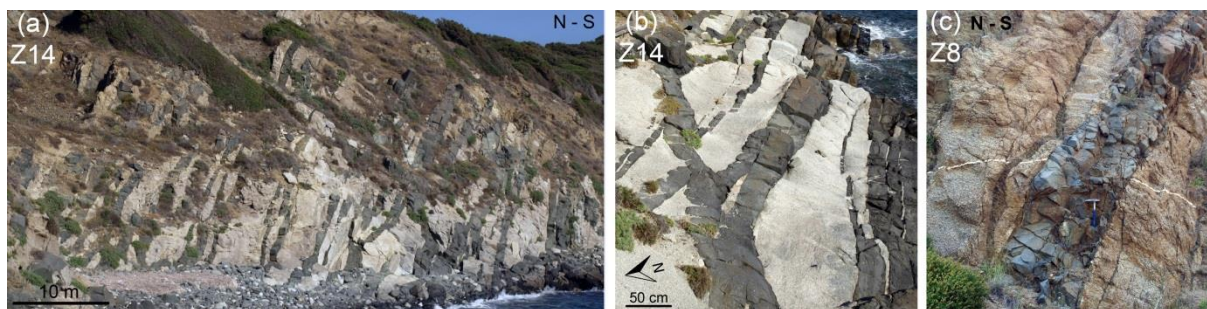
Fig. 3. 17. Field photographs. (a) View of the mafic dyke swarm along the coastal cliffs of zone 14. (b) Sub-horizontal outcrop from zone 14 showing mutually crosscutting mafic dykes. (c) Sub-vertical dyke in the road side of zone 8. A quartz vein in the granodiorite marks the apparent aperture of the dyke, which is sub-horizontal. Hammer for scale.

3.2.5.1. The dyke swarm and the fracture network

The 3D strike and dip orientation analysis of the dyke swarm confirms the prevalence of sub-vertical NNW-SSE trending dykes throughout the entire study area (Fig. 3. 18a). The spatial arrangement of fractures is much more complex, with multiple arrays (including sub-horizontal fracture sets, Fig. 3. 18b and c) and significant differences between fractures affecting the host granitoids and fractures affecting the dykes (Fig. 3. 18).

The N150° sub-vertical prevalent dyke orientation appears to coincide with one of the five main fracture sets in the host rocks (Figs. 3. 18a and b), a fact that is compatible with the two possibilities stated in section 3.4.4.1, that (i) most dykes could have exploited pre-existing joints or that (ii) dykes and dyke/parallel joints are contemporaneous. However, these dyke-parallel joints also conform one of the four main fracture sets inside some dykes (Fig. 3. 18c and f). A plausible conciliating scenario is that pre-existing joints in the granitoids were exploited during *dyking* and subsequently reactivated during cooling and post-cooling events. This implies active tectonics during and after the intrusion of the dyke swarm.

The scattering of poles to dyke walls around the mean NNW-SSE dyke orientation (Fig. 3. 18a) can be attributed to dykes intruded into previous joints in different orientations (e.g. Fig. 3. 17b). This is the case of a secondary group of sub-vertical dykes with mean orientation around N-S to NNE-SSW, which is present in some localities where they use to cut across the main set and have a distinctive lighter green colour (Fig. 3. 21b), being likely intruded along fractures in these orientations. Variations in strike and/or dip have also been observed along individual dykes, giving rise to continuous zigzagging stepped geometries (e.g. Figs. 3. 19d and e) and are probably equally related to the exploitation of previous joints. These features will be further described in the next sub-section. Marked differences exist between the joint system present in granitoids and that in the dykes, especially with regard to spacing, being jointing generally more pervasive in the dykes (e.g. Fig. 3. 18d). Fracture geometry and orientation also show differences in both lithologies, dykes having more systematically arranged joints (Fig. 3. 18). This can be attributed to the contrast in mechanical behaviour between mid- to coarse-grained felsic-intermediate granitoid types and fine-grained mafic dykes, producing markedly different fracture patterns. Moreover,
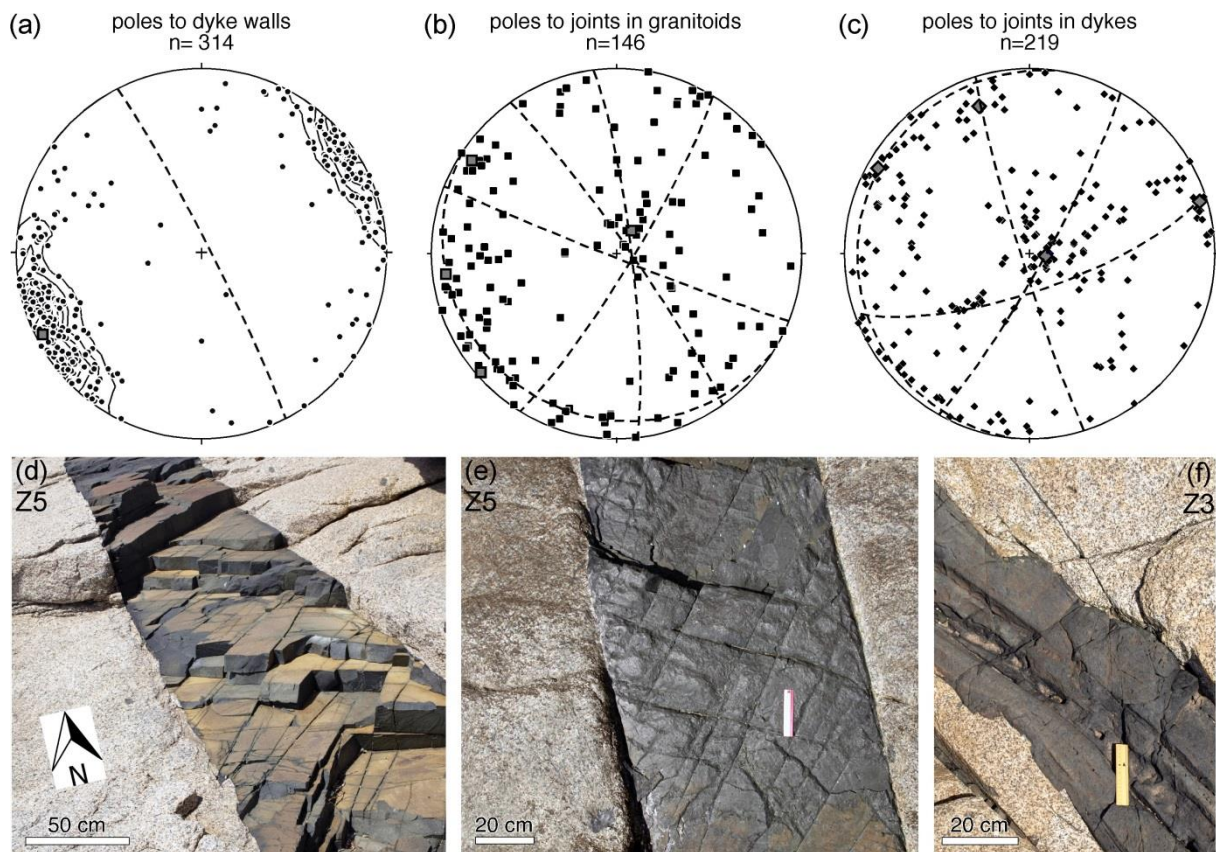
Fig. 3. 18. (a), (b) and (b) Lower hemisphere, equal area stereoplots of poles to dyke segments, fractures (mostly joints) in the granitoid host and joints inside the dykes, respectively. Contours at 2% per 1% area are depicted in (a). Dashed great circles in (b) and (c) represent mean planes of main fracture sets. (d), (e) and (f) Examples of fracture patterns around dykes from zones 5 and 3. Notice the larger joint spacing in granitoids compared to that inside the dykes. Also fracture geometry and orientation show differences in both lithologies.

these lithology-dependent contrasts in fracturing also likely reflect differentiated cooling and decompression conditions, as granitoids and mafic dykes represent separate intrusive events of distinct volumes and shapes. Actually, the internal fracture patterns of dykes in Fig. 3. 18d and e resemble typical cooling joints described in the literature (Correa-Gomes *et al*., 1991).

Deciphering mutual crosscutting relationships, and thus relative age, between different joint sets and between joints and dykes is not always straightforward. This is a consequence of the complex scenario of fracturing controlled by different processes (from cooling to tectonics, uplift and exhumation) and by factors such as the material intrinsic properties. This problem is not exclusive of this region but has been documented for other dyke swarms (e.g. Delaney *et al*., 1986; Peacock and Mann, 2005; Martinez-Poza *et al*., 2014).

3.2.5.2. Segmentation patterns related to dyke intrusion

As stated before, dykes observed at the mesoscale may display morphologies deviating from the 2D-linear or 3D-planar patterns that are predominant at the macroscale. The most common feature is segmentation, observed both on sub-horizontal and sub-vertical outcrops, and particularly noticeable in the thinner dykes that do not exceed ≈50cm in width (Fig. 3. 19).

Segmentation related to intrusion of veins and dykes has been widely investigated in the literature. It gives rise to a range of structures, including en echelon, stepped segments), offsetting and curved geometries, that can be used to infer dyke propagation direction, magma flow and paleostress conditions (Rubin, 1995). In the context of lithologically rather homogeneous host rocks, as in this study case, the main factors controlling dyke segmentation are (i) the interaction between regional stresses and local magma pressure, and (ii) host rock mechanical controls, so that dykes preferentially intrude along pre-existing fractures or foliation planes (Pollard and Aydin, 1984; Olson and Pollard, 1989; Hoek, 1991; Weinberger *et al*., 2000).
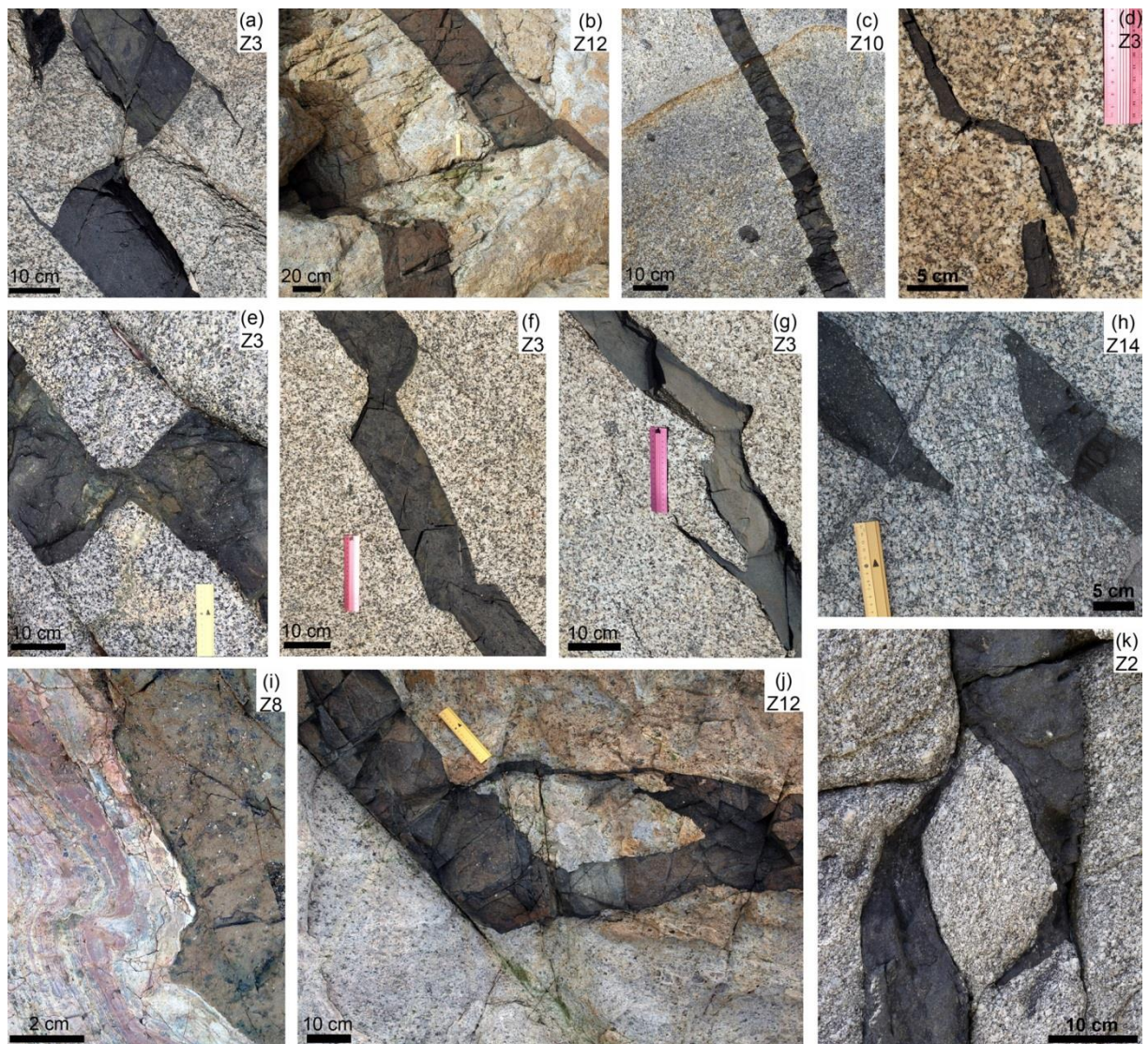
Fig. 3. 19. Examples of segmentation structures in dykes. Photographs taken on sub-horizontal outcrops except for (i) and (k) which are sub-vertical. (a) Right-stepped offset dyke. Note the slightly curved, nearing dyke tips in the internal part and the straight thin apophyses in the outer parts. (b) Another example of right-stepped dykes with little interaction structures and straight apophyses. Dyke arresting could be related to the presence of a fracture at a high angle to dykes. (c) Dyke with small right-stepping continuous offsets. (d) Dyke with right-stepping discontinuous and left-stepping continuous offsets. (e) A left-stepping continuous offset in a dyke along a pre-existing joint. Both the dyke walls and the previous joint are matching. (f) Right- and left-stepped continuous dyke. (g) Right-stepped dyke and a thin projection of the main dyke. The irregular geometry points to an origin of this continuous dyke by joining of two formerly separated dyke

segments. (h) Two overlapping en-echelon left-stepped dykes leaving a host-rock bridge. (i) A particular case of a mafic dyke intruded parallel to an older microgranitic dyke with a folded magmatic banding. The step in the mafic dyke is due to intrusion following the fold geometry in the felsic dyke. (j) Rafts of host rock due to dyke coalescence. (k) Although less common, segmentation is also present in vertical outcrops such as in this example of overlapping, almost coalescing dykes with interacting tips.

3.2.5.2.1. Discontinuous stepped dykes

These are defined by the en echelon-like arrangement of long dyke segments parallel to the dominant ~N140-N165° trend (Figs. 3. 19a, b, d, h and k). The resulting structures look like divergent or bisector-parallel en echelon arrays (Smith, 1996; Belayneh and Cosgrove, 2010). Arrays with right-stepping (Figs. 3. 19a, b and d) predominate over those with left-stepping (Fig. 3. 19h) and non-overlapping segments (Figs. 3. 19a, b and d) are more common than overlapping ones (Figs. 3. 19h and k). The interaction between two adjacent dyke segments may induce local stress perturbations (Pollard and Aydin, 1984; Ramsay and Lisle, 2000; Tentler and Amcoff, 2010), giving rise to horn-like structures defined by curving dyke tips and apophysis (Figs. 3. 19a, h and k). In the case of overlapping segments, a bridge of host rock between dyke segments can develop (Figs. 3. 19h and k). However, large curvatures are not common, a fact that is indicative of low to moderate dyke interaction and thus low magma pressure relative to far-field tectonic stresses (Olson and Pollard; 1989; Weinberger *et al.*, 2000). In some cases, a dyke-normal fracture or damaged zone is present across the offset zone between dyke segments (Figs. 3. 19b and h).

3.2.5.2.2. Continuous stepped dykes

Continuous dyke segmentation is also common in the studied swarm (Figs. 3. 19 and 3. 20). Right- and left-stepping arrays are equally common. Continuous segmentation can be generated by two main mechanisms. One is by the linkage and coalescence of formerly discontinuous stepped dykes by dilation across pre-existing or newly developed fractures (Nicholson and Pollard, 1985). In non-overlapping segments, the step represents the linking fracture or connector and thin projections of the main dyke may continue beyond the offset (e.g. Fig. 3. 19g). In the case of overlapping segments, raft structures may develop due to merging of opposite dyke tips (Fig. 3. 19j). Another plausible mechanism leading to continuous segmentation is magma propagation along the pre-existing joint network, alternately along the ≈N150° set joints (as long segments) and other secondary joint sets (as short segments). The developed steps and zigzags can sometimes be recognised as formed by this mechanism because of the matching of opposite dyke walls and previous joints (Figs. 3. 19d, e and f) and because the apparent dyke opening direction remains approximately constant. This becomes useful for the assessment of dyke dilation direction (Bussell, 1989; e.g. Martinez-Poza *et al.*, 2014; see next section).
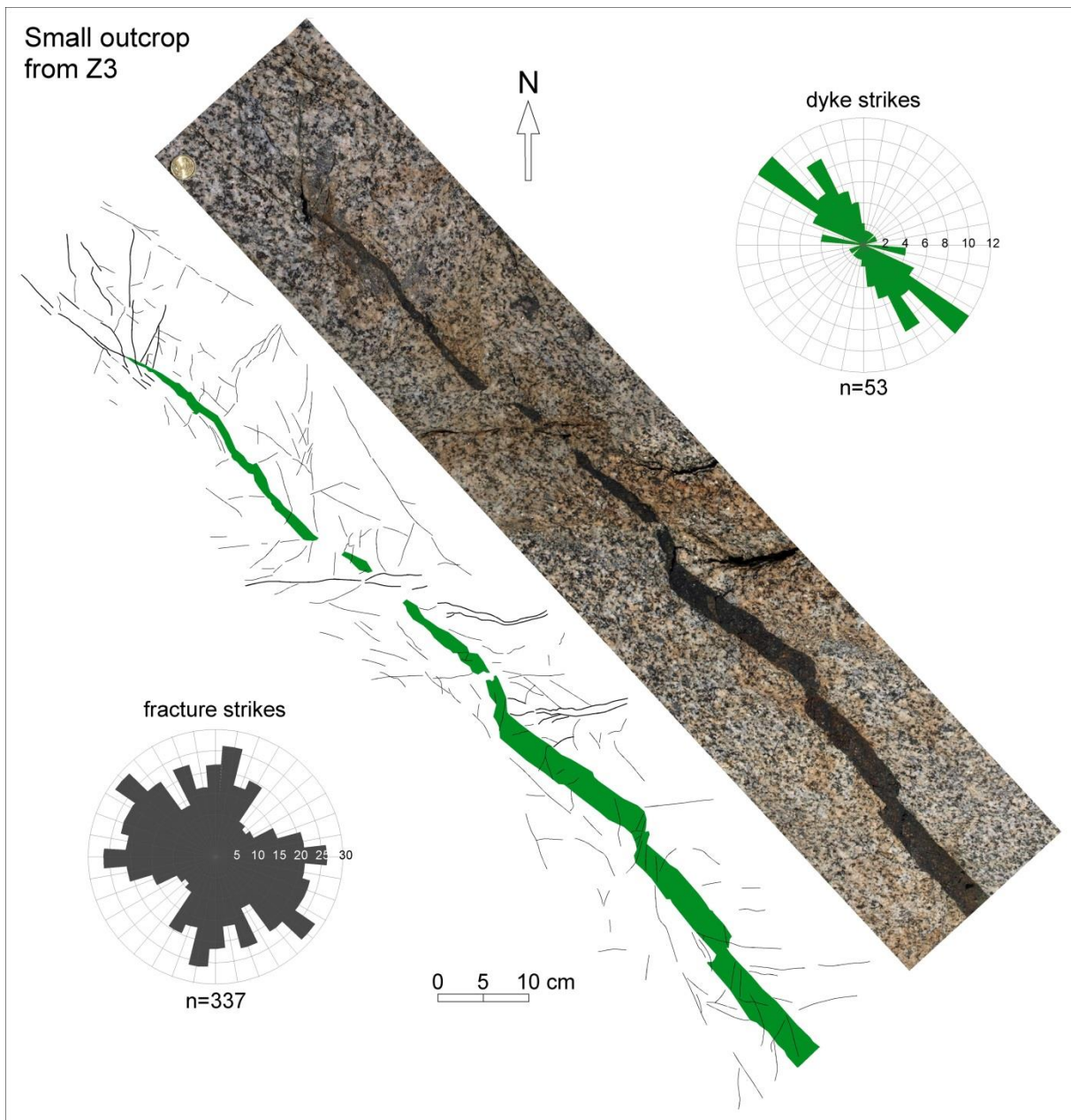
Fig. 3. 20. Photograph, structural sketch and rose diagrams of orientation frequency of dyke segments and fractures of a small sub-horizontal outcrop in Z3. Notice the progressive thinning and disruption of the dyke towards its tip and the regular right-stepping in the continuous segments. A damaged zone (likely syn-dyking fractures) is well developed in the granodiorite around the dyke tip and also present near the step overs.

A peculiar case of a continuous stepping has been observed in a mafic dyke intruded into an older microgranitic dyke (Fig. 3. 19i). The mafic dyke opened parallel to the folded magmatic banding present in the felsic dyke, thus adopting a stepped shape mimetic to the fold structure.

Fig. 3. 20 shows an example representative of dyke segmentation structures and their relation to fracture patterns. The dyke progressively narrows and disrupts into discontinuous segments along its last metre, while fracturing around the granodioritic host becomes more intense towards the dyke tip. The continuous segments are dominated by regular right-stepping, and a fracture

damaged zone (likely syn-dyking) is well developed in the granodiorite around the dyke tip and also present near the stepovers. This complex fracturing with fan-like patterns are typical of segmented dykes near their irregularities (Weinberger *et al*., 2000).

3.2.5.3. Segmentation related to syn- to post-dyking faulting

As observed before, localized fractures and deformation bands are commonly found around the steps or offset zones of segmented dykes (Figs. 3. 19b and h and Fig. 3. 20). Because these fractures are restricted to a small area around dykes they are interpreted as being developed during the dyking process. However, we observed another situation in which fractures or deformation bands extend farther away from the dykes into the host rocks (e.g. Fig. 3. 21a), giving rise to ambiguous structures of difficult interpretation. That is, are the right-lateral offsets displayed in Fig. 3. 21a former intrusive steps, or instead, are they the result of post-dyking dextral shears, or a combination of both? There are some other clearer situations in which dyke segments are offset with sharp cuts along fault surfaces (Figs. 3. 21b, c and e). Sinistral and dextral faults have close to N-S strikes and E-W strikes respectively, thus conforming anomalous conjugate sets with their acute angle bisector in the direction of extension (Fig. 3. 21d).

In Fig. 3. 21b, younger lighter dykes are partly offset, partly filling the sinistral faults, indicating that faults were already active during the last magmatic pulse. A low-angle normal fault affects a dyke and its host granitoid in Fig, 3. 21e. We infer that the anomalous orientation of normal and conjugate strike-slip faults is a consequence of reactivation of pre-existing fractures (probably joints) as faults during and after the last magmatic pulses.

3.2.6. Analysis of dyke net dilation direction

The observations made in the study area show evidences that most mafic dykes opened in a sub-horizontal NE-SW direction, approximately normal to the N150º mean dyke trend (Figs. 3. 16 and 3. 17). An accurate 3-D analysis has been carried out to estimate the orientation of the net dilation direction for the dyke swarm, applying the stereographic analytical technique of Bussell (1989). The approach is based on the concept that a dilation plane, defined by the offset edge and the apparent dilation direction, contains the average dilation direction. It has been applied in several studies of dyke emplacement (e.g. Baer and Beyth, 1990; Riley *et al*., 2005; Vétel and Cartwright, 2010; Martinez-Poza *et al*., 2014).

For this study, dilation planes were obtained from 23 different outcrops scattered around the whole study area by measuring the following elements (Fig. 3. 22a):

(1) Apparent dilation directions, which can be obtained from stepped dyke segments with matching walls and also from the offset of markers in the host rock that are cut by the mafic dykes (e.g. aplite and quartz veins, Fig. 3. 17c).
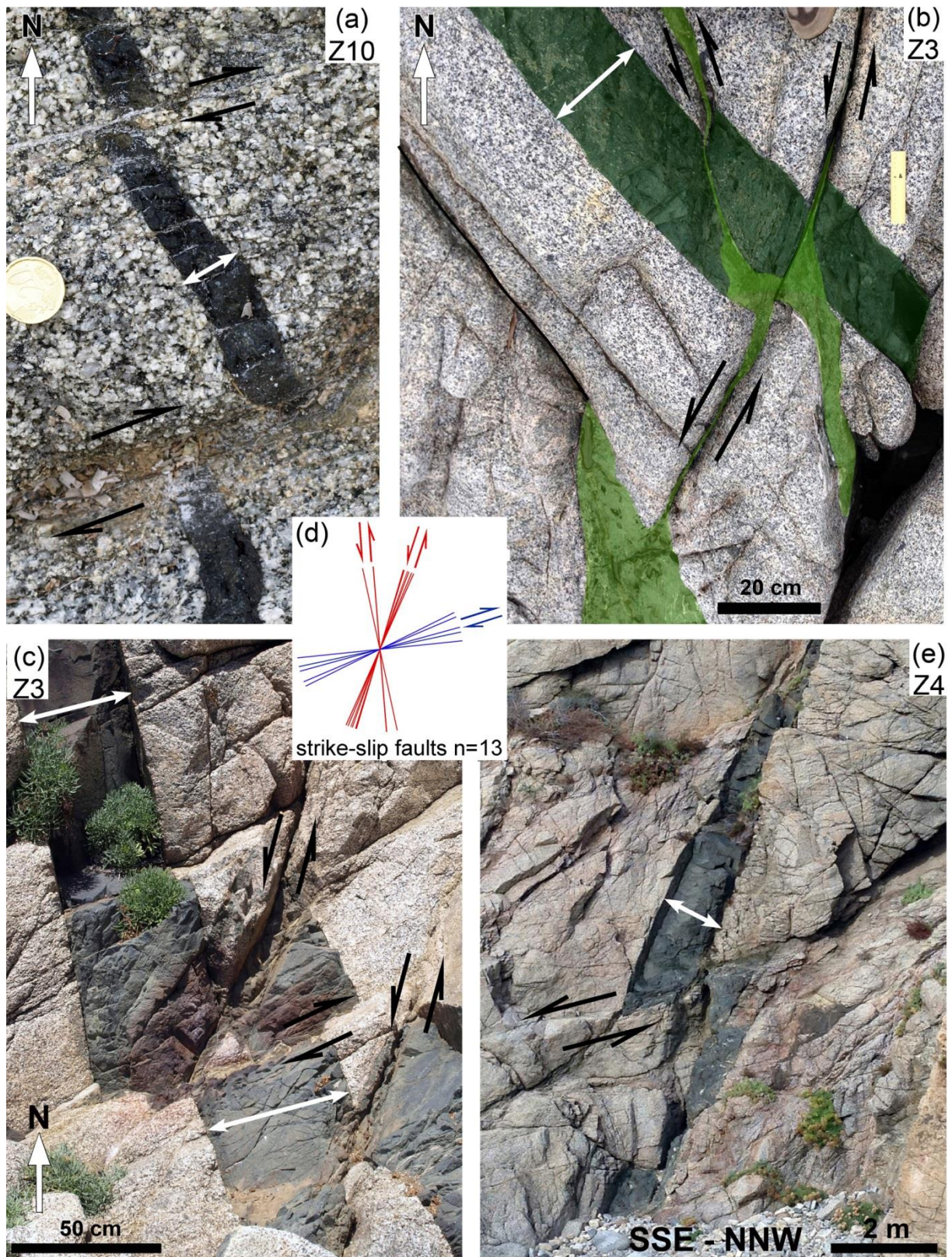
Fig. 3. 21. Examples of fault-related offset dykes. Photographs taken on sub-horizontal outcrops except for (e) which is sub-vertical. White double arrows indicate apparent dyke opening direction. (a) Apparent dextral shear fracture zones across granodiorite and mafic dyke. Many smaller fractures with no apparent displacement affect the central dyke segment. (b) Sinistral faults across granodiorite and a mafic dyke (dark). Younger, lighter dykes are partly offset, partly filling the faults, indicating that faults were active during the last magmatic event. (c) Dextral and sinistral shears affecting the host granodiorite and a mafic dyke. (d) Sketch summarizing the trends of the strike-slip faults. (e) Low angle normal fault affecting the host granodiorite and a mafic dyke.

(a) Example of application of Bussell (1989) method to a dyke from Z2
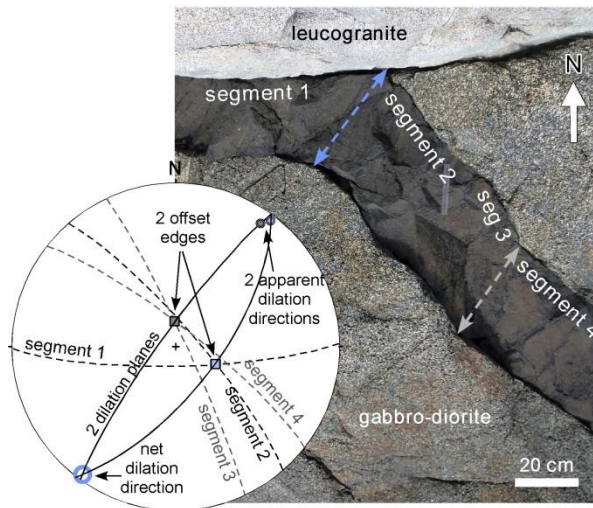
(b) Dilation planes (black great circles, n=56) and mean dilation direction (246/02), whole study area
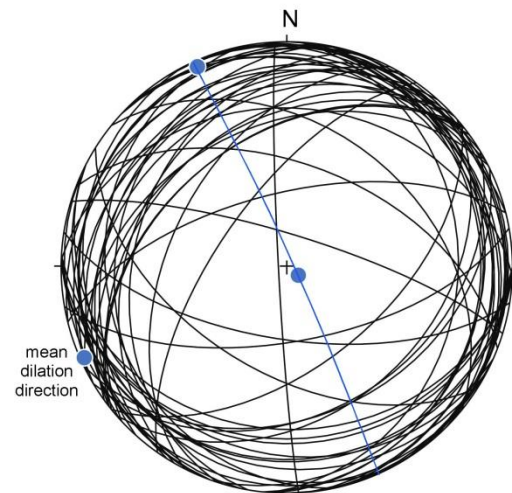
Fig. 3. 22. Illustration of dilation direction analysis performed on segmented dykes from the 14 zones by applying the Bussell (1989) method. (a) Example from zone 2 of how a true dilation direction is obtained from pairs of dyke offset edges and apparent dilation directions. (b) Stereoplot of the whole set of dilation planes and mean true dilation direction determined by the Bussell's method.

(2) Strikes and dips of pairs of adjacent non-parallel plane segments (surfaces of two adjacent stepped dyke segments or a dyke segment plus the surface of a vein in the host cut by the dyke) or their intersection lines (offset edges).

We determined a mean dilation direction from the best-fit intersection of multiple dilation planes. The obtained mean dilation direction for the whole sub-vertical dyke swarm is 246/02, i.e. a sub-horizontal ENE–WSW trending orientation (Fig. 3. 22b), which fits satisfactorily with the pole to the mean dyke orientation (Fig. 3. 18a) and the direction of maximum dyke thicknesses (Fig. 3. 16d), as expected to happen for close-to-pure extension fractures (Baer *et al*., 1994). This dilation direction is thus tentatively inferred to correlate with the orientation of the regional least compressive stress axis σ_3.

3.2.7. Regional stress field and magmatic pressure

A 3-D paleostress analysis was carried out in order to determine the regional tectonic environment at the time of emplacement of the mafic dyke swarm. We used the method by Jolly and Sanderson (1997), which is applicable to areas where pre-existing fractures (mostly joints) are reactivated as dilatant fractures. The method is based on a previous 3-D study by Baer *et al*. (1994) and on the approach of Delaney *et al*. (1986) for 2-D Mohr circle analysis. By this method, the relative state of stress and fluid/magma pressure can be estimated from patterns of poles to extension fractures (dykes and veins).

The determination of the 3-D Mohr circle is possible when the parameters driving pressure ratio and stress ratio are constrained. The driving pressure

ratio (R') is the result of the difference between the principal stress axis and the magmatic pressure (Baer *et al.*, 1994; equation 10), while the stress ratio (φ) expresses the relative magnitude of the principal stress axes (equation 11).

$$R' = \frac{P_m - \sigma_3}{\sigma_1 - \sigma_3} \quad (10)$$

$$\Phi = \frac{\sigma_2 - \sigma_3}{\sigma_1 - \sigma_3} \quad (11)$$

When φ=0, the stress ellipsoid is prolate, φ=1 represents an oblate ellipsoid, and 0<φ<1 means triaxial stresses with $\sigma_1 > \sigma_2 > \sigma_3$. The driving pressure ratio indicates the range of reactivation in the mode of fracture opening. If R'<0, no fractures are able to open in any orientation; if R'>0, fractures can open depending on the value of the stress ratio (Baer *et al*. 1994).

These two parameters are found after the use of stereographic projections which will provide the angles needed to construct the Mohr diagram. The stereographic distribution of poles to dyke walls can be interpreted as follows (see Martinez-Poza *et al.,* 2014 for a graphical explanation). A cluster distribution of poles around the minimum principal stress axis (σ_3) indicates that the magmatic pressure was lower than the intermediate stress axis (σ_2). On the other hand, if distribution of poles resembles a girdle with a small area free of poles around the maximum principal stress axis (σ_1), the magmatic pressure exceeded the intermediate stress axis (σ_2).

The symmetry in pole distribution gives the location of the principal stress axes (Jolly and Sanderson, 1997), which can be calculated by applying Bingham statistics (Mardia, 1972) using a software for stereographic projections. θ_1 is measured on the σ_2– σ_3 plane, θ_2 is measured on the σ_1– σ_3 plane and θ_3 is measured on the σ_1– σ_2 plane. If magma pressure is less than σ_2, the angles $2\theta_1$ and $2\theta_2$ define the cluster of poles. If magma pressure is higher than the intermediate stress σ_2, the angles $2\theta_2$ and $2\theta_3$ define the girdle of poles. The stress ratio and driving pressure values are calculated with the following equations (Jolly and Sanderson, 1997):

$$\Phi = \frac{\sigma_2 - \sigma_3}{\sigma_1 - \sigma_3} = \frac{\tau_{max1}}{\tau_{max2}} = \frac{1 + cos2\theta_2}{1 + cos2\theta_1} \quad (12)$$

$$\Phi = \frac{\sigma_2 - \sigma_3}{\sigma_1 - \sigma_3} = \frac{\tau_{max1}}{\tau_{max2}} = 1 - \frac{1 - cos2\theta_2}{1 - cos2\theta_3} \quad (13)$$

$$R' = \frac{P_m - \sigma_3}{\sigma_1 - \sigma_3} = \frac{a}{2\tau_{max2}} = \frac{(1 + cos2\theta_2)}{2} \quad (14)$$

Equation (12) applies to the situation where Pm < σ_2 and Equation (13) to that of $P_m > \sigma_2$.

The Jolly and Sanderson (1997) method has been applied to multiples studies, especially to tectonics of hydrothermal and magmatic vein and dyke systems

(André *et al*., 2001; McKeagney *et al*., 2004; Mazzarini and Isola, 2007; Mazzarini *et al*., 2011 and Mondal and Mamtani, 2013; Martínez-Poza *et al*., 2014).
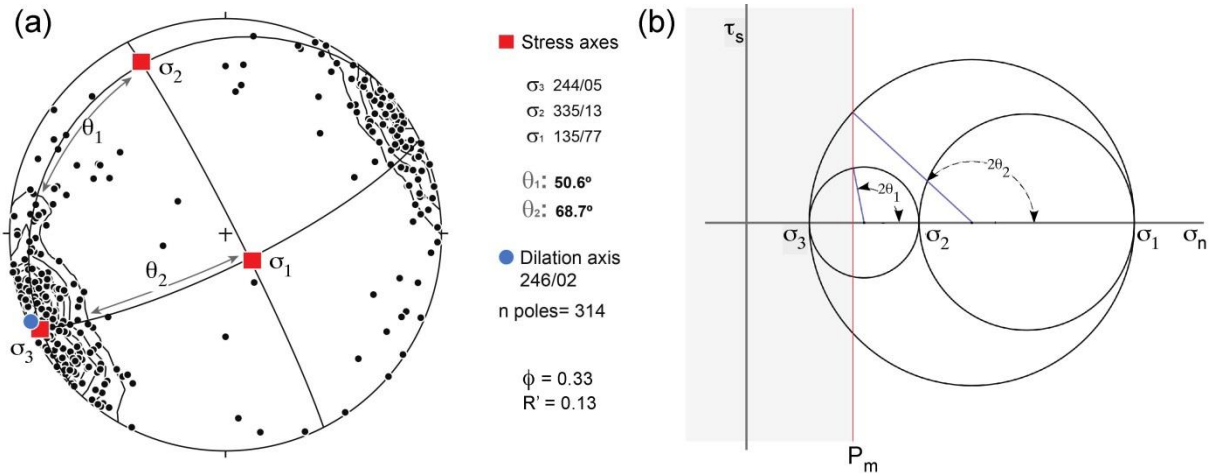

Fig. 3. 23. (a) Equal area, lower hemisphere stereoplot of poles to dyke segment walls from all measured dykes in Aiguablava (equivalent to Fig. 4a). Orientations of the principal stress axis (σ_1, σ_2, σ_3) are derived from the cluster-like distribution of dyke poles and the angles θ_1 and θ_2. The mean dilation direction obtained from application of the Bussell's method (Fig. 8) is depicted for comparison. (e) 3-D Mohr circle producing a stress ratio (φ) of 0.33 and a driving pressure ratio (R') of 0.13. P_m is the associated magmatic pressure which is lower than σ_2.

The stress analysis performed for the SE Sardinia dyke swarm has turned out to define the orientation of the three principal stress axes from the resulting sub-horizontal elongate cluster pattern of dyke wall poles (Fig. 3. 23a), which indicates that the magmatic pressure was smaller than the intermediate stress axis (Pm < σ_2). The resulting σ_1 is sub-vertical, compatible with a regional extensional tectonic regime, and σ_2 and σ_3 show sub-horizontal NNW-SSE and WSW-ENE trends respectively. σ_3 is sub-parallel to the sub-horizontal mean dyke opening direction obtained from Bussell's method (Fig. 3. 22b), both orientations being normal to the mean trend of the dyke swarm. Substituting the angles θ_1 and θ_2 (measured by stereographic analysis) into Equations (12) and (14), we can estimate the stress ratio (φ) and the driving pressure (R'). The obtained stress ratio is φ=0.33, while the driving pressure is R'= 0.13. The stress ratio correlates with a prolate stress ellipsoid (σ_1>>> σ_2> σ_3). The low value for R' agrees with a magmatic pressure inferior to σ_2. These values, together with the angles θ_1 and θ_2, were used to build the 3-D Mohr circle (Fig. 3. 23b).

3.2.8. Discussion

Based on a combination of several structural methods, the presented analysis of the SE Sardinia dyke swarm has allowed to characterize its main intrusive and structural features, as well as to gain insight into the mechanism of emplacement. A tectonic model for the emplacement of the dyke swarm is discussed in the next sub-section, followed by a comparison with the

Aiguablava dyke swarm in NE Iberia (previously interpreted on the basis of the same methodology), and, finally, an attempt of correlation between different Permian dyke swarms present in the western Mediterranean region.

3.2.8.1. Model for the intrusion of the SE Sardinia dyke swarm

We have shown that the granitoid host rocks embedding the mafic dykes are characterized by an extremely complex network of intersecting sub-vertical and sub-horizontal joint sets (Fig. 3. 16). Despite the difficulties encountered in giving a relative age to different fracture sets (pre-, syn, post-dyke intrusion), some evidences are found that the former fracture pattern at the time of dyke emplacement, likely developed during cooling and decompression of the granitoid pluton, included joint sets oriented parallel and oblique to the main N150º dyke trend (Figs. 3. 15 and 3. 18). A majority of dykes would have intruded and propagated parallel to or along joints in this NNW-SSE direction. Other secondary joint sets were exploited too, giving rise to segmentation structures such as continuous stepped dykes (Fig. 3. 19). In this way, we can state that the pre-existing joint network had an important control on the orientations for dyke intrusion. However, the strong prevalence of dyke orientation along sub-vertical ≈N150º surfaces and the matching of the normal to mean dyke plane with the calculated ENE-WSW net dilation direction (Fig. 3. 22), indicates that dyke intrusion was primarily controlled by the regional stress field.

We should remark that the given orientation values refer to present-time orientations and that these data cannot be extrapolated to the intrusion time (Permian) without a reconstruction of the relative position of the Corso-Sardinian block at that time, an aspect that will be discussed in sub-section 3.2.8.3. The performed paleostress analysis gives an estimation of the orientation and relative magnitudes of the tectonic principal stress axes operating at the time of intrusion (Fig. 3. 23). σ_1 was sub-vertical and σ_2 and σ_3 sub-horizontal, with σ_3 oriented ENE-WSW, perpendicular to the mean dyke swarm orientation and parallel to the mean dilation direction. The stress ratio φ = 0.33 corresponds to a close-to-prolate stress ellipsoid ($\sigma_1 >> \sigma_2 > \sigma_3$). There is a good correspondence between these paleostress values and field structures observed between dyke patterns in horizontal and vertical sections. That is, the higher variability in dyke orientation and degree of segmentation are observed in sub-horizontal exposures, and these are approximately parallel to the σ_2-σ_3, the plane of lower differential stress. Thus, the deduced paleostress values are in accordance with the observed segmentation pattern.

Emplacement of the mafic dyke swarm took place in the form of extension fractures during a regional extensional tectonic regime, as inferred from the sub-vertical principal stress axis (σ_1). Dykes preferentially opened perpendicular to their walls in a WSW-ENE direction. Despite the observed irregular dyke spacing distribution, the average crustal extension percentage associated to dyke intrusion estimated for the SE Sardinia region is considerably large (29%). The calculated low driving pressure ratio (R' = 0.13) and its closeness to the stress ratio (φ=0.33) imply that magma pressure was lower than the intermediate principal stress ($P_m < \sigma_2$, Fig. 3. 23). This is consistent with field

observations on the predominance of straight dykes over irregular patterns (Figs. 3. 16, 3. 17 and 3. 18). Moreover, when segmentation structures are present (Figs. 3. 19 and 3. 20), they show quite regular geometries, and curved apophysis and horns are scarce, reflecting limited local perturbation of the stress field by magmatic pressure.

Finally, dyke intrusion seems to have been favoured (and partly controlled) by the presence of pre-existing joints in the granitoid host rocks. Thus, the final 3-D pattern of the dyke swarm likely resulted from the interaction between these inherited fractures and the external tectonic stress tensor active during dyke emplacement.

3.3.8.2. Comparison with the Aiguablava dyke swarm (Catalan Coastal Ranges)

One of the aims of this work was to make a comparison with the Aiguablava lamprophyre dyke swarm in the Catalan Coastal Ranges of NE Iberia. The principal reasons for establishing this correlation is their apparent similarity and the fact that these two fragments of the Variscan belt are supposed to have been closely adjacent to each other by the time of magmatic activity in the Middle Permian. Since the approach and methods were the same in both studies, qualitative and quantitative results can be directly compared. Again, we should notice that data referred to spatial orientation (dyke strikes, stress axes orientations) cannot be directly compared without a previous restoration of the original relative positions of the respective crustal blocks (see next section). As regard to the rest of evaluated parameters, there are more similarities than differences between both settings.

In SE Sardinia, the smaller orientation range of dykes that are able to dilate implies a smaller driving pressure (R') compared to the Aiguablava case, the magmatic pressure being less than the intermediate stress (σ_2), whereas for Aiguablava the magmatic pressure equals σ_2. On the other hand, the slightly different stress ratios (Φ) correlates with slightly larger σ_2-σ_3 differential stress in SE Sardinia. Combining both facts, it results that intrusion of the SE Sardinia dyke swarm would have been more facilitated by tectonic stresses, i.e. tectonic activity, consistent with the observed larger development of fractures and reactivation of pre-existing fractures as fault planes in SE Sardinia. That would mean that the intrusion of the SE Sardinia dyke swarm would have been favoured by the active extensional crustal tectonics more than the Aiguablava intrusions, which is also in correspondence with the larger values achieved for amounts such as the maximum dyke thickness and the average percentage of regional extension, which are more than double in SE Sardinia compared to Aiguablava.

3.2.8.3. Attempt of correlation with other Permian mafic dyke swarms of the western Mediterranean region

The Variscan basement of Sardinia, as part of the Corso-Sardinian block, experienced a complex plate-scale history from its original intra-Pangea configuration (Late Paleozoic) to present times. This has relevant implications

into the interpretation of the former spatial distribution of the studied dyke swarm. Any attempt to illustrate Sardinian basement structures and to correlate them with those from other segments of the Variscan crust necessitates a restoration of at least the two principal post-Permian events that contributed to modify its original configuration. These are (i) rotation of the Corso-Sardinian block together with the Iberian microplate with respect to the stable Eurasian plate during Cretaceous times, and (ii) rotation of the Corso-Sardinian block relative to the Western European plate during the Neogene.

A tentative restoration of the Western Mediterranean region to the Triassic times is schematically represented in Figure 3. 24, including the effects of these two major tectonic events. This is based on qualitative and semi-quatitative values of crustal rotations and displacements and present orientation of dyke swams obtained from the literature.

3.2.8.3.1. Effects of Neogene rifting event

A counter-clockwise rotation of the Corso-Sardinian block relative to the Western European plate producing the opening of the Liguro-Provençal Basin took place during the Neogene rifting event, probably in the early Miocene (Arthaud and Matte, 1966, 1977; Alvarez, 1972; Westphal et al., 1976; Matte, 2001; Gattacceca et al., 2007). Different plate tectonic models have been used to describe this event (Alvarez et al. 1973; de Jong et al. 1973; Manzoni, 1975; Cohen, 1981; Montigny et al. 1981; Vigliotti et al, 1990; Speranza et al. 2002; Rollet et al., 2002; Ferrandini et al., 2003). An anti-clockwise rotation of the Corso-Sardo block between 30º and 50º with respect to the stable Western European plate results from averaging different values from the literature.

3.2.8.3.2. Effects of eo-Alpine tectonics

This consisted in an anti-clockwise rotation and sinistral displacement of the Corso-Sardinian block together with the Iberian microplate with respect to the stable Eurasian plate, involving the opening of the Bay of Biscay a the sinistral translation along the North Pyrenean Fault during Cretaceous (Aptian) times. Also different plate tectonic models have been used to describe these movements. The various proposed reconstructions differ on the rotation amount (20° to 40º) and on the amount of displacement along the North Pyrenean Fault (Matte, 1986; Olivet, 1996; Lefort and Agarwal, 1999; Gong et al., 2008). Moreover, the Iberian plate also encompassed the Balearic Islands, the Briançonaise block, nowadays in the western Alps (Stampfli, 1993) and pressumably involved the Maures-Tanneron massif in southern France.

3.2.8.3.3. Possible effects of Permian shearing and rotations

The tentative reconstruction to Triassic times depicted in Fig. 3. 24 results from restoration of the described anti-clockwise rotation associated to the Neogene rifting event and the eo-Alpine sinistral translation and rotation. The resulting pattern of dyke swarms is characterized by rather variable orientations. Notice,

for instance, the marked divergences in trend between the Catalan and the Sardinian dykes.

Mid- to Late-Permian mafic calc-alkaline to alkaline dyke swarms are widespread not only in the Corso-Sardinian block (Ronca *et al.*, 1999; Buraglini and Traversa, 2000) and in the Catalan Coastal Ranges (Martínez-Poza *et al.*, 2014), but also elsewhere in the Maures-Tanneron massif (Duchesne *et al.*, 2013), Massif Central (Perini *et al.*, 2004), Pyrenean Axial Zone (Debon and Zimmerman, 1993; Lasheras *et al* 1999; Lago *et al.*, 2004; Gil-Imaz *et al.*, 2012) and Iberian Massif (Orejana *et al.*, 2008; Scarrow *et al.*, 2011).

During the Late Carboniferous – Late Permian, there are palaeomagnetic evidences from Sardinia that support the presence of differential block rotation (Zijderveld *et al.*, 1970; Edel *et al.*, 1981; Edel, 2000; Moser *et al.*, 2005; Emmer *et al.*, 2005, Aubele *et al.* 2014). These movements have been generally related to a crustal-scale shear zone between Laurasia and Gondwana during post-Variscan times (Arthaud and Matte, 1977; Edel, 2000). This event is probably related to the transformation of Pagea B into Pangea A (Muttoni *et al.*, 2003).
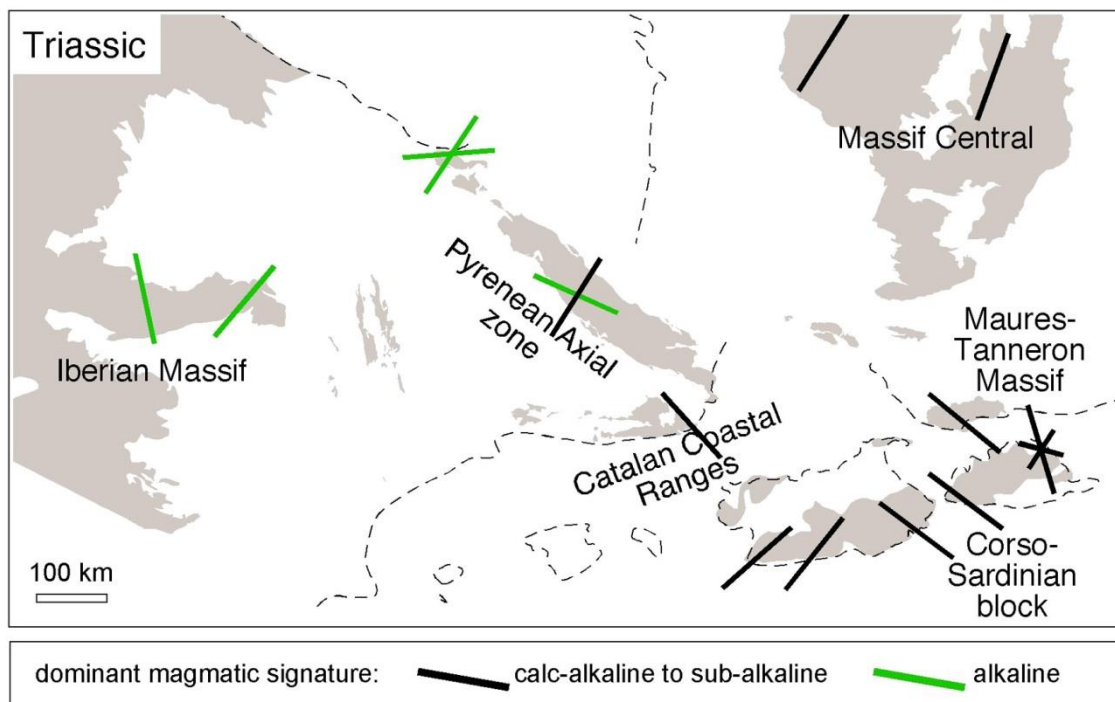

Fig. 3. 24. **Tentative reconstruction of the distribution during Triassic times of the SW European Variscan massifs and the main trends of Permian mafic dykes. Distribution of Variscan massifs has been modified from Carreras and Druguet (2014). Dyke orientations restored from original data compiled from Lasheras *et al.*, 1999; Ronca *et al.*, 1999; Buraglini and Traversa, 2000; Lago *et al.*, 2004; Gaggero *et al*, 2007; Orejana *et al.*, 2008; Scarrow *et al.*, 2011; Duchesne *et al.*, 2013; Martínez-Poza et al., 2014 and this work (see main text for further details).**

Helbing *et al.* (2006), based on the different trends of post-Variscan mafic dykes in NE and SE Sardinia, postulate a periclinal structure attributed to the Alpine cycle. However, according to Kischer *et al.* (2011), based on a palaeomagnetic study carried out in Jurassic sediments from Sardinia (Kirscher et al., 2011), all these movements took place before the Triassic, corroborating the models

based on Permian movements. The proposed model by Kischer *et al* (2011) sets that the shearing and wrenching process in the post-Variscan intra-Pangea area is presumably the responsible of the rotations of faulted blocks during the Permian in Sardinia (Chen *et al.*, 2006, Emmer *et al.*, 2005). In a more recent palaeomagnetic study performed on 13 late Variscan-Early Permian dykes from Sardinia, Aubele *et al.* (2014) postulates that Sardinia fragmented into two or three crustal blocks after dyke emplacement, which experienced differential relative rotations, as is also indicated by the differences in overall strike directions.

Our preliminary interpretation takes into account these possible, but still uncertain effects of pre-Triassic tectonics. The differential rotations associated with localized strike-slip movements might have operated interacting with regional extension during the Late Permian, contemporaneously with the emplacement of the large complex of mafic dykes which conforms part of the Western Mediterranean magmatic province.

3.2.9. Conclusions

A swarm of mafic porphyritic to lamprophyric dykes with a rather regular sub-vertical NNW-SSE orientation are exposed in SE Sardinia, being intruded in Permian times into the Late Variscan granitoids of the Sàrrabus massif. We have performed a multi-approach study in order to structurally characterize the dyke swarm and associated structures in the host rocks and to assess the stress state and tectonic regime at the time of the mafic dyking.

The dyke swarm has a mean ~N150º trend, with secondary sets at ~N77º and ~N10º, the last set likely corresponds to a posterior magmatic pulse.

The fracture network (mostly joints) affecting both, the granitoid host rocks and the dykes, is not as straightforward to interpret. Joints have multiple orientations clustered in four or more sets, with patterns in granitoid and dykes being noticeably different. There is evidence that some of the pre-existing joint sets were exploited by dykes and that other joints were reactivated as faults during and after dyke intrusion.

The paleostress analysis yields σ_1 sub-vertical, indicating that an extensional tectonic regime predominated in the area during the emplacement of the dyke swarm. σ_2 and σ_3 are sub-horizontal, with σ_3 ENE-WSW, sub-parallel to the mean dilation direction inferred from dyke orientation data and normal to the mean trend of the dykes.

The stress ratio is $\Phi=0.33$, corresponding to a prolate stress ellipsoid, with σ_1 much larger than the other two principal stress axes.

The driving pressure ratio is R'=0.13, demonstrating that the magmatic pressure (P_m) was relatively low, lower than σ_2.

An additional analysis, aimed to estimate regional extension, gave a mean true extension value of ~29% for the whole study area.

In this context, intrusion of the NNW-SSE dyke swarm occurred under low fluid pressure conditions and preferentially into a pre-existing joint nerwork that was partly reactivated as extension fractures during a regional extensional event.

The main trend of the SE Sardinian dyke swarm has been compared with that of other contemporary mafic dykes in the nearby areas of the Variscan orogen. This has been made by restoring the effects of the two main post-intrusion rotation events of crustal blocks related to Neogene and eo-Alpine tectonics. The performed reconstruction gives a rather complex, non-parallel crustal-scale pattern of dyke orientation. Several factors could account for such a complex pattern, among which we can point out differential rotations associated with localized strike-slip movements that might have been operating coevally with regional extension during Permian times. Further work is necessary to fully understand the geodynamics of the large western Mediterranean Permian magmatic province.